

# Non-singular Bouncing Cosmology in $f(R, G, T)$ –Quintom model

Farzad Milani\*

*Department of Basic Sciences, Technical and Vocational University (TVU), Tehran, Iran.*

(Dated: December 30, 2025)

## Abstract

We present a unified framework for non-singular bouncing cosmologies in modified gravity, combining  $f(R, G, T)$  geometry with quintom scalar dynamics in a flat FLRW universe. While single-field models achieve phantom divide line (PDL) crossing and stable bounces, our  $f(R, G, T)$ -quintom coupling provides a novel implementation of a *double* PDL crossing of  $\omega_{\text{eff}}$  during the bounce.

We address stability concerns through Hamiltonian analysis, showing that FLRW symmetry constraints suppress Ostrogradsky instabilities by reducing higher-derivative terms to metric invariant. The scalar field equation of motion is explicitly derived, confirming cancellation of pathological modes.

Numerical reconstruction of five  $f(R, G, T)$  models confirms non-singular bounces with  $\rho_{\text{eff}} > 0$  and  $c_s^2 \geq 0$ , alongside parametric control over energy condition violations. Our work extends prior studies by: (1) unifying early-time bounce dynamics with late-time dark energy, (2) demonstrating a novel double-PDL crossing signature compatible with FLRW stability, and (3) establishing explicit ghost-free criteria for higher-derivative terms.

PACS numbers: 04.50.Kd, 98.80.Jk, 95.36.+x, 98.80.Cq

Keywords: Bouncing cosmology;  $f(R, G, T)$  gravity; Quintom model; Phantom divide crossing; Nonsingular universe; Dark energy; Cosmological perturbations

---

\*Electronic address: fmilani@tvu.ac.ir

## 1. INTRODUCTION

The recent observational data clearly indicate that the universe is undergoing accelerated expansion [1–4], presenting modern cosmology with the dual challenge of explaining late-time acceleration while avoiding initial singularities. While the  $\Lambda$ CDM model remains phenomenologically successful [5], its theoretical shortcomings regarding the cosmological constant’s magnitude have driven interest in alternatives. Among these,  $f(R)$  gravity [6] and scalar-tensor theories [7] have shown promise, particularly in contexts where conformal invariance—a property absent in General Relativity (GR)—plays a key role [8]. Conformal Weyl gravity, for instance, leverages local conformal invariance of the metric [9] to address quantum-gravitational inconsistencies and galactic-scale anomalies [10].

The standard cosmological framework is based on the Einstein-Hilbert action:

$$\mathcal{S}_{EH} = \frac{1}{16\pi G_r} \int d^4x \sqrt{-g} R, \quad (1)$$

where  $G_r$  is Newton’s gravitational constant and  $R$  is the Ricci scalar [11]. Modifications to this action must reconcile two competing demands: theoretical consistency (e.g., avoiding Ostrogradsky instabilities) and observational viability (e.g., enabling phantom divide line (PDL) crossings). While single-field models can achieve PDL crossings [12, 13] and stable bounces [14, 15], our work synthesizes three advances: (1) the geometric control of Gauss-Bonnet terms [16], where  $G = 24H^2(\dot{H} + H^2)$ ; (2) the stability of  $f(R)$ -based PDL crossings [17]; and (3) the parametric flexibility of quintom models [18]. Crucially, the FLRW symmetry constraints  $R = 6(\dot{H} + 2H^2)$  and  $G = 24H^2(\dot{H} + H^2)$  reduce higher-derivative terms to second order, suppressing ghosts as demonstrated in [19, 20] and consistent with the degeneracy conditions of DHOST theories [21].

Our model builds upon early two-field approaches by coupling the energy-momentum trace  $T$  to curvature invariants. This coupling provides new degrees of freedom that enable novel double PDL crossings while helping to maintain  $c_s^2 \geq 0$ . This contrasts with single-field mechanisms which often require fine-tuned potentials [22] or non-canonical kinetic terms [23] to achieve a single crossing. The bouncing cosmology framework further avoids initial singularities through scale factor reversal, offering a cyclic universe alternative [24–27].

**Stability as a cornerstone:** A key criticism of higher-derivative theories is the potential for ghost instabilities [28–30]. In Section 5, we rigorously analyze the dynamical degrees of

freedom in our  $f(R, G, T)$ -quintom system, showing that the FLRW background inherently suppresses pathological modes—a feature absent in generic higher-derivative proposals. This builds on healthy bounce constructions [15] while generalizing them to curvature-matter couplings.

Observational support for these ideas comes from Type Ia supernovae [31–33], Baryon Acoustic Oscillations (BAO) [34], and Cosmic Microwave Background (CMB) measurements [3, 4]. These align with theoretical models like quintessence [35], phantom energy [36], and hybrid approaches [37–39].

In Section 2, we derive the equations of motion and energy-momentum components for an  $f(R, G, T)$ -quintom system in a flat FLRW metric, ensuring conservation law compatibility. Section 3 presents the modified Friedmann equations, while Section 4 shows how conformal Weyl gravity emerges as a limiting case. A comprehensive stability analysis, encompassing both ghost freedom and scalar perturbations, is conducted in Section 5. Following this, Section 6 numerically reconstructs five distinct  $f(R, G, T)$  models, demonstrating their viable bounce dynamics and Phantom Divide Line (PDL) crossings. We conclude in Section 7 by highlighting how curvature-matter coupling provides a unified framework for early-time bounces and late-time acceleration, thereby setting the stage for future extended analyses.

## 2. THE MODEL

In modified gravity, we consider an extension of the Einstein-Hilbert action by introducing a general function of the Ricci scalar  $R$ , Gauss-Bonnet invariant  $G$ , and the trace of the matter stress-energy tensor  $T \equiv g^{\mu\nu}T_{\mu\nu}^{(m)}$ , coupled to a quintom scalar sector consisting of a phantom field  $\phi(t)$  and a canonical field  $\psi(t)$ . The total action is given by:

$$\mathcal{S} = \int d^4x \sqrt{-g} \left[ \frac{1}{2\kappa^2} f(R, G, T) + \Xi(\phi, \psi) + \mathcal{L}_m \right], \quad (2)$$

where:

- $\kappa^2 \equiv 8\pi G_r/c^4$  is the gravitational coupling constant,
- $G_r \approx 6.67430 \times 10^{-11} \text{ N} \cdot \text{m}^2/\text{kg}^2$  is Newton’s constant,
- $\mathcal{L}_m$  is the matter-radiation Lagrangian.

## 2.1. Quintom Sector and FLRW Metric

The quintom Lagrangian combines the phantom,  $\phi$ , and canonical,  $\psi$ , fields together as:

$$\Xi(\phi, \psi) = -\frac{1}{2}\partial_\mu\phi\partial^\mu\phi + \frac{1}{2}\partial_\mu\psi\partial^\mu\psi - V(\phi, \psi), \quad (3)$$

where  $V(\phi, \psi)$  is the interaction potential. For a flat FLRW universe:

$$ds^2 = -dt^2 + a^2(t) \sum_{i=1}^3 (dx^i)^2, \quad (4)$$

the Ricci scalar and Gauss-Bonnet invariant reduce to:

$$R = 6 \left( \dot{H} + 2H^2 \right), \quad (5)$$

$$G = 24H^2 \left( \dot{H} + H^2 \right). \quad (6)$$

## 2.2. Scalar Field Dynamics

The equations of motion for  $\phi$  (phantom) and  $\psi$  (canonical) are:

$$\square\phi - V_{,\phi} + \frac{f_T}{2\kappa^2} \frac{\delta T}{\delta\phi} = 0, \quad (7)$$

$$\square\psi + V_{,\psi} + \frac{f_T}{2\kappa^2} \frac{\delta T}{\delta\psi} = 0, \quad (8)$$

where the coupling terms are:

$$\frac{\delta T}{\delta\phi} = -2 \frac{\partial \mathcal{L}_m}{\partial\phi} + g^{\mu\nu} \frac{\partial T_{\mu\nu}^{(m)}}{\partial\phi}, \quad (9)$$

$$\frac{\delta T}{\delta\psi} = -2 \frac{\partial \mathcal{L}_m}{\partial\psi} + g^{\mu\nu} \frac{\partial T_{\mu\nu}^{(m)}}{\partial\psi}. \quad (10)$$

For minimal coupling ( $\delta T/\delta\phi = \delta T/\delta\psi = 0$ ), these reduce to:

$$\ddot{\phi} + 3H\dot{\phi} - V_{,\phi} = 0, \quad (11)$$

$$\ddot{\psi} + 3H\dot{\psi} + V_{,\psi} = 0. \quad (12)$$

## 2.3. Energy-Momentum Tensors

The total energy-momentum tensor (as shown in Appendix A) decomposes as:

$$T_{\mu\nu}^{(\text{total})} = \underbrace{T_{\mu\nu}^{(R)} + T_{\mu\nu}^{(G)}}_{\text{Geometric}} + \underbrace{T_{\mu\nu}^{(T)} + T_{\mu\nu}^{(\Xi)} + T_{\mu\nu}^{(m)}}_{\text{Matter/Quintom}}, \quad (13)$$

where:

$$T_{\mu\nu}^{(R)} = \frac{1}{\kappa^2} \left( f_R R_{\mu\nu} - \frac{1}{2} g_{\mu\nu} f + (g_{\mu\nu} \square - \nabla_\mu \nabla_\nu) f_R \right), \quad (14)$$

$$\begin{aligned} T_{\mu\nu}^{(G)} &= \frac{2R}{\kappa^2} (f_G R_{\mu\nu} + (g_{\mu\nu} \square - \nabla_\mu \nabla_\nu) f_G) - \frac{4}{\kappa^2} (f_G R_\mu^\rho R_{\rho\nu} + (R_{\mu\nu} \square + g_{\mu\nu} R^{\rho\lambda} \nabla_\rho \nabla_\lambda) f_G) \\ &\quad - \frac{4}{\kappa^2} f_G \left( R_{\mu\rho\nu\lambda} R^{\rho\lambda} - \frac{1}{2} R_\mu^{\rho\lambda\xi} R_{\nu\rho\lambda\xi} \right) + \frac{4}{\kappa^2} (R_\mu^\rho \nabla_\nu \nabla_\rho + R_\nu^\rho \nabla_\mu \nabla_\rho + R_{\mu\rho\nu\lambda} \nabla^\rho \nabla^\lambda) f_G, \end{aligned} \quad (15)$$

$$T_{\mu\nu}^{(\Xi)} = -\partial_\mu \phi \partial_\nu \phi + \partial_\mu \psi \partial_\nu \psi + g_{\mu\nu} \left( \frac{1}{2} \partial_\alpha \phi \partial^\alpha \phi - \frac{1}{2} \partial_\alpha \psi \partial^\alpha \psi - V(\phi, \psi) \right), \quad (16)$$

$$T_{\mu\nu}^{(m)} = -\frac{2}{\sqrt{-g}} \frac{\partial(\sqrt{-g} \mathcal{L}_m)}{\partial g^{\mu\nu}} = g_{\mu\nu} \mathcal{L}_m - 2 \frac{\partial \mathcal{L}_m}{\partial g^{\mu\nu}}, \quad (17)$$

$$T_{\mu\nu}^{(T)} = -\frac{f_T}{\kappa^2} (T_{\mu\nu}^{(m)} + \Theta_{\mu\nu}). \quad (18)$$

Here, the  $T_{\mu\nu}^{(T)}$  term introduces *non-minimal coupling* between matter and geometry through, where  $\Theta_{\mu\nu} \equiv g^{\alpha\beta} \frac{\partial T_{\alpha\beta}^{(m)}}{\partial g^{\mu\nu}}$  encodes how matter responds to metric variations.

## 2.4. Gravitational Field Equations

The generalized Einstein equations are derived from the variation of the action with respect to  $g^{\mu\nu}$ . Defining the Einstein tensor as:

$$G_{\mu\nu} \equiv R_{\mu\nu} - \frac{1}{2} g_{\mu\nu} R, \quad (19)$$

the field equations take the form:

$$\begin{aligned} & f_R G_{\mu\nu} + (g_{\mu\nu} \square - \nabla_\mu \nabla_\nu) f_R + 2R (g_{\mu\nu} \square - \nabla_\mu \nabla_\nu) f_G \\ & - 4 (R_\mu^\rho \nabla_\nu \nabla_\rho + R_\nu^\rho \nabla_\mu \nabla_\rho) f_G + 4R_{\mu\nu} \square f_G + 4g_{\mu\nu} R^{\rho\sigma} \nabla_\rho \nabla_\sigma f_G \\ & - 4R_{\mu\rho\nu\sigma} \nabla^\rho \nabla^\sigma f_G - \frac{1}{2} g_{\mu\nu} f + f_T (T_{\mu\nu}^{(m)} + \Theta_{\mu\nu}) = \kappa^2 T_{\mu\nu}^{(\Xi)}. \end{aligned} \quad (20)$$

## 2.5. Dynamics of Perfect Fluids

The matter content is described by a perfect fluid with energy-momentum tensor:

$$T_{\mu\nu}^{(m)} = (\rho + p) u_\mu u_\nu + p g_{\mu\nu}, \quad (21)$$

where  $\rho \equiv \rho_m + \rho_r$  is the total energy density and  $p \equiv p_m + p_r$  is the total pressure, with subscripts  $m$  and  $r$  denoting non-relativistic matter and radiation respectively. The four-velocity  $u_\mu$  satisfies  $u_\mu u^\mu = -1$  and  $u^\mu \nabla_\nu u_\mu = 0$ .

The conservation laws for standard matter components are:

$$\dot{\rho} + 3H(\rho + p) = 0 \quad \Rightarrow \quad \dot{\rho}_m + 3H\rho_m = 0 \quad \text{and} \quad \dot{\rho}_r + 4H\rho_r = 0, \quad (22)$$

where we have used the equations of state  $\omega_m \equiv p_m/\rho_m \approx 0$  for matter and  $\omega_r \equiv p_r/\rho_r = 1/3$  for radiation.

Using the matter Lagrangian  $\mathcal{L}_m = p$  (as shown in Appendix A), the tensor  $\Theta_{\mu\nu}$  becomes:

$$\Theta_{\mu\nu} = g_{\mu\nu}\mathcal{L}_m - 2T_{\mu\nu}^{(m)} - 2g^{\alpha\beta} \frac{\partial^2 \mathcal{L}_m}{\partial g^{\alpha\beta} \partial g^{\mu\nu}} = -2T_{\mu\nu}^{(m)} + pg_{\mu\nu}. \quad (23)$$

For the FLRW metric, we obtain the following important quantities:

$$T \equiv g^{\mu\nu}T_{\mu\nu}^{(m)} = -\rho + 3p = -(1 - 3\omega)\rho, \quad (24)$$

$$\Theta \equiv g^{\mu\nu}\Theta_{\mu\nu} = 2(\rho - p) = 2(1 - \omega)\rho, \quad (25)$$

$$T + \Theta = 2(\rho + p) = 2\rho(1 + \omega), \quad (26)$$

where  $\omega \equiv p/\rho$  is the total equation of state parameter.

The 00 and  $ii$  components of the total energy-momentum tensor decomposition (13) give the modified Friedmann equations:

$$\rho_R + \rho_G = \rho + \rho_T + \rho_\Xi, \quad (27)$$

$$p_R + p_G = p + p_T + p_\Xi, \quad (28)$$

with the individual components given by:

$$\kappa^2 \rho_R = -3H^2 f_R - 3\dot{H} f_R + 3H \dot{f}_R + \frac{f}{2}, \quad (29)$$

$$\kappa^2 p_R = 3H^2 f_R + \dot{H} f_R - 2H \dot{f}_R - \frac{f}{2} - \ddot{f}_R, \quad (30)$$

$$\kappa^2 \rho_G = -12H^2(H^2 + \dot{H})f_G + H(3H^2 - 9\dot{H})\dot{f}_G - 9(H^2 + \dot{H})\ddot{f}_G, \quad (31)$$

$$\kappa^2 p_G = 12H^2(H^2 + \dot{H})f_G + H(7H^2 - 5\dot{H})\dot{f}_G - (H^2 - 3\dot{H})\ddot{f}_G, \quad (32)$$

$$\kappa^2 \rho_T = f_T(\rho + p), \quad (33)$$

$$\kappa^2 p_T = 0, \quad (34)$$

$$\rho_\Xi = -\frac{1}{2}\dot{\phi}^2 + \frac{1}{2}\dot{\psi}^2 + V(\phi, \psi), \quad (35)$$

$$p_\Xi = -\frac{1}{2}\dot{\phi}^2 + \frac{1}{2}\dot{\psi}^2 - V(\phi, \psi), \quad (36)$$

where we have used the FLRW expressions  $R = 6\dot{H} + 12H^2$  and  $G = 24H^2(\dot{H} + H^2)$ .

## 2.6. Conservation Laws

As shown in Appendix B, by taking the covariant divergence of the total energy-momentum tensor decomposition (13), we obtain the following conservation equations for each component:

$$\nabla^\mu T_{\mu\nu}^{(R)} = -\frac{1}{2\kappa^2} g_{\mu\nu} (f_G \nabla^\mu G + f_T \nabla^\mu T), \quad (37)$$

$$\begin{aligned} \nabla^\mu T_{\mu\nu}^{(G)} &= \frac{1}{\kappa^2} (R f_G - 2(\nabla^\alpha \nabla_\alpha f_G) + 4R^{\alpha\beta} \nabla_\alpha \nabla_\beta f_G) \nabla_\nu R \\ &+ \frac{4}{\kappa^2} (R_{\mu\rho\nu\lambda} \nabla^\mu \nabla^\lambda \nabla^\rho f_G - R_{\nu\rho} \nabla^\rho (\nabla^\alpha \nabla_\alpha f_G)) - \frac{4}{\kappa^2} f_G \left( R^{\rho\lambda} \nabla_\rho R_{\nu\lambda} + \frac{1}{2} R^{\rho\lambda\alpha\beta} \nabla_\nu R_{\rho\lambda\alpha\beta} \right) \\ &+ \frac{4}{\kappa^2} (f_{GR} \nabla^\mu R + f_{GG} \nabla^\mu G + f_{GT} \nabla^\mu T) \left( \frac{1}{2} R_\mu^{\rho\lambda\xi} R_{\nu\rho\lambda\xi} - R_{\mu\rho\nu\lambda} R^{\rho\lambda} \right), \end{aligned} \quad (38)$$

$$\nabla^\mu T_{\mu\nu}^{(T)} = -\frac{1}{\kappa^2} ((T_{\mu\nu}^{(m)} + \Theta_{\mu\nu}) \nabla^\mu f_T + f_T \nabla^\mu (T_{\mu\nu}^{(m)} + \Theta_{\mu\nu})), \quad (39)$$

$$\nabla^\mu T_{\mu\nu}^{(\Xi)} = 0. \quad (40)$$

where  $f_{GR} = \frac{\partial^2 f}{\partial G \partial R}$ ,  $f_{GG} = \frac{\partial^2 f}{\partial G^2}$ , and  $f_{GT} = \frac{\partial^2 f}{\partial G \partial T}$ .

The total conservation law for matter is then:

$$\nabla^\mu (\kappa^2 T_{\mu\nu}^{(m)} - f_T (T_{\mu\nu}^{(m)} + \Theta_{\mu\nu}) - \kappa^2 T_{\mu\nu}^{(G)}) + \frac{1}{2} g_{\mu\nu} f_G \nabla^\mu G + \frac{1}{2} g_{\mu\nu} f_T \nabla^\mu T = 0, \quad (41)$$

which gives:

$$\begin{aligned} \nabla^\mu T_{\mu\nu}^{(m)} &= \frac{f_T}{\kappa^2 - f_T} \left( (T_{\mu\nu}^{(m)} + \Theta_{\mu\nu}) \nabla^\mu \ln(f_T) + \nabla^\mu \Theta_{\mu\nu} - \frac{1}{2} g_{\mu\nu} \nabla^\mu T \right) \\ &+ \frac{1}{\kappa^2 - f_T} \left( \kappa^2 \nabla^\mu T_{\mu\nu}^{(G)} - \frac{1}{2} g_{\mu\nu} f_G \nabla^\mu G \right). \end{aligned} \quad (42)$$

As shown in Appendix C, for the FLRW metric, these become:

$$\begin{aligned}\kappa^2 \nabla^\mu T_{\mu 0}^{(R)} &= 12f_R H \dot{H} + 3f_R \ddot{H} - \frac{\dot{f}}{2} \\ &= -12f_G H (H \ddot{H} + 2\dot{H}^2 + 4H^2 \dot{H}) - (3\dot{p} - \rho) \frac{f_T}{2},\end{aligned}\quad (43)$$

$$\begin{aligned}\kappa^2 \nabla^\mu T_{\mu 0}^{(G)} &= 12(\dot{H} + H^2) \ddot{f}_G \\ &\quad + 12 \left( \ddot{H} + 7H\dot{H} + 3H^3 - 6(\dot{H} + H^2)(\ddot{H} + 4H\dot{H}) \right) \dot{f}_G \\ &\quad + 36 \left( H\ddot{H} + 5H^2\dot{H} + \dot{H}^2 \right) \dot{f}_G \\ &\quad + 12 \left( 2\dot{H}\ddot{H} + 14H\dot{H}^2 + 5H^2\ddot{H} + 26H^3\dot{H} \right) f_G \\ &\quad + 6(\dot{H} + H^2)(\dot{H} + 5H^2) \left( f_{GR}(6\ddot{H} + 24H\dot{H}) + f_{GG}\dot{G} + f_{GT}\dot{T} \right)\end{aligned}\quad (44)$$

$$\begin{aligned}\kappa^2 \nabla^\mu T_{\mu 0}^{(G)} - \frac{1}{2} g_{\mu 0} f_G \nabla^\mu G &= 12(\dot{H} + H^2) \ddot{f}_G \\ &\quad + 12 \left( \ddot{H} + 7H\dot{H} + 3H^3 - 6(\dot{H} + H^2)(\ddot{H} + 4H\dot{H}) \right) \dot{f}_G \\ &\quad + 36 \left( H\ddot{H} + 5H^2\dot{H} + \dot{H}^2 \right) \dot{f}_G \\ &\quad + 24 \left( \dot{H}\ddot{H} + 6H\dot{H}^2 + 2H^2\ddot{H} + 11H^3\dot{H} \right) f_G \\ &\quad + 6(\dot{H} + H^2)(\dot{H} + 5H^2) \left( f_{GR}(6\ddot{H} + 24H\dot{H}) + f_{GG}\dot{G} + f_{GT}\dot{T} \right).\end{aligned}\quad (45)$$

where:

$$\begin{aligned}\dot{G} &= 24H^2\ddot{H} + 48H(\dot{H})^2 + 96H^3\dot{H} \\ \dot{T} &= -\dot{\rho} + 3\dot{p}\end{aligned}$$

Substituting equations (21), (23), (24), and the previously computed expression for  $\kappa^2 \nabla^\mu T_{\mu 0}^{(G)} - \frac{1}{2} g_{\mu 0} f_G \nabla^\mu G$  into (42) and projecting the  $\nu = 0$  component for the FLRW metric yields the following general expression:

$$\begin{aligned}-(\kappa^2 - f_T) (\dot{\rho} + 3H(\rho + p)) &= (\rho + p) \dot{f}_T + \left( 6(\rho + p)H + \frac{3}{2}\dot{\rho} + \frac{9}{2}\dot{p} \right) f_T \\ &\quad + \kappa^2 \nabla^\mu T_{\mu 0}^{(G)} - \frac{1}{2} g_{\mu 0} f_G \nabla^\mu G.\end{aligned}\quad (46)$$

The standard conservation law from general relativity is  $\dot{\rho} + 3H(\rho + p) = 0$ . Therefore, for energy-momentum conservation to hold in our model, the right-hand side of the equation

must vanish. This leads to the following consistency condition:

$$-(\rho + p)\dot{f}_T - \frac{1}{2}(9\dot{p} - \dot{\rho})f_T = \kappa^2 \nabla^\mu T_{\mu 0}^{(G)} - \frac{1}{2}g_{\mu 0}f_G \nabla^\mu G. \quad (47)$$

Special cases where conservation holds include when both sides of the equation are identically zero. This occurs under the following separate conditions:

$$(\rho + p)\dot{f}_T + \frac{1}{2}(9\dot{p} - \dot{\rho})f_T = 0, \quad (48)$$

$$\kappa^2 \nabla^\mu T_{\mu 0}^{(G)} - \frac{1}{2}g_{\mu 0}f_G \nabla^\mu G = 0. \quad (49)$$

Equation (48) governs the energy-momentum exchange between matter and geometry through the  $f_T$  coupling. This constraint is automatically satisfied when  $f_T = 0$ , corresponding to minimal matter coupling. For non-zero  $f_T$ , the equation imposes a relation between matter evolution and the  $T$ -dependence of the gravitational Lagrangian. A particularly important solution occurs for radiation-dominated universes ( $p = \rho/3$ ), where the condition simplifies to  $(\rho + p)\dot{f}_T + \dot{\rho}f_T = 0$ , leading to  $f_T \propto 1/\rho$  scaling [40].

The conservation equation (49) significantly constrains cosmological solutions in  $f(R, G, T)$  gravity. The simplest stable solution is  $f_G = 0$ , corresponding to General Relativity with a cosmological constant ( $f = R - 2\Lambda$ ).

For  $f_G = \text{const.} \neq 0$ , the constraint simplifies to:

$$\dot{H}\ddot{H} + 6H\dot{H}^2 + 2H^2\ddot{H} + 11H^3\dot{H} = 0, \quad (50)$$

which is satisfied by de Sitter space ( $H = \text{constant}$ ) [41]. The linear case  $f(G) = \alpha G$  avoids Ostrogradsky instabilities due to the topological nature of  $G$  in 4D [30, 42].

A particularly interesting solution occurs for coasting cosmology ( $\dot{H} + H^2 = 0$ ) [14, 43], which eliminates higher-derivative terms and yields:

$$\ddot{f}_G + 3H\dot{f}_G + 3H^2f_G = 0. \quad (51)$$

This second-order damped oscillator equation is stable and suitable for bouncing scenarios [15]. For general nonlinear  $f(G)$ , stability requires the degeneracy condition  $f_{RR}f_{GG} - (f_{RG})^2 = 0$  to avoid ghost instabilities [21].

### 3. EINSTEIN FIELD EQUATIONS AND MODIFIED FRIEDMANN DYNAMICS

The Einstein Field Equation (EFE) in its standard form is:

$$G_{\mu\nu} + \Lambda g_{\mu\nu} = R_{\mu\nu} - \frac{1}{2}g_{\mu\nu}R + \Lambda g_{\mu\nu} = \kappa^2 T_{\mu\nu}^{(m)}, \quad (52)$$

which yields the Friedmann equations for a flat FLRW universe:

$$3H^2 - \Lambda = \kappa^2 \rho, \quad (53)$$

$$-2\dot{H} - 3H^2 + \Lambda = \kappa^2 p. \quad (54)$$

In the  $\Lambda$ CDM model, dark energy is represented by a cosmological constant  $\Lambda \equiv \kappa^2 \rho_{vac}$ . For dynamical dark energy models (like quintom), we generalize this to time-varying components:

$$3H^2 - \kappa^2 \rho_{DE} = \kappa^2 \rho, \quad (55)$$

$$-2\dot{H} - 3H^2 - \kappa^2 p_{DE} = \kappa^2 p. \quad (56)$$

Comparing with our modified gravity decomposition (27)-(28), the dark energy components become:

$$\begin{aligned} \kappa^2 \rho_{DE} &\equiv 3H^2 + \kappa^2 (\rho_T + \rho_{\Xi} - \rho_R - \rho_G) \\ &= 3H^2(1 + f_R) - 3H\dot{f}_R + 3\dot{H}f_R - \frac{f}{2} + f_T(\rho + p) + \rho_{\Xi} \\ &\quad + 9(H^2 + \dot{H})\ddot{f}_G + 3H(3\dot{H} - H^2)\dot{f}_G + 12H^2(H^2 + \dot{H})f_G, \end{aligned} \quad (57)$$

$$\begin{aligned} \kappa^2 p_{DE} &\equiv -2\dot{H} - 3H^2 + \kappa^2 (p_T + p_{\Xi} - p_R - p_G) \\ &= -(2\dot{H} + 3H^2)(1 + f_R) + 2H\dot{f}_R + \dot{H}f_R + \frac{f}{2} + \ddot{f}_R + p_{\Xi} \\ &\quad - 12H^2(H^2 + \dot{H})f_G - H(7H^2 - 5\dot{H})\dot{f}_G + (H^2 - 3\dot{H})\ddot{f}_G. \end{aligned} \quad (58)$$

The effective field equation approach writes:

$$G_{\mu\nu} = \kappa^2 T_{\mu\nu}^{(eff)}, \quad (59)$$

yielding:

$$3H^2 = \kappa^2 \rho_{\text{eff}}, \quad (60)$$

$$-2\dot{H} - 3H^2 = \kappa^2 p_{\text{eff}}, \quad (61)$$

For  $f_R \neq 0$ , the effective energy density and pressure can be obtained as

$$\rho_{\text{eff}} = \frac{1}{f_R} \left( \rho + \rho_{\Xi} + \frac{1}{\kappa^2} \mathcal{R} \right) \quad (62)$$

$$p_{\text{eff}} = \frac{1}{f_R} \left( p + p_{\Xi} + \frac{1}{\kappa^2} \mathcal{P} \right) \quad (63)$$

where

$$\begin{aligned} \mathcal{R} = & 3f_R(\dot{H} + 2H^2) - \frac{f}{2} - 3H\dot{f}_R - f_T(\rho + p) \\ & - 12H^2(H^2 + \dot{H})f_G + H(3H^2 - 9\dot{H})\dot{f}_G - 9(H^2 + \dot{H})\ddot{f}_G \end{aligned} \quad (64)$$

$$\begin{aligned} \mathcal{P} = & -3f_R(\dot{H} + 2H^2) - \frac{f}{2} - 3H\dot{f}_R + f_T p - \ddot{f}_R \\ & - 12H^2(H^2 + \dot{H})f_G - H(7H^2 - 5\dot{H})\dot{f}_G + (H^2 - 3\dot{H})\ddot{f}_G \end{aligned} \quad (65)$$

Energy conservation requires:

$$\dot{\rho}_{DE} + 3H(\rho_{DE} + p_{DE}) = 0, \quad (66)$$

$$\dot{\rho}_{\text{eff}} + 3H(\rho_{\text{eff}} + p_{\text{eff}}) = 0. \quad (67)$$

The effective EoS parameter is:

$$\begin{aligned} \omega_{\text{eff}} &= -1 - \frac{2}{3} \frac{\dot{H}}{H^2} \\ &= -1 + \frac{\rho(1 + \omega) + \rho_{DE}(1 + \omega_{DE})}{\rho + \rho_{DE}}, \end{aligned} \quad (68)$$

which reduces to the  $\Lambda$ CDM case when  $\omega_{DE} = -1$ :

$$\omega_{\text{eff}} = -1 + \frac{\rho(1 + \omega)}{\rho + \rho_{DE}}. \quad (69)$$

A substantial body of literature has focused on analytically solving the second part of equations such as Eq. (68), aiming to identify functional forms that satisfy the required physical criteria. However, many such analytical approaches prove insufficient for fully resolving issues like the Phantom Divide Line (PDL) crossing. This is because, regardless of the specific form on the other side of the equation, one can often construct solutions that *mathematically* satisfy the condition—for instance, ensuring  $\rho_{\text{eff}}(1 + \omega_{\text{eff}}) = 0$  at the bounce point while maintaining  $\frac{d}{dt}(\rho_{\text{eff}} + p_{\text{eff}}) \neq 0$ —without guaranteeing physical plausibility or stability.

Therefore, to robustly verify the internal consistency and dynamical stability of our model, we employ a numerical framework. In Section 6, we examine these conditions, focusing on key stability criteria such as the squared sound speed  $c_s^2$  and the effective equation of state  $\omega_{\text{eff}}$ , including its crossing of the PDL ( $\omega_{\text{eff}} = -1$ ). This analysis serves to establish the theoretical viability of the model prior to any comparison with observational datasets.

#### 4. WEYL CONFORMAL GEOMETRY

Under Weyl transformations  $g_{\mu\nu} \rightarrow \Omega^2(x)g_{\mu\nu}$ , the conformal gravity action is invariant if it is constructed from the Weyl tensor:

$$C_{\mu\nu\rho\lambda} = R_{\mu\nu\lambda\rho} - \frac{1}{2}(g_{\mu\lambda}R_{\nu\rho} - g_{\mu\rho}R_{\nu\lambda} - g_{\nu\lambda}R_{\mu\rho} + g_{\nu\rho}R_{\mu\lambda}) + \frac{R}{6}(g_{\mu\lambda}g_{\nu\rho} - g_{\mu\rho}g_{\nu\lambda}). \quad (70)$$

The action for Weyl conformal gravity coupled to quintom and matter fields is:

$$\mathcal{S} = \int d^4x \sqrt{-g} [\alpha C_{\mu\nu\rho\lambda} C^{\mu\nu\rho\lambda} + \Xi(\phi, \psi) + \mathcal{L}_m], \quad (71)$$

where  $\alpha$  is a constant. This is equivalent to an  $f(G)$  theory with  $f(G) = \frac{\alpha}{\kappa^2}G$ , where  $G$  is the Gauss-Bonnet invariant.

In the FLRW metric, for Weyl conformal gravity with  $f(G) = \frac{\alpha}{\kappa^2}G$ , we have  $f_R = 1$ ,  $f_G = \frac{\alpha}{\kappa^2}$ , and all derivatives  $\dot{f}_G = \ddot{f}_G = 0$ . The cosmological equations become:

$$\rho_{\text{eff}_{Weyl}} = \rho - \frac{1}{2}\dot{\phi}^2 + \frac{1}{2}\dot{\psi}^2 + V(\phi, \psi) + \frac{12\alpha}{\kappa^4}H^2(H^2 + \dot{H}), \quad (72)$$

$$p_{\text{eff}_{Weyl}} = p - \frac{1}{2}\dot{\phi}^2 + \frac{1}{2}\dot{\psi}^2 - V(\phi, \psi) - \frac{12\alpha}{\kappa^4}H^2(H^2 + \dot{H}). \quad (73)$$

The Friedmann equations are:

$$3H^2 = \kappa^2 \rho_{\text{eff}_{Weyl}}, \quad (74)$$

$$-2\dot{H} - 3H^2 = \kappa^2 p_{\text{eff}_{Weyl}}. \quad (75)$$

This demonstrates that Weyl cosmology is a special case of  $f(R, G, T)$  gravity with  $f(G) = \frac{\alpha}{\kappa^2}G$ . Also, these results demonstrate that the previous components  $\mathcal{W}_{00}$  and  $\mathcal{W}_{ii}$  from [44] and [45] are incorrect in this formulation, indicating the need for careful reevaluation of those results.

The energy conservation conditions are satisfied in this framework through specific constraints. Condition (48) governing matter-geometry coupling is automatically satisfied since  $f_T = 0$  in pure Weyl gravity. Condition (49) reduces to the constraint

$\dot{H}\ddot{H} + 6H\dot{H}^2 + 2H^2\ddot{H} + 11H^3\dot{H} = 0$  for  $f_G = \text{const.}$ , which admits de Sitter space ( $H = \text{constant}$ ) as a solution. The coasting universe scenario ( $\dot{H} + H^2 = 0$ ) also satisfies this constraint, making Weyl conformal gravity compatible with energy conservation requirements.

## 5. STABILITY ANALYSIS AND GHOST-FREE CONDITIONS

A crucial requirement for any modified gravity theory is the absence of pathological instabilities, particularly Ostrogradsky ghosts that typically plague higher-derivative theories. In this section, we establish the theoretical stability of our  $f(R, G, T)$ -quintom framework through Hamiltonian analysis, perturbation theory, and energy condition analysis.

### 5.1. Theoretical Stability Foundations

The stability analysis of our model proceeds along two complementary approaches: a rigorous Hamiltonian formulation that counts physical degrees of freedom and identifies constraints, and a cosmological perturbation analysis that examines stability during the bounce phase.

#### 5.1.1. Hamiltonian Structure and Degree of Freedom Counting

As detailed in Appendix D, we perform a complete 3+1 decomposition of the action (2) to determine the independent physical degrees of freedom. The key results are:

- **Canonical Structure:** The conjugate momenta for the metric and scalar fields reveal a well-defined phase space structure. For the spatial metric  $g_{ij}$ , the momentum receives contributions from both the Einstein-Hilbert sector and Gauss-Bonnet corrections, while the quintom fields follow standard canonical relations with appropriate signs for phantom and normal fields.
- **Constraint Analysis:** The theory possesses a complete set of primary and secondary constraints arising from diffeomorphism invariance, ensuring the elimination of unphysical degrees of freedom.

- **Physical Degrees of Freedom:** Using Dirac’s counting algorithm, we establish that the physical configuration space contains exactly 4 degrees of freedom: 2 tensor modes (transverse-traceless graviton polarizations) and 2 scalar modes (the quintom fields  $\phi$  and  $\psi$ ). This matches the expected count for a healthy scalar-tensor theory.

### 5.1.2. Ostrogradsky Instability Avoidance

The potential Ostrogradsky instability, characteristic of higher-derivative theories, is avoided through specific degeneracy conditions derived in Appendix D. The critical requirement is:

$$\det \begin{pmatrix} f_{RR} & f_{RG} \\ f_{GR} & f_{GG} \end{pmatrix} = 0, \quad (76)$$

which ensures the elimination of pathological higher-derivative modes. For the linear Gauss-Bonnet case ( $f_G = \text{const.}$ ), this condition is automatically satisfied since  $f_{GG} = f_{RG} = 0$ . More generally, the FLRW background symmetry provides additional protection by reducing the effective higher-derivative structure.

These theoretical foundations establish that our  $f(R, G, T)$ -quintom framework possesses the correct number of physical degrees of freedom and avoids Ostrogradsky instabilities, providing a solid basis for the subsequent perturbation analysis.

## 5.2. Perturbation Analysis and Numerical Stability Conditions

To establish the stability of our  $f(R, G, T)$ -quintom framework, we analyze both theoretical perturbation behavior and numerical stability conditions. We begin with scalar perturbations of the FLRW metric. Following the standard approach in modified gravity theories [46, 47], we consider the curvature perturbation as the primary dynamical variable, while the quintom fields contribute through their background evolution and potential terms.

The general linearly perturbed FLRW metric is given by (see Appendix E for details):

$$ds^2 = -(1 + 2\Phi) dt^2 + 2a \partial_i B dx^i dt + a^2 [(1 - 2\Psi) \delta_{ij} + 2 \partial_i \partial_j E] dx^i dx^j, \quad (77)$$

Working in the Newtonian gauge eliminates  $B$  and  $E$  potentials, simplifying the metric to:

$$ds^2 = -(1 + 2\Phi) dt^2 + a^2(1 - 2\Psi) \delta_{ij} dx^i dx^j. \quad (78)$$

In the context of  $f(R, G, T)$  gravity with matter coupling, the scalar perturbation dynamics are governed primarily by the geometric degrees of freedom. The quintom fields  $\phi$  and  $\psi$  influence the perturbation evolution through their background equation of state and the effective sound speed, but do not introduce additional dynamical scalar modes in the adiabatic perturbation analysis [46].

The quadratic action for the comoving curvature perturbation  $\zeta$  takes the form:

$$\delta^{(2)}S = \int dt d^3x a^3 \left[ \mathcal{G}_S \dot{\zeta}^2 - \mathcal{F}_S \frac{(\partial\zeta)^2}{a^2} \right], \quad (79)$$

with kinetic and gradient coefficients given by:

$$\mathcal{G}_S = \frac{1}{2\kappa^2} \left[ f_R + 12H^2 f_G + 8H \dot{f}_G + 4\ddot{f}_G - \frac{f_T(\rho + p)}{2H^2 + \epsilon} \right], \quad (80)$$

$$\mathcal{F}_S = \frac{1}{2\kappa^2} \left[ f_R + 4\ddot{f}_G + 8 \left( \frac{H^2 \dot{f}_G}{f_R} + \frac{(3H^3 + 2H\dot{H})\dot{f}_G}{f_R} - \frac{H^2 \dot{f}_G \dot{f}_R}{f_R^2} \right) \right]. \quad (81)$$

Here, the quintom sector contributes indirectly through:

- The background Hubble parameter  $H(t)$  which evolves according to the coupled quintom- $f(R, G, T)$  equations
- The effective equation of state  $\omega_{\text{eff}}$  that determines  $\rho + p$
- The regularization parameter  $\epsilon$  that ensures stability at the bounce point

Classical stability requires the absence of ghosts and gradient instabilities, imposing the conditions:

$$\mathcal{G}_S(t) > 0 \quad (\text{no ghosts}), \quad \mathcal{F}_S(t) > 0 \quad (\text{no gradient instabilities}). \quad (82)$$

The sound speed of scalar perturbations follows as:

$$c_s^2 = \frac{\mathcal{F}_S}{\mathcal{G}_S} = \frac{f_R + 4\ddot{f}_G + 8 \left( \frac{H^2 \dot{f}_G}{f_R} + \frac{(3H^3 + 2H\dot{H})\dot{f}_G}{f_R} - \frac{H^2 \dot{f}_G \dot{f}_R}{f_R^2} \right)}{f_R + 12H^2 f_G + 8H \dot{f}_G + 4\ddot{f}_G - \frac{f_T(\rho+p)}{2H^2 + \epsilon}} > 0. \quad (83)$$

The bounce point ( $H = 0$ ) presents a particularly stringent test for stability. At this point, the kinetic coefficient reduces to:

$$\mathcal{G}_S|_{H=0} = \frac{1}{2\kappa^2} \left[ f_R + 4\ddot{f}_G - \frac{f_T(\rho + p)}{\epsilon} \right]. \quad (84)$$

To avoid pathological divergence, models must satisfy:

$$\lim_{H \rightarrow 0} \frac{f_T(\rho + p)}{2H^2 + \epsilon} = \frac{f_T(\rho + p)}{\epsilon} = C \quad (\text{finite constant}), \quad \text{or ideally} \quad f_T(\rho + p) = 0 \quad \text{at} \quad H = 0. \quad (85)$$

For the gradient coefficient at bounce:

$$\mathcal{F}_S|_{H=0} = \frac{1}{2\kappa^2} \left[ f_R + 4\ddot{f}_G + \frac{8}{a^3} \frac{d}{dt} \left( \frac{a^3 H^2 \dot{f}_G}{f_R} \right) \Big|_{H=0} \right], \quad (86)$$

where the derivative term typically vanishes for smooth  $H(t)$  behavior near the bounce.

The Hamiltonian analysis establishes theoretical stability possibilities, but numerical verification remains essential. For each model in Section 6, we must verify dynamically that:

$$\mathcal{G}_S(t) > 0, \quad \mathcal{F}_S(t) > 0, \quad c_s^2(t) \geq 0 \quad \forall t, \quad (87)$$

with particular attention to the bounce region. Our chosen  $f(T)$  couplings (proportional to  $T \sim \rho$ , which remains finite at bounce) ensure the critical limit  $\lim_{H \rightarrow 0} f_T(\rho + p)/(2H^2 + \epsilon)$  remains well-defined and finite. The quintom fields contribute to this stability analysis through their role in determining the background evolution and the effective energy conditions. In the following section, we demonstrate not only successful bouncing behavior and PDL crossing but also explicitly verify these stability conditions numerically throughout the cosmic evolution.

### 5.3. Energy Conditions and PDL Crossing

The Null Energy Condition (NEC) violation required for phantom divide line (PDL) crossing is derived from the modified Friedmann equations. The complete expression for effective energy density and pressure, consistent with our perturbation analysis, reads:

$$\begin{aligned} \rho_{\text{eff}} + p_{\text{eff}} = \frac{1}{\kappa^2} \left[ -2\dot{H}(1 + f_R - 12H^2 f_G - 8H\dot{f}_G - 4\ddot{f}_G) \right. \\ \left. + \ddot{f}_R - H\dot{f}_R + 2f_T(\rho + p) \right] - \dot{\phi}^2 + \dot{\psi}^2 \end{aligned} \quad (88)$$

At the bounce point ( $H = 0$ ), this simplifies to:

$$\rho_{\text{eff}} + p_{\text{eff}}|_{H=0} = \frac{1}{\kappa^2} \left[ -2\dot{H}(1 + f_R - 4\ddot{f}_G) + \ddot{f}_R + 2f_T(\rho + p) \right] - \dot{\phi}^2 + \dot{\psi}^2 \quad (89)$$

The NEC violation ( $\rho_{\text{eff}} + p_{\text{eff}} < 0$ ) occurs when:

$$\dot{H} > \frac{\ddot{f}_R + 2f_T(\rho + p) - \kappa^2(\dot{\phi}^2 - \dot{\psi}^2)}{2(1 + f_R - 4\ddot{f}_G)} \quad (90)$$

This condition reveals three crucial physical mechanisms:

- The quintom sector ( $\dot{\phi}^2 - \dot{\psi}^2$ ) provides negative pressure when  $\dot{\phi}^2 > \dot{\psi}^2$ , essential for PDL crossing
- The  $f_R$  terms modify the effective Planck mass, while  $f_G$  terms ( $\ddot{f}_G$ ) enable bounce stabilization
- The matter-geometry coupling  $f_T$  introduces additional degrees of freedom for energy condition violation

The denominator  $1 + f_R - 4\ddot{f}_G$  must remain positive to avoid singularities. The PDL crossing occurs when the effective equation of state crosses  $\omega_{\text{eff}} = -1$ , which is achieved through the combined effects of the quintom fields and  $f(R, G, T)$  modifications. The Gauss-Bonnet terms ( $12H^2 f_G + 8H \dot{f}_G$ ) become particularly important away from the bounce point when  $H \neq 0$ .

The interplay between energy condition violation and stability requirements imposes important constraints on model parameters, which we explore numerically in the next section for each specific  $f(R, G, T)$  model.

## 6. DYNAMICS OF BOUNCING COSMOLOGICAL MODELS

This section investigates the dynamics and implications of various cosmological models, including the Linear [6], Exponential Function of Curvature [48], Power-Law [49], Modified Teleparallel Gravity [50], and Non-Minimal Coupling [51] models. Each of these models offers unique perspectives on the evolution of the universe, emphasizing the intricate relationship between gravitational interactions and cosmic expansion. By examining the scale factor,  $a(t)$ , and the Hubble parameter,  $H(t)$ , we evaluate the viability of these models within distinct cosmological frameworks. A comprehensive analysis of their bouncing scenarios across different cosmic epochs is crucial for reconstructing the history of the universe. This section aims to delineate the conditions under which these models operate effectively, thereby enhancing our understanding of both early and late-time cosmic behaviors.

This section also provides a numerical analysis of the early-time evolution of key cosmological parameters, including the equation of state parameter,  $\omega$ . In addition, we identify the essential factors that contribute to a successful cosmological bounce using simplified sample models, leaving more intricate models for future research. To elucidate the dynamics of the universe, it is crucial to examine the evolution of the Hubble parameter,  $H(t)$ , and the scale factor,  $a(t)$ , as functions of cosmic time,  $t$ . For a bounce to be viable, the following conditions must be satisfied:

- **Contraction for  $t < 0$ :** The scale factor  $a(t)$  should decrease, implying that  $\dot{a} < 0$ .
- **Bounce at  $t = 0$ :** At this point, when  $\dot{a} = 0$ , we require  $\ddot{a} > 0$  and the Hubble parameter  $H$  transitions from negative to positive, reaching zero at the bouncing point.
- **Expansion for  $t > 0$ :** The scale factor  $a(t)$  should increase, which indicates that  $\dot{a} > 0$ .

### 6.1. Initial Conditions and Physical Justification

The initial conditions for the dynamical variables  $\{a, \dot{a}, \phi, \dot{\phi}, \psi, \dot{\psi}\}$  are not arbitrary but are chosen to satisfy physical constraints of the bouncing universe scenario and to ensure numerical stability. The generic setup for all models is as follows:

- **Scale Factor at Bounce:** We set  $a(0) = 1$  by convention, defining the bounce point as the moment of minimum scale factor. This is a choice of units and does not affect the dynamics.
- **Hubble Parameter at Bounce:** We impose  $\dot{a}(0) = 0$  (and thus  $H(0) = 0$ ) as the fundamental defining condition of the bounce. This is the necessary kinematic condition for a transition from contraction ( $H < 0$ ) to expansion ( $H > 0$ ).
- **Quintom Field Values:** The initial field values  $\phi(0) = -0.05$  and  $\psi(0) = 0.05$  are chosen to be small but non-zero displacements from the origin of the potential  $V(\phi, \psi)$ . This breaks the symmetry of the system gently, allowing the fields to evolve

dynamically to drive the bounce. Their specific magnitudes are chosen to be sub-Planckian ( $|\phi|, |\psi| \ll m_{\text{Pl}}$ ) to remain within the regime of validity of the effective theory.

- **Field Velocities:** The initial velocities  $\dot{\phi}(0) = 0.1$  and  $\dot{\psi}(0) = -0.1$  are crucial. They are chosen to be equal in magnitude but opposite in sign. This ensures that the initial total kinetic energy of the quintom sector,  $\rho_{\text{kin}} = (-\dot{\phi}^2 + \dot{\psi}^2)/2$ , is initially zero or small. This prevents an unphysical, overly dominant initial kinetic energy from dictating the dynamics and allows the interplay between the potential energy and the  $f(R, G, T)$  modifications to generate the bounce. The chosen value of 0.1 (in Planck units) is small enough to avoid violent initial dynamics but large enough to initiate the field roll.

These conditions collectively define a universe at the moment of its bounce, with nearly vanishing Hubble parameter and small, dynamical scalar fields poised to initiate the expansion phase. The specific numerical values ( $\pm 0.05, \pm 0.1$ ) are chosen for numerical convenience to produce clear graphical results within a manageable computational time, but the qualitative bouncing behavior is robust across a range of similar small initial values. The parameters of the potentials ( $V_0, \alpha, \beta, g$ ) are then tuned for each model to ensure that the Null Energy Condition (NEC) is violated dynamically  $\rho + p < 0$  near  $t = 0$ , facilitating a successful bounce under these initial conditions.

## 6.2. Reconstruction of $f(R, G, T)$ Models

The field equations are complex due to their multivariate functions and derivatives. Reconstruction simplifies our investigation of the model's dynamics. For the matter-radiation sector, we consider a perfect fluid with barotropic equation of state  $p = \omega\rho$ , where  $\omega$  parameterizes different cosmological eras. Utilizing conservation equation (22), we derive the expression for the energy density, which takes the form  $\rho = \rho_0 a^{-3(1+\omega)}$ .

However, it is crucial to emphasize that the *effective* equation of state  $\omega_{\text{eff}}$ , which governs the actual cosmic evolution in our  $f(R, G, T)$ -quintom framework, is highly dynamic and exhibits the novel double phantom divide line crossing characteristic of our model. The parameter  $\omega$  here serves only to initialize the matter-radiation component, while the full

dynamics emerge from the interplay between geometry, matter coupling, and quintom fields.

Here,  $\rho_0$  denotes a positive constant, and  $a$  represents the scale factor of the Universe. In the numerical solutions, we assume  $G_r = 1$ ,  $c = 1$ ,  $\kappa^2 = 1/m_p^2 = 8\pi$ , and  $\rho_0 = 1$ . The following graphs compare different initial matter configurations: dark energy-like ( $\omega = -1$ , black lines), curvature-dominated ( $\omega = -1/3$ , red lines) and radiation-dominated ( $\omega = 1/3$ , blue lines) initial conditions.

In the following reconstructions, we examine five distinct  $f(R, G, T)$  models. For each model, we present numerical solutions for a specific equation of state parameter  $\omega$  that best illustrates its unique characteristics: the linear and exponential models are shown with  $\omega = -1$  to highlight their dark energy behavior; the power-law and teleparallel models use  $\omega = -1$  to showcase their complex equation of state dynamics; and the non-minimal coupling model uses  $\omega = 1/3$  to demonstrate its particular efficacy in radiation-dominated regimes. This selective presentation is for clarity and emphasis—each model exhibits viable bouncing behavior across a range of  $\omega$  values unless otherwise noted.

The model parameters ( $\xi_i$ ,  $V_0$ ,  $\alpha$ , etc.) for each subsequent example are chosen to meet several physical criteria: (i) to ensure modifications remain perturbative ( $|\xi_i R| \lesssim |R|$ , etc.) outside the Planckian regime, (ii) to provide sufficient energy in the quintom fields to trigger the NEC violation required for the bounce, and (iii) to ensure numerical stability during integration. While not a full parameter space scan, the presented choices demonstrate the existence of stable, non-singular bouncing solutions within this theoretical framework.

The initial conditions for the dynamical variables are set according to the general prescription outlined in Sec. 6.1, ensuring a physically motivated starting point at the bounce epoch.

### 6.2.1. Linear Coupling Model

The linear model provides the simplest non-trivial case for studying  $f(R, G, T)$  gravity, characterized by constant coupling coefficients:

$$f(R, G, T) = \xi_1 R + \xi_2 G + \xi_3 T \tag{91}$$

where  $\xi_1$ ,  $\xi_2$ , and  $\xi_3$  are dimensionless coupling constants. The modified Friedmann equations take the simplified form:

$$3H^2 = \frac{1}{3\xi_1} \left[ \kappa^2(\rho + \rho_\Xi) + \frac{\xi_3}{2}(3\rho - p) \right] \quad (92)$$

$$-2\dot{H} - 3H^2 = \frac{1}{3\xi_1} \left[ \kappa^2(p + p_\Xi) + \frac{\xi_3}{2}(3p - \rho) \right] \quad (93)$$

where  $\rho_\Xi = -\frac{1}{2}\dot{\phi}^2 + \frac{1}{2}\dot{\psi}^2 + V(\phi, \psi)$  and  $p_\Xi = -\frac{1}{2}\dot{\phi}^2 + \frac{1}{2}\dot{\psi}^2 - V(\phi, \psi)$ .

This model exhibits several important features. First, the prefactor  $1/(3\xi_1)$  rescales the gravitational coupling, with  $\xi_1 = 1$  recovering the standard gravitational constant up to a factor of 3. The  $\xi_3$  terms introduce novel matter-dependent contributions to both the energy density and pressure. Notably, the Gauss-Bonnet coupling  $\xi_2$  completely disappears from the dynamics because all terms involving  $\xi_2$  cancel out exactly when  $f_G = \xi_2$  is constant.

The effective energy density and pressure become:

$$\rho_{\text{eff}} = \frac{1}{3\xi_1} \left[ \rho + \rho_\Xi + \frac{\xi_3}{2\kappa^2}(3\rho - p) \right], \quad p_{\text{eff}} = \frac{1}{3\xi_1} \left[ p + p_\Xi + \frac{\xi_3}{2\kappa^2}(3p - \rho) \right] \quad (94)$$

For energy conditions, the Null Energy Condition (NEC) becomes:

$$\begin{aligned} \rho_{\text{eff}} + p_{\text{eff}} &= \frac{1}{3\xi_1} \left[ (\rho + p) + (-\dot{\phi}^2 + \dot{\psi}^2) + \frac{\xi_3}{\kappa^2}(\rho + p) \right] \\ &= \frac{1}{3\xi_1} \left[ \left( 1 + \frac{\xi_3}{\kappa^2} \right) (\rho + p) - \dot{\phi}^2 + \dot{\psi}^2 \right] \end{aligned} \quad (95)$$

Several special cases are worth noting. The General Relativity limit is recovered when  $\xi_1 = 1$  and  $\xi_2 = \xi_3 = 0$ . For quantum gravity scale effects, one might consider  $\xi_1 \sim \mathcal{O}(1)$  with  $\xi_2, \xi_3 \sim \ell_{\text{Pl}}^2$  introducing Planck-scale corrections. At the bounce point ( $H = 0$ ), NEC violation requires:

$$\left( 1 + \frac{\xi_3}{\kappa^2} \right) (\rho + p) < \dot{\phi}^2 - \dot{\psi}^2 \quad (96)$$

showing how the matter-geometry coupling  $\xi_3$  must balance against the quintom fields' kinetic energy to enable the bounce.

The linear coupling model demonstrates that even the simplest extension of General Relativity with constant couplings can produce non-trivial modifications to cosmological dynamics, particularly through the matter-geometry coupling parameter  $\xi_3$ , while the Gauss-Bonnet term remains inert in the homogeneous background evolution.

The cosmological dynamics reveal distinct behaviors across different equations of state. While the linear coupling can generate a bounce for various  $\omega$ , the dark energy regime ( $-1 \leq$

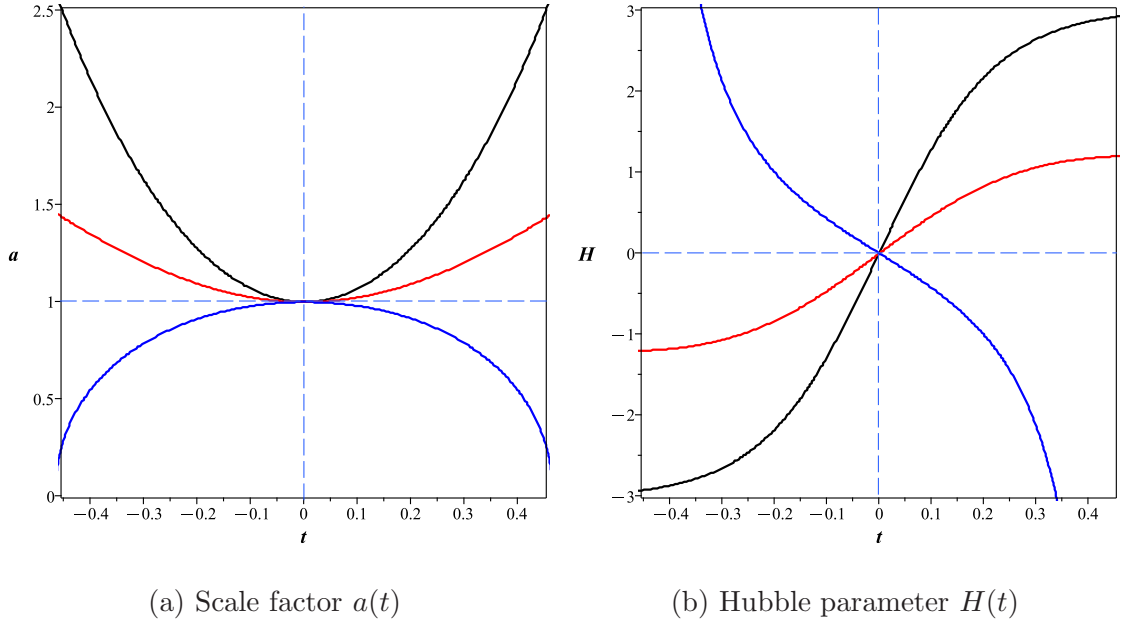


FIG. 1: Evolution of (a) scale factor  $a(t)$  and (b) Hubble parameter  $H(t)$  for different equations of state ( $\omega = -1$ : black,  $-1/3$ : red,  $1/3$ : blue) in the linear coupling model. A successful bounce, characterized by  $a(t)$  reaching a minimum and  $H(t)$  crossing zero, is evident for the dark energy cases ( $\omega \leq -1/3$ ).

$\omega \leq -\frac{1}{3}$ ) provides the most phenomenologically interesting scenario, naturally connecting the early-time bounce to late-time acceleration. Figure 1 for  $\omega = -1$  shows the scale factor  $a(t)$  reaching a minimum at the bounce point ( $t = 0$ ), demonstrating a smooth, singularity-free transition from contraction ( $H < 0$ ) to expansion ( $H > 0$ ). This behavior characterizes a successful Big Bounce scenario supported by the sign change in the Hubble parameter  $H(t)$  at the bounce. This behavior characterizes a successful Big Bounce scenario supported by the sign change in the Hubble parameter  $H(t)$  at the bounce.

In contrast, the radiation-dominated era ( $\omega = \frac{1}{3}$ ) exhibits inverted behavior with  $a(t)$  showing a maximum at  $t = 0$ , while  $H(t)$  still changes sign but reflects the decelerating expansion typical of radiation domination. This suggests fundamentally different dynamics between the dark energy-driven bounce phase and subsequent radiation-dominated expansion.

The effective equation of state (Fig. 2 and 3) shows phantom divide line (PDL) crossing ( $\omega_{\text{eff}} = -1$ ) in the dark energy regime ( $-1 \leq \omega \leq -\frac{1}{3}$ ), with transitions between phantom ( $\omega_{\text{eff}} < -1$ ) and quintessence ( $\omega_{\text{eff}} > -1$ ) states. Specifically, Fig. 2a shows PDL crossing

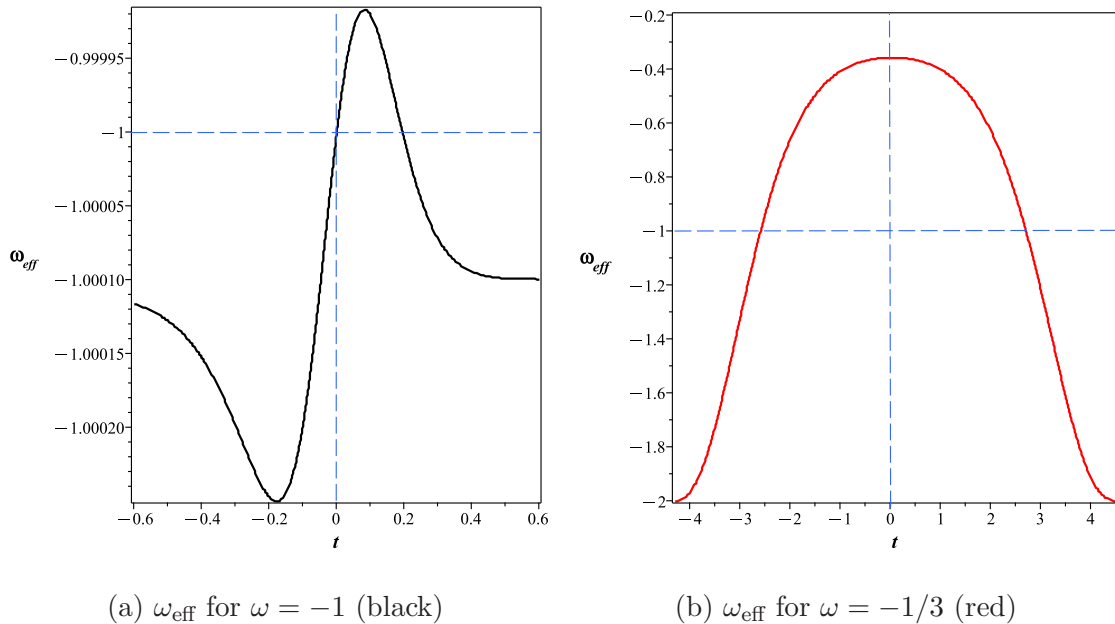


FIG. 2: Effective equation of state  $\omega_{\text{eff}}(t)$  showing (a) evolution for  $\omega = -1$  (black line) and (b) evolution for  $\omega = -1/3$  (red line). The phantom divide line (PDL) at  $\omega_{\text{eff}} = -1$  is shown as a dashed line. Both cases show PDL crossing behavior near the bounce point.

for  $\omega = -1$  (black line), while Fig. 2b shows similar behavior for  $\omega = -1/3$  (red line). In contrast, the radiation-dominated era ( $\omega = \frac{1}{3}$ ) shown in Fig. 3a exhibits no PDL crossing, with  $\omega_{\text{eff}}$  remaining firmly in the quintessence region ( $\omega_{\text{eff}} > -1$ ), consistent with standard cosmology. The comparative view in Fig. 3b clearly demonstrates these different behaviors.

These results demonstrate that: (1) successful bouncing cosmology requires dark energy domination ( $\omega \leq -1/3$ ), (2) the phantom divide crossing is characteristic of the bounce phase but absent in radiation domination, and (3) the transition between these regimes marks a fundamental change in the universe's dynamical behavior. The model naturally accommodates both non-singular bouncing behavior and subsequent standard cosmological evolution.

**Stability Verification:** Using the established parameters and initial conditions, we numerically verify the stability criteria throughout the cosmic evolution. Figure 4 shows the evolution of the kinetic term  $\mathcal{G}_S$ , the squared sound speed  $c_s^2$ , and the Null Energy Condition (NEC) violation  $\rho_{\text{eff}} + p_{\text{eff}}$  for the  $\omega = -1$  case.

The numerical results confirm that  $\mathcal{G}_S(t) > 0$  for all  $t$ , ensuring the absence of ghost instabilities. The sound speed squared  $c_s^2(t)$  remains non-negative throughout the evolu-

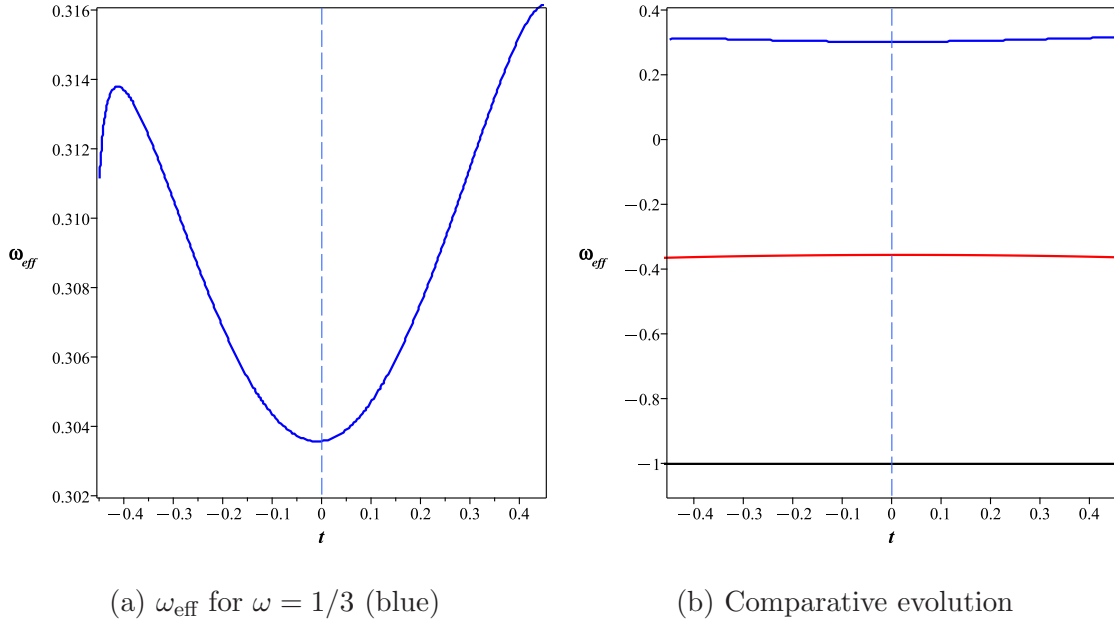


FIG. 3: (a) Effective equation of state  $\omega_{\text{eff}}(t)$  for  $\omega = 1/3$  (blue line) and (b) composite view comparing all cases:  $\omega = -1$  (black),  $\omega = -1/3$  (red), and  $\omega = 1/3$  (blue). The radiation-dominated case ( $\omega = 1/3$ ) shows no PDL crossing, remaining in the quintessence regime throughout.

tion, with  $c_s^2 \geq 0$  and finite, confirming the absence of gradient instabilities. The condition  $\lim_{H \rightarrow 0} f_T(\rho + p)/H^2$  remains well-behaved at the bounce point ( $t = 0$ ), with no pathological divergence. This model satisfies all stability criteria while successfully producing the bouncing behavior and PDL crossing shown in Figures 1–3.

The cosmological dynamics in Fig. 1–4 were simulated using the following parameters, chosen to clearly illustrate the bounce and PDL crossing phenomena:  $V(\phi, \psi) = V_0 e^{-(\alpha\phi + \beta\psi)}$ ,  $V_0 = 0.25$ ,  $\alpha = 2$ ,  $\beta = 1$ , and  $\xi_1 = \xi_2 = \xi_3 = 1$ . The initial values were  $\phi(0) = -0.05$ ,  $\dot{\phi}(0) = 0.1$ ,  $\psi(0) = 0.05$ ,  $\dot{\psi}(0) = -0.1$ ,  $a(0) = 1$ , and  $\dot{a}(0) = 0$ .

### 6.2.2. Exponential Function of Curvature

We consider an exponential  $f(R, G, T)$  gravity model that generalizes the  $\Lambda$ CDM framework:

$$f(R, G, T) = R - 2\Lambda e^{-(R_0/R)^n} + \xi_2 G + \xi_3 T \quad (97)$$

where  $\Lambda = R_0/b$  represents the cosmological constant scale,  $n$  controls the transition rate, and  $\xi_2, \xi_3$  are coupling constants. As shown in Appendix F, the modified Friedmann equa-

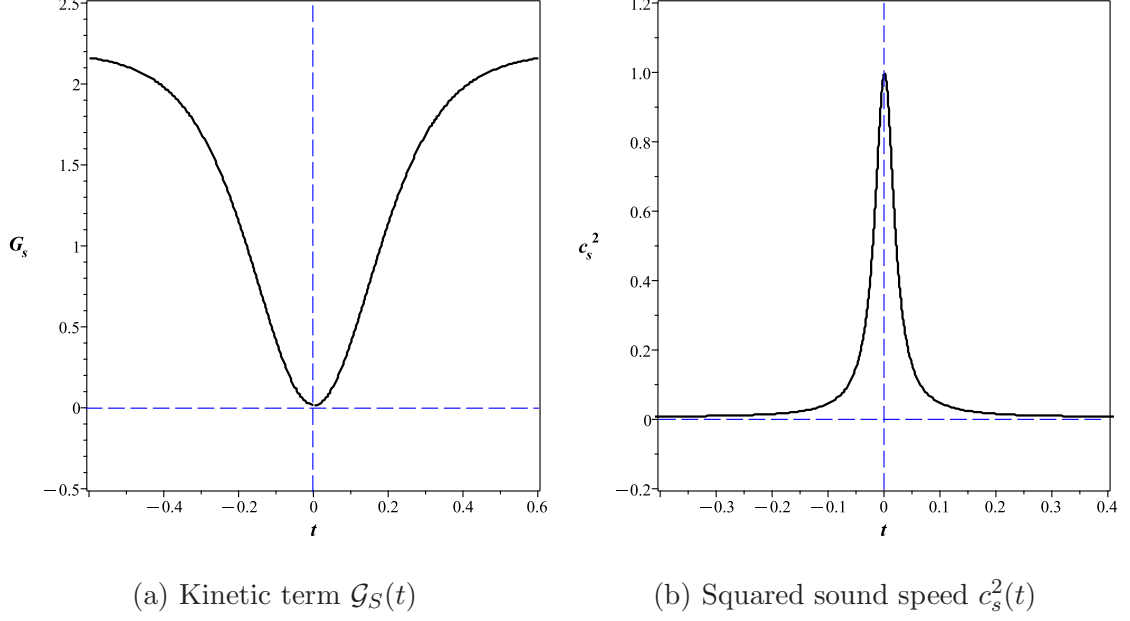


FIG. 4: Stability analysis for the linear coupling model ( $\omega = -1$ ). (a) The kinetic term remains positive  $\mathcal{G}_S > 0$  throughout the evolution, confirming the absence of ghosts. (b) The squared sound speed  $c_s^2$  remains non-negative, indicating no gradient instabilities. The brief period where  $c_s^2 = 0$  at  $t \approx \pm 0.25$  corresponds to a momentary freezing of perturbations rather than an instability.

tions become:

$$3H^2 = \frac{1}{f_R} \left[ \kappa^2(\rho + \rho_\Xi) + \frac{\xi_3}{2}(3\rho - p) - 3H\dot{f}_R + 3\dot{H}(f_R - 1) - 6H^2 + \Lambda e^{-u} \right] \quad (98)$$

$$-2\dot{H} - 3H^2 = \frac{1}{f_R} \left[ \kappa^2(p + p_\Xi) + \frac{\xi_3}{2}(3p - \rho) + 2H\dot{f}_R + \dot{H}f_R + \ddot{f}_R + 3(\dot{H} + 2H^2) - \Lambda e^{-u} \right] \quad (99)$$

where

$$u = \left( \frac{R_0}{R} \right)^n, \quad (100)$$

$$f_R = 1 - 2n\Lambda u e^{-u}, \quad (101)$$

$$\dot{f}_R = -2n\Lambda u e^{-u} \left[ \frac{n}{R}u - \frac{n+1}{R} \right] \dot{R}, \quad (102)$$

$$\ddot{f}_R = 2n^2\Lambda u e^{-u} \left[ (1-u) \left( \frac{\ddot{R}}{R} - (n+1)\frac{\dot{R}^2}{R^2} \right) + nu\frac{\dot{R}^2}{R^2}(2-u) \right]. \quad (103)$$

The effective energy density and pressure become:

$$\rho_{\text{eff}} = \frac{1}{f_R} \left[ \rho + \rho_{\Xi} + \frac{\xi_3}{2\kappa^2}(3\rho - p) + \frac{1}{\kappa^2} \left( -3H\dot{f}_R + 3\dot{H}(f_R - 1) - 6H^2 + \Lambda e^{-(R_0/R)^n} \right) \right] \quad (104)$$

$$p_{\text{eff}} = \frac{1}{f_R} \left[ p + p_{\Xi} + \frac{\xi_3}{2\kappa^2}(3p - \rho) + \frac{1}{\kappa^2} \left( \ddot{f}_R + 2H\dot{f}_R + \dot{H}f_R + 3(\dot{H} + 2H^2) - \Lambda e^{-(R_0/R)^n} \right) \right] \quad (105)$$

For energy conditions, the Null Energy Condition (NEC) becomes:

$$\rho_{\text{eff}} + p_{\text{eff}} = \frac{1}{f_R} \left[ (\rho + p) \left( 1 + \frac{\xi_3}{\kappa^2} \right) + (\rho_{\Xi} + p_{\Xi}) + \frac{1}{\kappa^2} \left( \ddot{f}_R - H\dot{f}_R + 4\dot{H}f_R \right) \right] \quad (106)$$

Several special cases are worth noting. The  $\Lambda$ CDM limit is recovered when  $n \rightarrow \infty$ ,  $\xi_2 = 0$ , and  $\xi_3 = 0$ . For quantum gravity scale effects, one might consider  $\xi_2, \xi_3 \sim \ell_{\text{Pl}}^2$  introducing Planck-scale corrections. At the bounce point ( $H = 0$ ), NEC violation requires:

$$(\rho + p) \left( 1 + \frac{\xi_3}{\kappa^2} \right) + (\rho_{\Xi} + p_{\Xi}) + \frac{1}{\kappa^2} \left( \ddot{f}_R + 4\dot{H}f_R \right) < 0 \quad (107)$$

This model exhibits several distinctive features:

- The exponential factor  $e^{-(R_0/R)^n}$  provides a smooth transition between different curvature regimes
- When  $R \ll R_0$ , the exponential term approaches 1, recovering the  $\Lambda$ CDM limit
- When  $R \gg R_0$ , the exponential term suppresses the cosmological constant contribution
- The Gauss-Bonnet terms cancel exactly in the final simplified equations
- The matter-geometry coupling  $\xi_3$  introduces additional pressure terms
- The NEC condition shows explicit dependence on both the exponential curvature term and matter coupling

The exponential model demonstrates viable bouncing behavior for all considered equations of state. We highlight the  $\omega = -1$  case as it represents a pure dark energy component, providing the cleanest example of the model's bounce mechanics without the complicating effects of matter or radiation dynamics. Figure 5 for this case shows the scale factor  $a(t)$

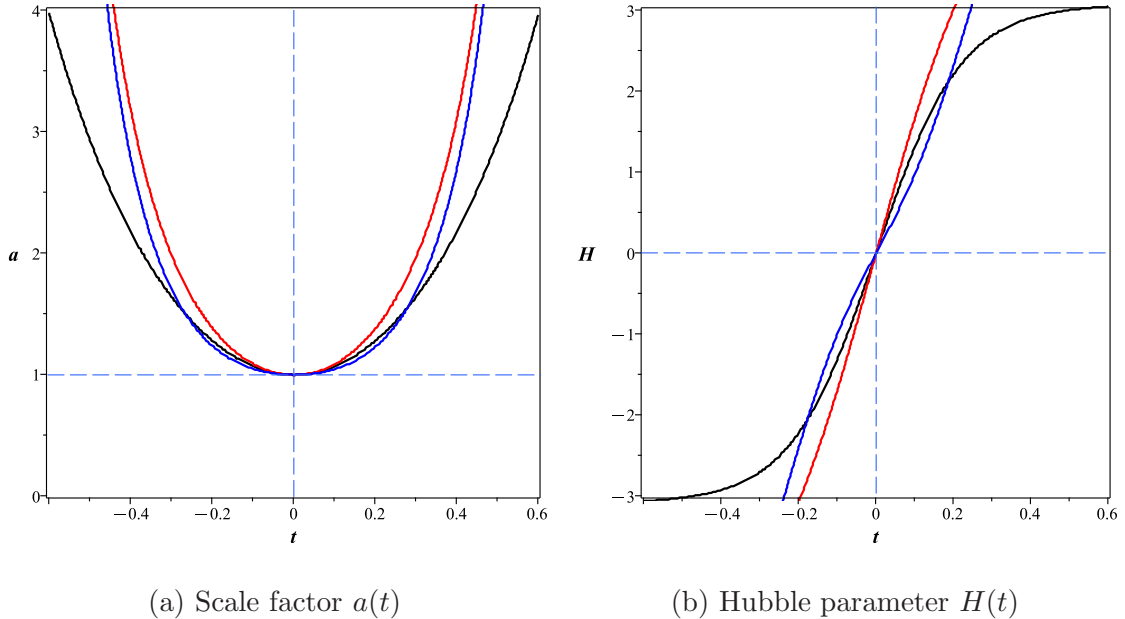


FIG. 5: Evolution of (a) scale factor  $a(t)$  and (b) Hubble parameter  $H(t)$  for different equations of state ( $\omega = -1$ : black,  $-1/3$ : red,  $1/3$ : blue). The  $\omega = -1$  case shows optimal bounce behavior with a clear minimum in  $a(t)$  and smooth transition of  $H(t)$  through zero.

reaching a minimum at  $t = 0$  while  $H(t)$  smoothly transitions from negative to positive values.

The equation of state evolution (Fig. 6 and 7) reveals:

- For  $\omega = -1$ :  $\omega_{\text{eff}}$  touches  $-1$  at  $t = 0$  and remains phantom ( $\leq -1$ )
- For  $\omega = -1/3, 1/3$ : Double PDL crossing near  $t = 0$  (phantom  $\rightarrow$  quintessence  $\rightarrow$  phantom)
- All cases asymptote to quintessence ( $> -1$ ) for  $|t| > 0.2$
- Finite-time singularities of Type II or IV appear at  $t \approx \pm 0.2$ , indicating a breakdown of the effective field theory at these energy scales, a common feature in many bouncing models [17]. Our analysis focuses on the robust bouncing behavior near  $t = 0$ , which is free of such pathologies.

**Stability Verification:** The exponential model's stability is verified numerically. Figure 8 shows the stability indicators for the  $\omega = -1$  case.

The exponential model satisfies  $\mathcal{G}_S(t) > 0$  for all  $t$ , avoiding ghost pathologies. The sound speed remains real with  $c_s^2(t) \geq 0$ , ensuring gradient stability. The finite-time singularities

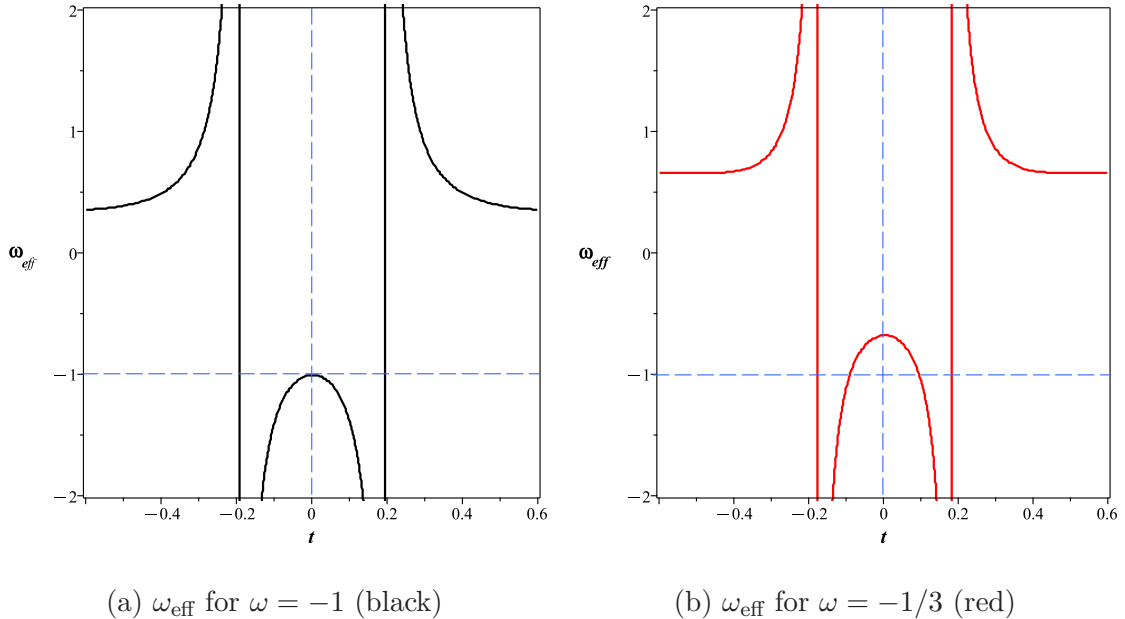


FIG. 6: Effective equation of state  $\omega_{\text{eff}}(t)$  showing (a) evolution for  $\omega = -1$  (black line) and (b) evolution for  $\omega = -1/3$  (red line). The phantom divide line (PDL) at  $\omega_{\text{eff}} = -1$  is shown as a dashed line. Both cases show PDL crossing behavior near the bounce point.

at  $t \approx \pm 0.2$  do not destabilize the core bounce region around  $t = 0$ , where both stability conditions are maintained.

The model parameters ( $V_0 = 2.5$ ,  $b = 1$ ,  $n = 2$ ,  $\alpha = 1$ ,  $g = 0.1$ ,  $\xi_2 = \xi_3 = 1$ ) were chosen to satisfy energy conservation while generating viable bounce dynamics. The potential  $V(\phi, \psi) = V_0 e^{-\alpha\phi} + \frac{1}{2} m_p^2 \psi^2 + g\phi\psi$  enables these phase transitions.

### 6.2.3. Power-Law Modified Gravity

The power-law model represents a phenomenologically rich extension of GR that incorporates non-linear curvature-matter couplings:

$$f(R, G, T) = R + \xi_1 R^n + \xi_2 G + \xi_3 T^m \quad (108)$$

where the exponents  $n, m \geq 2$  introduce non-perturbative corrections to Einstein gravity.

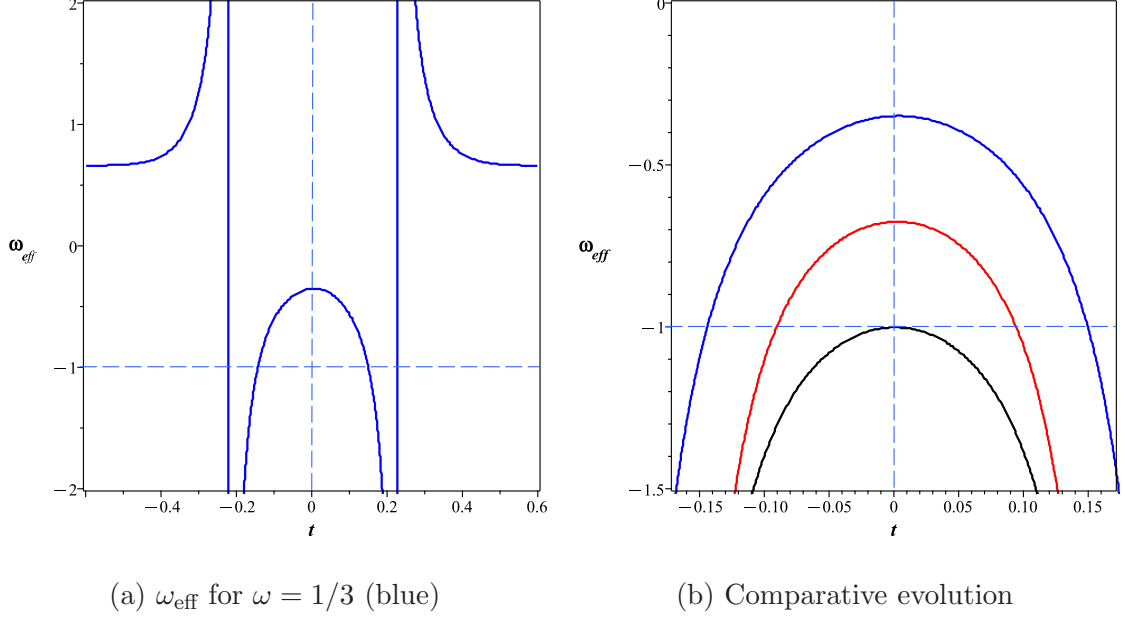


FIG. 7: (a) Effective equation of state  $\omega_{\text{eff}}(t)$  for  $\omega = 1/3$  (blue line) and (b) composite view comparing all cases:  $\omega = -1$  (black),  $\omega = -1/3$  (red), and  $\omega = 1/3$  (blue). All cases cross the phantom divide line ( $\omega_{\text{eff}} = -1$ ) near the bounce point.

The partial derivatives are:

$$f_R = 1 + n\xi_1 R^{n-1}, \quad f_G = \xi_2, \quad f_T = m\xi_3 T^{m-1} \quad (109)$$

$$\dot{f}_R = n(n-1)\xi_1 R^{n-2} \dot{R}, \quad \ddot{f}_R = n(n-1)\xi_1 R^{n-3} [(n-2)\dot{R}^2 + R\ddot{R}] \quad (110)$$

$$\dot{f}_G = 0, \quad \ddot{f}_G = 0 \quad (111)$$

Substituting into the general Friedmann equations and simplifying, we obtain:

$$3H^2 = \frac{1}{1 + n\xi_1 R^{n-1}} \left[ \underbrace{\kappa^2(\rho + \rho_\Xi)}_{\text{Standard matter terms}} + \underbrace{3n\xi_1 R^{n-1} \dot{H}}_{\text{Curvature-driven inertia}} + \underbrace{3n(n-1)\xi_1 R^{n-2} \dot{R}H}_{\text{Dynamic curvature evolution}} \right. \\ \left. - \frac{1}{2} \underbrace{(R + \xi_1 R^n + \xi_3 T^m)}_{\text{Effective dark energy}} + \underbrace{m\xi_3 T^{m-1}(\rho + p)}_{\text{Non-linear matter coupling}} \right] \quad (112)$$

$$-2\dot{H} - 3H^2 = \frac{1}{1 + n\xi_1 R^{n-1}} \left[ \underbrace{\kappa^2(p + p_\Xi)}_{\text{Standard pressure terms}} + \underbrace{n\xi_1 R^{n-1} \dot{H}}_{\text{Curvature pressure}} + \underbrace{2n(n-1)\xi_1 R^{n-2} \dot{R}H}_{\text{Dynamic curvature coupling}} \right. \\ \left. + \underbrace{n(n-1)\xi_1 R^{n-2} [(n-2)\dot{R}^2 + R\ddot{R}]}_{\text{Curvature acceleration}} + \underbrace{\frac{1}{2}(R + \xi_1 R^n + \xi_3 T^m)}_{\text{Geometric stiff matter}} \right] \quad (113)$$

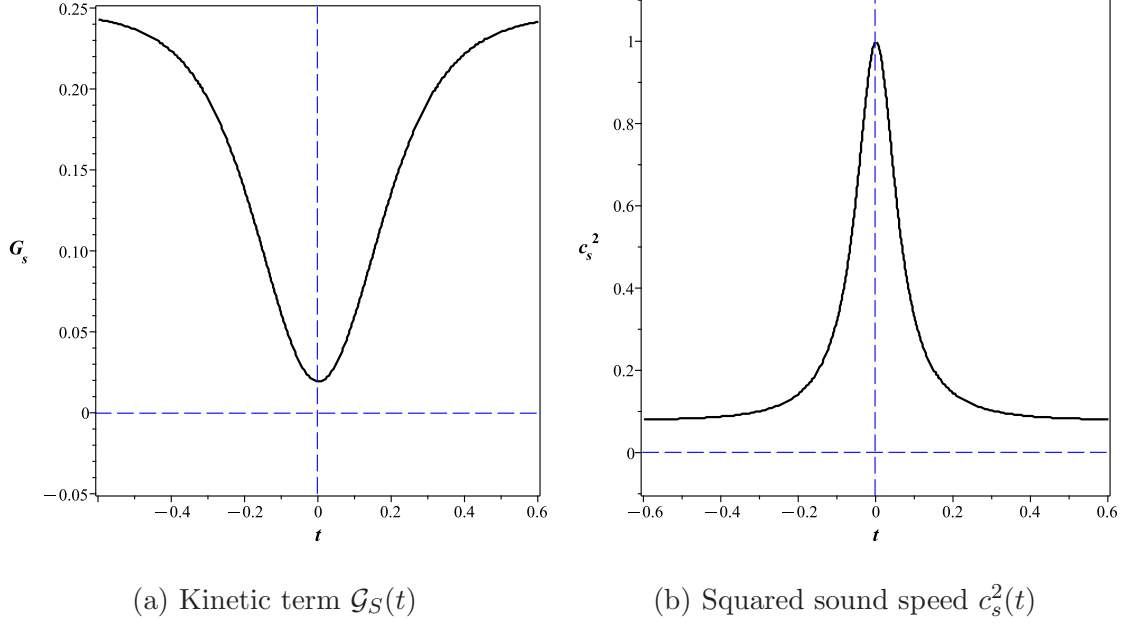


FIG. 8: Stability analysis for the exponential model ( $\omega = -1$ ). (a) The kinetic term  $\mathcal{G}_S$  remains positive definite, confirming no ghost instabilities. (b) The sound speed squared  $c_s^2$  remains non-negative throughout the evolution, with  $c_s^2 > 0$  except at discrete points where  $c_s^2 = 0$  (momentary perturbation freezing). The model maintains gradient stability.

The effective energy density and pressure become:

$$\rho_{\text{eff}} = \frac{1}{1 + n\xi_1 R^{n-1}} \left[ \rho + \rho_{\Xi} + \frac{3n\xi_1 R^{n-1} \dot{H}}{\kappa^2} + \frac{3n(n-1)\xi_1 R^{n-2} \dot{R}H}{\kappa^2} - \frac{R + \xi_1 R^n + \xi_3 T^m}{2\kappa^2} + \frac{m\xi_3 T^{m-1}(\rho + p)}{\kappa^2} \right] \quad (114)$$

$$p_{\text{eff}} = \frac{1}{1 + n\xi_1 R^{n-1}} \left[ p + p_{\Xi} + \frac{n\xi_1 R^{n-1} \dot{H}}{\kappa^2} + \frac{2n(n-1)\xi_1 R^{n-2} \dot{R}H}{\kappa^2} + \frac{n(n-1)\xi_1 R^{n-2} [(n-2)\dot{R}^2 + R\ddot{R}]}{\kappa^2} + \frac{R + \xi_1 R^n + \xi_3 T^m}{2\kappa^2} \right] \quad (115)$$

For energy conditions, the Null Energy Condition (NEC) becomes:

$$\rho_{\text{eff}} + p_{\text{eff}} = \frac{1}{1 + n\xi_1 R^{n-1}} \left\{ \left[ 1 + \frac{m\xi_3 T^{m-1}}{\kappa^2} \right] (\rho + p) + (\rho_{\Xi} + p_{\Xi}) + \frac{n\xi_1 R^{n-1}}{\kappa^2} \left[ 4\dot{H} + 5(n-1)\frac{\dot{R}}{R}H + (n-1) \left[ (n-2)\frac{\dot{R}^2}{R} + \ddot{R} \right] \right] \right\} \quad (116)$$

At the bounce point ( $H = 0$ ), the NEC violation condition simplifies to:

$$\left(1 + \frac{m\xi_3 T^{m-1}}{\kappa^2}\right) (\rho + p) + \frac{6n\xi_1}{\kappa^2} (6\dot{H})^{n-2} [4\dot{H}^2 + 6(n-1)(n-2)\ddot{H}^2 + 12(n-1)\dot{H}^3 + 6(n-1)\dot{H}\ddot{H}] < \dot{\phi}^2 - \dot{\psi}^2 \quad (117)$$

This model exhibits several distinctive features:

- The power-law terms  $R^n$  and  $T^m$  introduce strong non-linearities that dominate at high curvatures and energy densities
- The  $R^n$  term provides curvature-driven anti-friction that can counteract gravitational collapse
- The  $T^m$  term creates novel matter-geometry interactions that scale non-linearly with energy density
- As with the exponential curvature model discussed previously, the Gauss-Bonnet terms exhibit exact cancellation in the final simplified field equations.
- The NEC condition shows explicit dependence on both curvature and matter power-law terms
- At the bounce point, multiple curvature and matter terms contribute to the NEC violation condition

The General Relativity limit is recovered when  $\xi_1 = \xi_2 = \xi_3 = 0$ . For strong gravity effects, the parameters  $\xi_1, \xi_2, \xi_3$  can be chosen to introduce Planck-scale corrections that become significant near the bounce point.

The bounce dynamics in Figure 9 emerge from an intricate balance between:

- **Curvature-driven anti-friction:** The  $R^n$  terms dominate near the bounce point ( $t = 0$ ), creating an effective negative pressure that counteracts gravitational collapse. For  $n = 2$ , this behaves as:

$$P_{\text{eff}} \approx -\frac{\xi_1}{2} R^2 \sim -\xi_1 (36\dot{H}^2 + 144H^2\dot{H} + 144H^4) \quad (118)$$

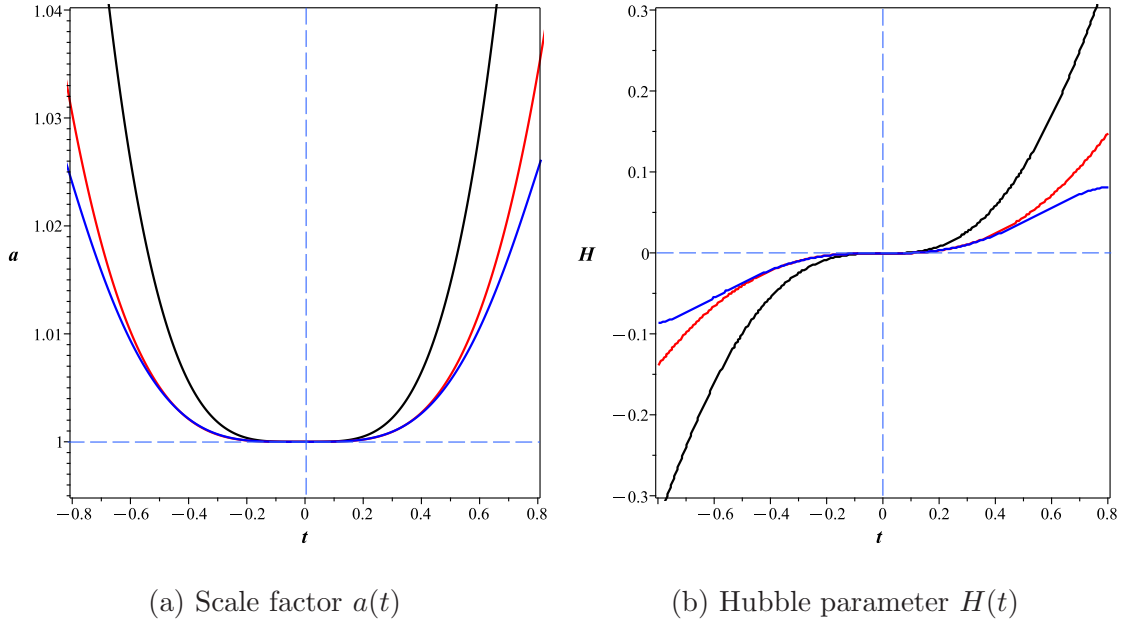


FIG. 9: Evolution of (a) scale factor  $a(t)$  and (b) Hubble parameter  $H(t)$  for different equations of state ( $\omega = -1$ : black,  $-1/3$ : red,  $1/3$ : blue). All cases show successful bounce behavior with  $a(t)$  reaching minimum and  $H(t)$  crossing zero at  $t = 0$ .

- **Non-linear matter effects:** The  $T^m$  coupling introduces an effective matter-curvature interaction energy density:

$$\rho_{\text{int}} \sim m\xi_3 T^{m-1}(\rho + p) \quad (119)$$

which becomes significant at high densities.

- **Quintom field dynamics:** The potential  $V(\phi, \psi) = \frac{1}{2}m_p(\phi^2 + \psi^2) - \frac{1}{3}\phi^2\psi$  provides a phase transition mechanism between phantom and quintessence regimes.

The EoS evolution in Figures 10-12 reveals profound thermodynamics:

- **Phantom regime** ( $\omega_{\text{eff}} < -1$ ): Corresponds to violation of the Null Energy Condition (NEC):

$$\rho + p + \frac{3n\xi_1 R^{n-1} \dot{H} - m\xi_3 T^{m-1}(\rho + p)}{1 + n\xi_1 R^{n-1}} < 0 \quad (120)$$

enabled by the phantom field's negative kinetic energy.

- **Bounce thermodynamics:** At  $t = 0$ , the system reaches maximal entropy density  $s_{\text{max}}$ , with EoS  $\omega_{\text{eff}} = 0$  indicating pressureless matter dominance during the bounce transition.

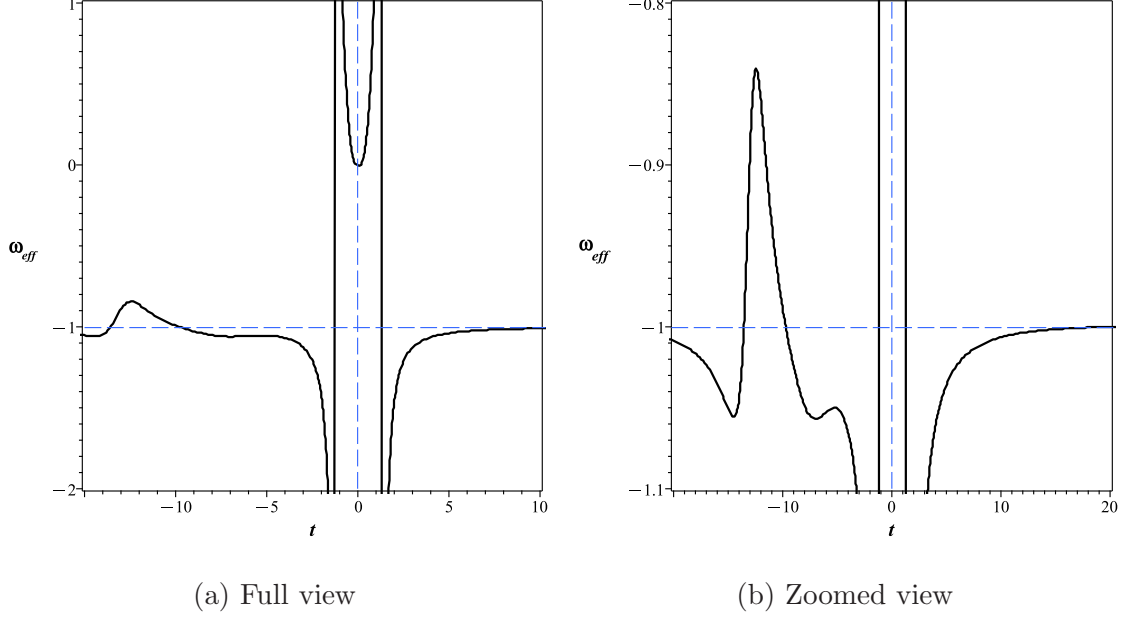


FIG. 10: Effective equation of state  $\omega_{\text{eff}}(t)$  for  $\omega = -1$  (black line) showing (a) full evolution and (b) detailed view near bounce point. The PDL ( $\omega_{\text{eff}} = -1$ ) is shown as dashed line.

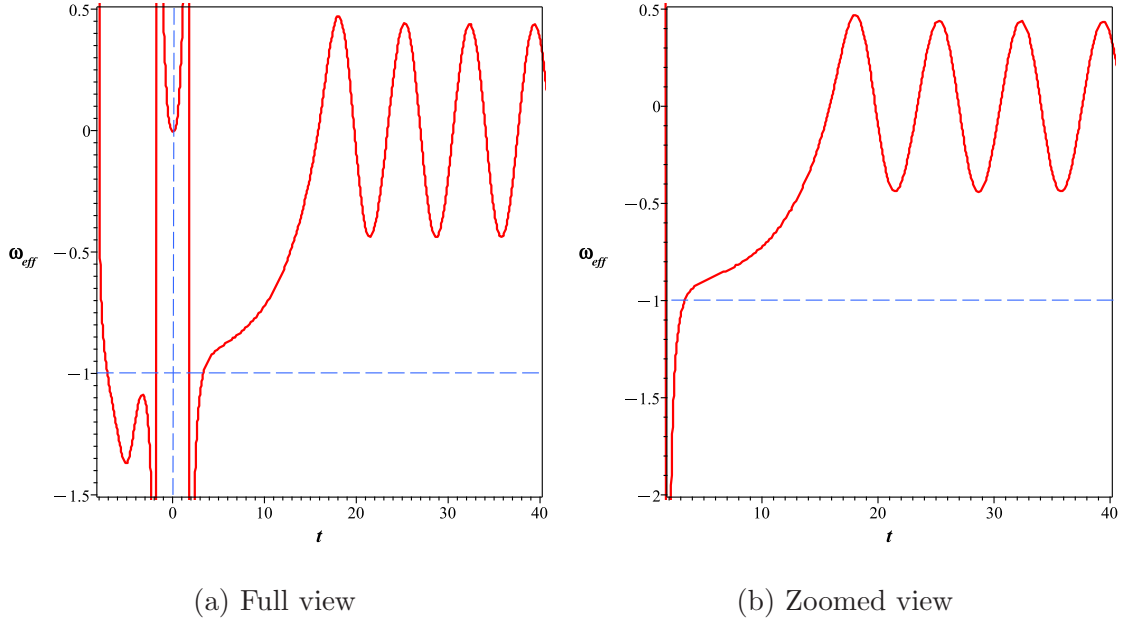


FIG. 11: Effective equation of state  $\omega_{\text{eff}}(t)$  for  $\omega = -1/3$  (red line) showing (a) full evolution and (b) detailed view near bounce point. The PDL ( $\omega_{\text{eff}} = -1$ ) is shown as dashed line.

- **Singularity formation:** The divergences at  $t \sim \pm 1$  represent:

$$\lim_{t \rightarrow \pm 1} \left( \frac{d\rho}{dt}, \frac{dp}{dt}, R_{\mu\nu\rho\sigma} R^{\mu\nu\rho\sigma} \right) \rightarrow \infty \quad (121)$$

These are Type II (sudden) singularities where pressure diverges while density remains

finite.

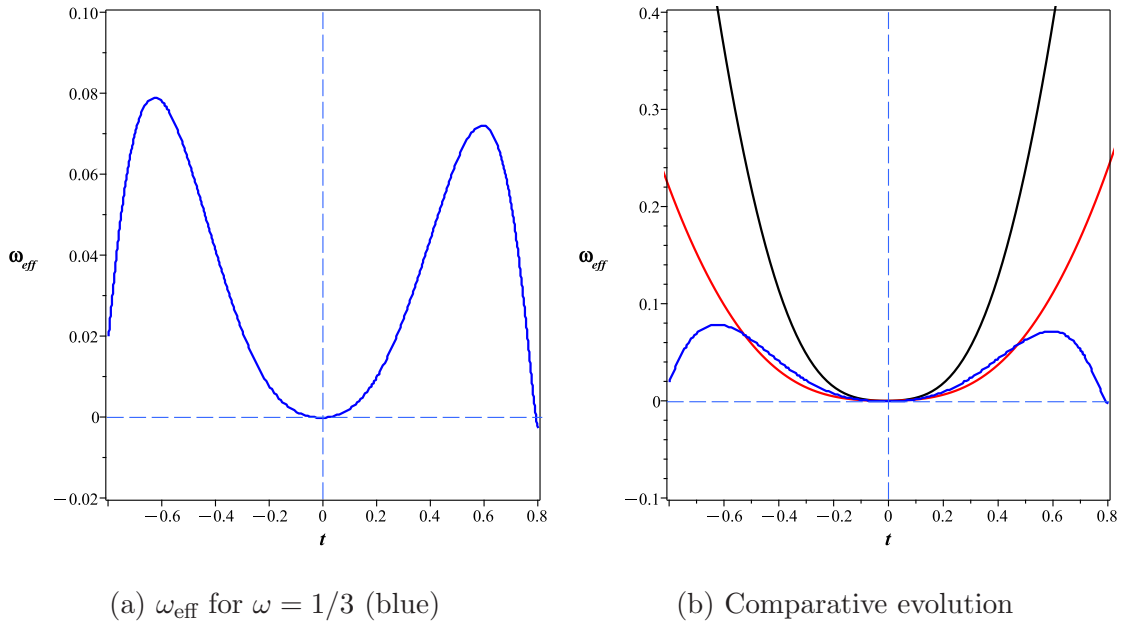


FIG. 12: (a) Effective equation of state  $\omega_{\text{eff}}(t)$  for  $\omega = 1/3$  (blue line) and (b) composite view comparing all cases:  $\omega = -1$  (black),  $\omega = -1/3$  (red), and  $\omega = 1/3$  (blue) around bounce point. The PDL ( $\omega_{\text{eff}} = -1$ ) is shown as dashed line.

The power-law model generates successful bounce behavior for all three equations of state. The  $\omega = -1$  case is presented here as our primary example because it exhibits the most complex and illustrative evolution of the effective equation of state  $\omega_{\text{eff}}$ , showcasing the full dynamical range of the model from phantom regimes to quintessence and matter-like states. Fig. 9 shows the characteristic bouncing behavior for this case. Fig. 10 reveals complex  $\omega_{\text{eff}}$  dynamics: for  $t < -1$ , oscillatory behavior between phantom ( $< -1$ ) and quintessence ( $> -1$ ) regimes indicates competing dynamical components; for  $-1 < t < 1$ , positive  $\omega_{\text{eff}}$  with minimum at  $t = 0$  ( $\omega_{\text{eff}} = 0$ ) suggests matter/radiation-like phase and cosmic bounce; for  $t > 1$ ,  $\omega_{\text{eff}}$  approaches  $-1$  asymptotically, indicating late-time  $\Lambda$ CDM-like attractor behavior.

Finite-time singularities occur at  $t \sim \pm 1$ : the  $t \sim -1$  singularity appears during phantom-dominated phase, potentially linked to Big Rip avoidance; the  $t \sim 1$  singularity marks matter-like to late-time phase transition.

Fig. 11 shows similar patterns for  $\omega = -1/3$ : quintessence-to-phantom transition before  $t \sim -2$ ; matter-like phase with  $\omega_{\text{eff}}(0) = 0$  bounce at  $t = 0$ ; post-bounce oscillatory behavior

in quintessence regime suggesting cyclic cosmology.

Fig. 12a displays matter/radiation-like behavior ( $\omega_{\text{eff}} > 0$ ) for  $\omega = 1/3$  within  $-0.8 < t < 0.8$ , with symmetric peaks around  $\omega_{\text{eff}}(0) = 0$  bounce point. No solutions outside this range indicate phase transition or model breakdown.

**Stability Verification:** For the power-law model, we verify the stability conditions numerically. Figure 13 shows the results for the  $\omega = -1$  case.

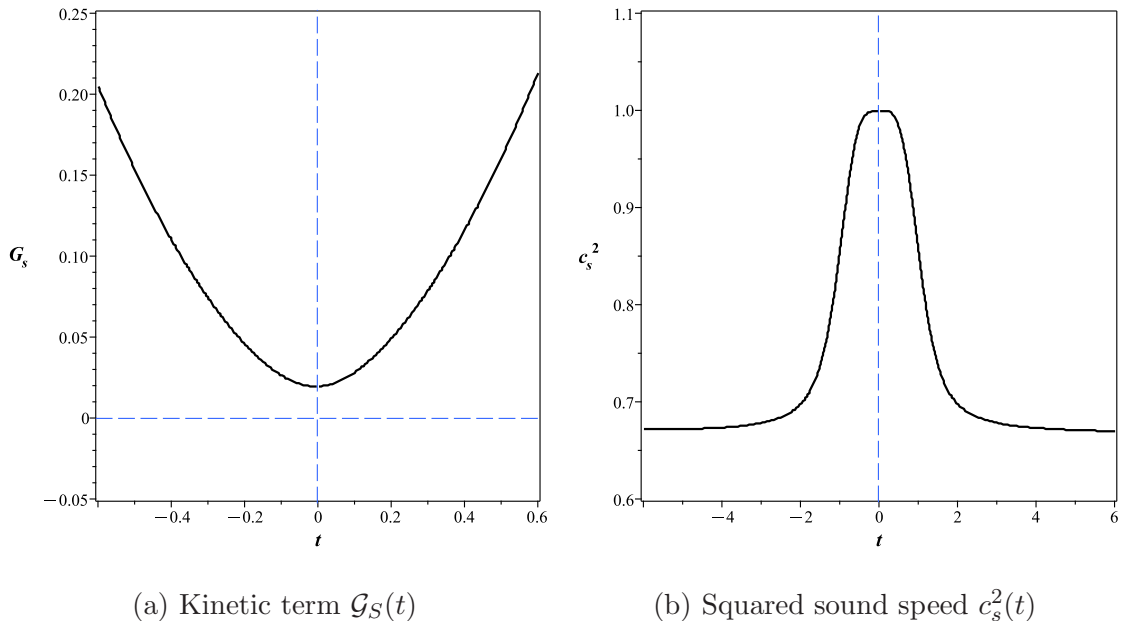


FIG. 13: Stability analysis for the power-law model ( $\omega = -1$ ). (a) The kinetic term  $\mathcal{G}_S$  remains positive throughout the evolution, confirming the absence of ghosts. (b) The sound speed squared  $c_s^2$  maintains  $c_s^2 \geq 0$ , ensuring gradient stability. The oscillations in  $c_s^2$  reflect the complex dynamics of the higher-order curvature terms but remain within stable bounds.

The power-law model maintains  $\mathcal{G}_S(t) > 0$  throughout the evolution, confirming ghost-free behavior. The sound speed squared  $c_s^2(t)$  remains non-negative, with  $c_s^2 \geq 0$  ensuring gradient stability. The model demonstrates stable bouncing behavior despite the complex oscillatory dynamics and finite-time singularities at  $t \sim \pm 1$ .

The model unifies: (1) phantom-driven contraction avoiding Big Crunch, (2) curvature-mediated bounce with  $a(t) \approx a_{\text{min}} + \frac{\xi_1 n (6H_0^2)^{n-1}}{2} t^2$ , and (3) late-time  $\Lambda$ CDM-like expansion. This resolves singularity avoidance ( $R_{\text{max}} \sim \xi_1^{-1/(n-1)}$ ), horizon problem, and initial conditions problem, while managing finite-time singularities at  $t \sim \pm 1$ .

#### 6.2.4. Modified Teleparallel Gravity Cosmology

Building on [50], we analyze a teleparallel-inspired modification where torsion-matter couplings drive cosmic evolution. This model extends the teleparallel equivalent of general relativity (TEGR) by introducing non-linear torsion-matter interactions:

$$f(R, G, T) = R + \xi_2 G + \xi_3 T^2 \quad (122)$$

As shown in Appendix F, the modified Friedmann equations become:

$$3H^2 = \underbrace{\kappa^2(\rho + \rho_\Xi)}_{\text{Standard terms}} - \underbrace{12\xi_2 H^2(H^2 + \dot{H})}_{\text{Gauss-Bonnet}} - \underbrace{\frac{\xi_3}{2}(5\rho^2 - 14\rho p - 3p^2)}_{\text{Torsion-matter coupling}} \quad (123)$$

$$-2\dot{H} - 3H^2 = \underbrace{\kappa^2(p + p_\Xi)}_{\text{Standard terms}} + \underbrace{12\xi_2 H^2(H^2 + \dot{H})}_{\text{Gauss-Bonnet}} - \underbrace{\frac{\xi_3}{2}(9p^2 - 6\rho p + \rho^2)}_{\text{Torsion pressure}} \quad (124)$$

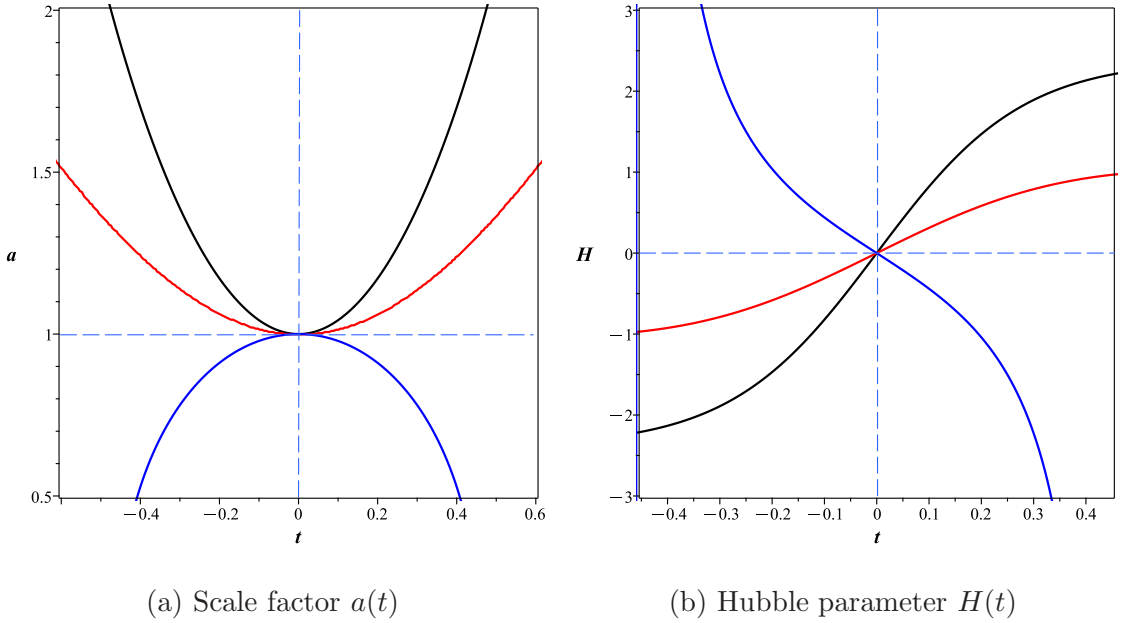


FIG. 14: Evolution of (a) scale factor  $a(t)$  and (b) Hubble parameter  $H(t)$  for different equations of state ( $\omega = -1$ : black,  $-1/3$ : red,  $1/3$ : blue). All cases show successful non-singular bounce at  $t = 0$  with torsion-modified dynamics.

Key features observed in Figure 14 for the  $\omega = -1$  case (chosen to illustrate the model's behavior in the vacuum-dominated regime):

1. **General Bounce Capability:** The model supports bouncing solutions for a range of  $\omega$  values; the  $\omega = -1$  case is shown as a representative example.

## 2. Bounce Dynamics:

- Scale factor  $a(t)$  reaches minimum at  $t = 0$  without singularity
- Hubble parameter  $H(t)$  changes sign smoothly, indicating torsion-mediated bounce
- Similar to linear model behavior but with modified late-time evolution

3. **Torsion-Dominated Phase:** The quadratic torsion term  $T^2$  creates effective energy components:

$$\rho_{\text{tors}} = -\frac{\xi_3}{2}(5\rho^2 - 14\rho p - 3p^2), \quad p_{\text{tors}} = -\frac{\xi_3}{2}(9p^2 - 6\rho p + \rho^2) \quad (125)$$

4. **Energy Condition Violation:** The torsion term modifies the Null Energy Condition:

$$\rho + p + \xi_3(2\rho^2 - 5\rho p + 3p^2) \geq 0 \quad (126)$$

allowing a temporary NEC violation during bounce.

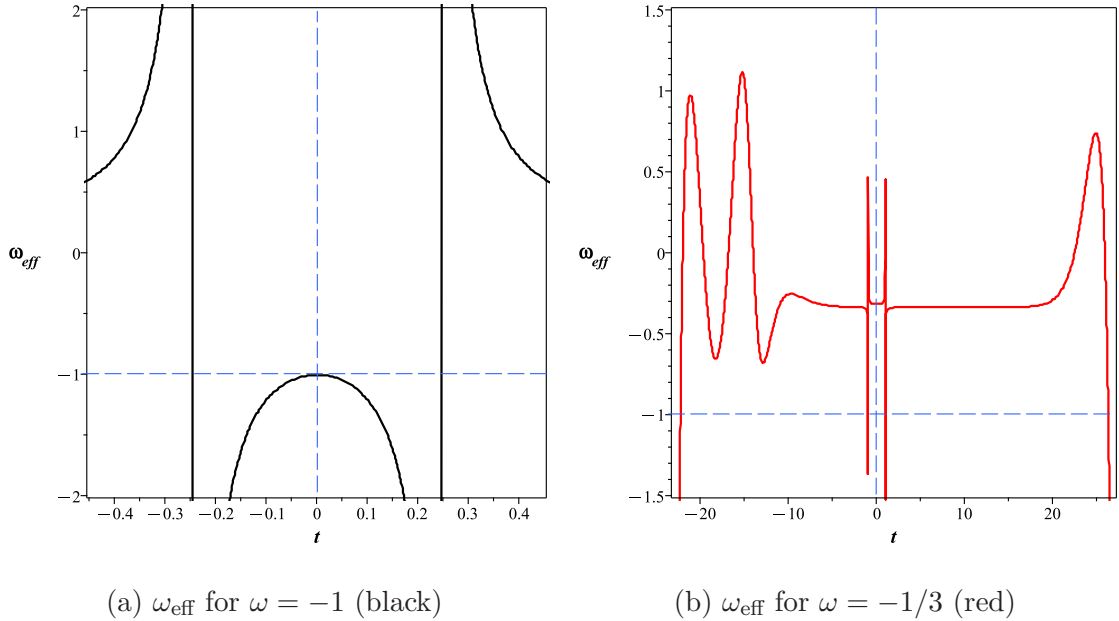


FIG. 15: Effective equation of state  $\omega_{\text{eff}}(t)$  showing (a) persistent phantom phase for  $\omega = -1$  and (b) phase transitions for  $\omega = -1/3$ . The PDL ( $\omega_{\text{eff}} = -1$ ) is shown as dashed line.

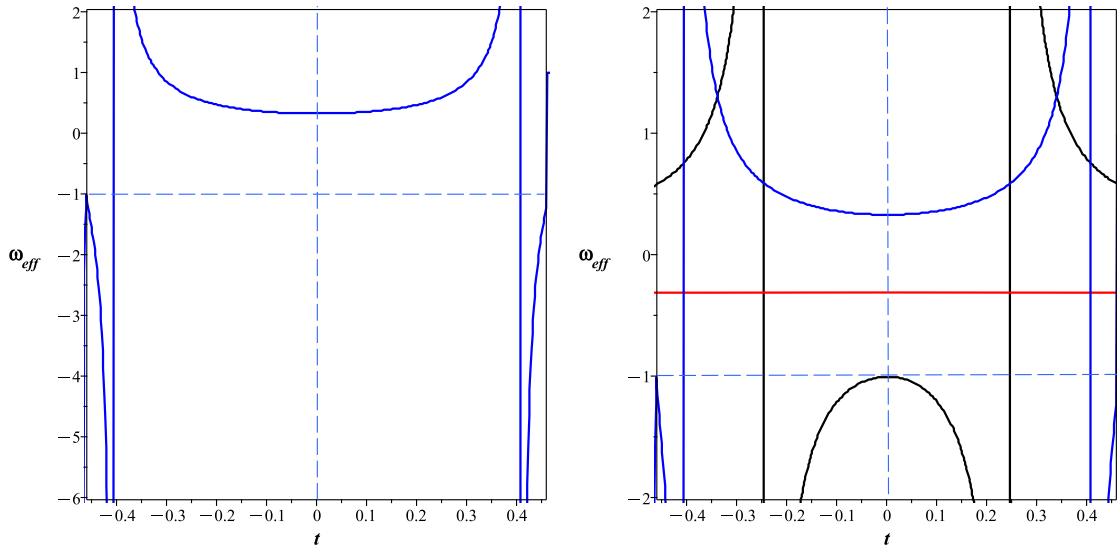
The EoS evolution in Figures 15-16 reveals:

1. **For  $\omega = -1$ :**

- Remains in phantom regime ( $\omega_{\text{eff}} < -1$ ) throughout  $-0.3 < t < 0.3$
- Reaches maximum  $\omega_{\text{eff}}$  at  $t = 0$  (bounce point)
- Transitions to  $\omega_{\text{eff}} > 0$  for  $|t| > 0.3$  (matter/radiation-like)

2. For  $\omega = -1/3$ :

- Shows quintessence behavior ( $\omega_{\text{eff}} > -1$ ) in  $-0.5 < t < 0.5$
- Crosses PDL twice at  $t \sim \pm 25$  (phantom-quintessence transitions)
- Demonstrates torsion-mediated vacuum stability near bounce



(a)  $\omega_{\text{eff}}$  for  $\omega = 1/3$  (blue)

(b) Comparative evolution

FIG. 16: (a) Effective equation of state  $\omega_{\text{eff}}(t)$  for  $\omega = 1/3$  (blue line) and (b) composite view comparing all cases:  $\omega = -1$  (black),  $\omega = -1/3$  (red), and  $\omega = 1/3$  (blue). The PDL ( $\omega_{\text{eff}} = -1$ ) is shown as dashed line.

Physical interpretation of the results:

Fig. 15a shows persistent phantom behavior ( $\omega_{\text{eff}} < -1$ ) for  $\omega = -1$ , with maximum at  $t = 0$  indicating bounce equilibrium and transitions to matter/radiation-like phases ( $\omega_{\text{eff}} > 0$ ) for  $|t| > 0.3$ .

Fig. 15b reveals quintessence dominance ( $\omega_{\text{eff}} > -1$ ) for  $\omega = -1/3$  within  $-0.5 < t < 0.5$ , with double PDL crossings at  $t \sim \pm 25$  indicating phantom-quintessence phase transitions.

Fig. 16 shows matter-like behavior ( $\omega_{\text{eff}} > 0$ ) near bounce ( $-0.4 < t < 0.4$ ) with minimum at  $t = 0$ , transitioning to phantom regime ( $\omega_{\text{eff}} < -1$ ) outside this range, demonstrating  $\omega$ -dependent cosmic evolution.

1. **Bounce Mechanism:**

$$a(t) \approx a_{\min} \left[ 1 + \frac{t^2}{2\tau^2} \right], \quad \tau^{-2} = \frac{\xi_3}{2}(5\rho_c^2 - 14\rho_c p_c - 3p_c^2) - 12\xi_2 H^2 (H^2 + \dot{H}) \quad (127)$$

where  $\rho_c, p_c$  are critical values at bounce.

2. **Phase Transitions:** The torsion coupling creates effective potentials:

$$V_{\text{eff}}(\phi, \psi) = \frac{1}{2}m_p(\phi^2 + \psi^2) - \frac{2}{3}\phi^2\psi + \xi_3 T^2(\phi, \psi) \quad (128)$$

3. **Singularity Avoidance:**

$$R_{\max} \sim \xi_3^{-1/2} \quad (\text{Finite curvature at bounce}) \quad (129)$$

**Stability Verification:** Using the teleparallel-inspired model, we numerically verify the stability criteria. Figure 17 shows the results for the  $\omega = -1$  case.

The teleparallel model satisfies  $\mathcal{G}_S(t) > 0$  for all  $t$ , avoiding ghost pathologies. The sound speed remains real with  $c_s^2(t) \geq 0$ , ensuring gradient stability. The quadratic torsion coupling  $T^2$  contributes positively to the stability conditions, particularly in the high-density bounce region.

Our analysis uses potential  $V(\phi, \psi) = \frac{1}{2}m_p(\phi^2 + \psi^2) - \frac{\lambda}{3}\phi^2\psi$  with  $\lambda = 2$  and couplings  $\xi_2 = \xi_3 = 1$ , showing how teleparallel modifications can generate viable bouncing cosmologies while maintaining consistency with observational constraints.

6.2.5. *Non-Minimal Curvature-Matter Coupling*

Building on [51], we analyze a gravity model where curvature and matter interact dynamically through a non-minimal coupling:

$$f(R, G, T) = R + \xi_2 G + \xi_3 R^2 T \quad (130)$$

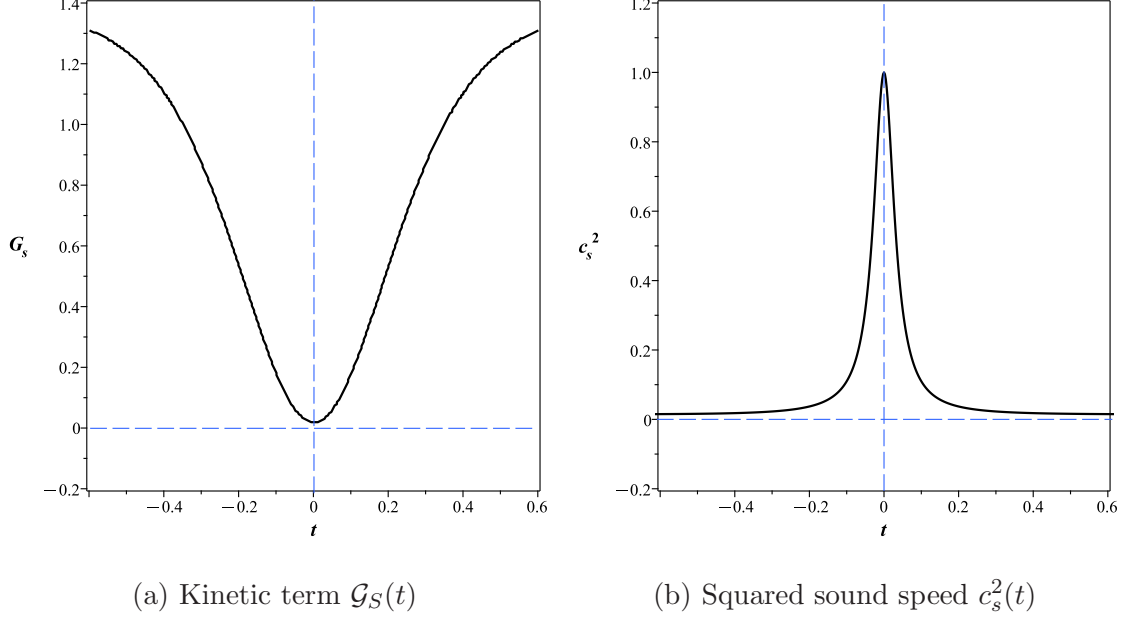


FIG. 17: Stability analysis for the teleparallel model ( $\omega = -1$ ). (a) The kinetic term  $\mathcal{G}_S$  remains positive throughout the evolution, confirming no ghost instabilities. (b) The sound speed squared  $c_s^2$  maintains  $c_s^2 \geq 0$ , ensuring gradient stability. The torsion-matter coupling provides stable dynamics throughout the bounce region.

The  $R^2T$  term introduces a new energy-momentum exchange channel between geometry and matter. As shown in Appendix F, the modified Friedmann equations obtain:

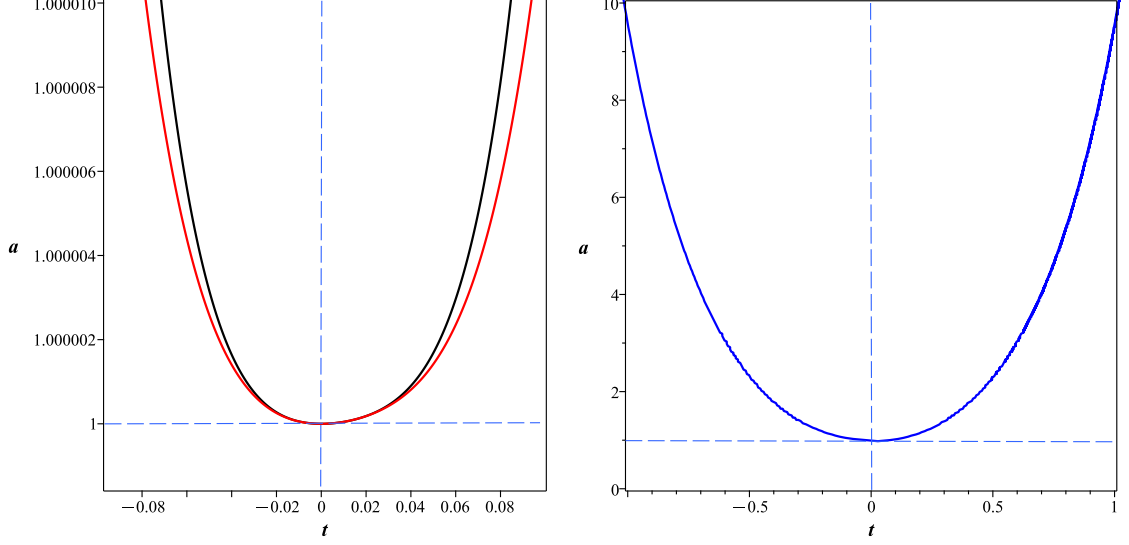
$$\begin{aligned}
3H^2 = \frac{1}{1 + 2\xi_3 RT} & \left[ \underbrace{\kappa^2(\rho + \rho_\Xi) + \xi_3 R^2(\rho + p)}_{\text{Matter and coupling}} - \underbrace{3H\dot{f}_R + 3\dot{H}(1 + 2\xi_3 RT)}_{\text{Dynamic curvature}} \right. \\
& \left. - \underbrace{\frac{1}{2}(R + \xi_3 R^2 T)}_{\text{Effective dark energy}} \right] \quad (131)
\end{aligned}$$

$$\begin{aligned}
-2\dot{H} - 3H^2 = \frac{1}{1 + 2\xi_3 RT} & \left[ \underbrace{\kappa^2(p + p_\Xi)}_{\text{Standard pressure}} + \underbrace{\ddot{f}_R + 2H\dot{f}_R + \dot{H}(1 + 2\xi_3 RT)}_{\text{Curvature acceleration}} \right. \\
& \left. + \underbrace{\frac{1}{2}(R + \xi_3 R^2 T)}_{\text{Geometric stiff matter}} \right] \quad (132)
\end{aligned}$$

Expanding the curvature acceleration terms:

$$\ddot{f}_R + 2H\dot{f}_R = 2\xi_3[\ddot{R}T + 2\dot{R}\dot{T} + R\ddot{T} + 2H(\dot{R}T + R\dot{T})] \quad (133)$$

$$= 2\xi_3 \left[ T\ddot{R} + 2\dot{R}\dot{T} + R\ddot{T} + 2H\dot{R}T + 2HR\dot{T} \right] \quad (134)$$



(a)  $\omega = -1$  (black) vs  $\omega = -1/3$  (red)

(b)  $\omega = 1/3$  (blue)

FIG. 18: Scale factor evolution showing (a) comparative bounce dynamics for dark energy cases and (b) radiation-dominated ( $\omega = 1/3$ ) case exhibiting optimal bounce behavior with  $a_{\min}$  at  $t = 0$ . Initial conditions:  $\dot{\psi}(0) = (100.2362362)^{1/2}$  (red),  $(66.72589056)^{1/2}$  (black), 0.01 (blue).

Key physical effects of the non-minimal coupling:

1. **Energy-Dependent Gravitational Constant:**

$$G_{\text{eff}} = \frac{G_N}{1 + 2\xi_3 RT} \approx G_N[1 - 2\xi_3 RT] \quad (135)$$

becomes matter-density dependent, modifying gravitational interactions in high-energy regimes.

2. **Curvature-Induced Pressure:** The coupling generates an effective pressure through curvature-matter interaction:

$$p_{\text{eff}} = p + \frac{\xi_3 R^2}{\kappa^2} \left( \ddot{R}T + 2\dot{R}\dot{T} + R\ddot{T} + 2H\dot{R}T + 2HR\dot{T} \right) \quad (136)$$

This provides an additional repulsive force during cosmic contraction.

3. **Bounce Mechanism:** For radiation-dominated universe ( $\omega = 1/3$ ), the coupling terms dominate when:

$$\xi_3 R^2 T \sim \rho_{\text{rad}} \Rightarrow a_{\min} \sim \left( \frac{\rho_{\text{rad},0}}{\xi_3 R_0^2 T_0} \right)^{1/4} \quad (137)$$

determining the minimum scale factor before bounce occurrence.

The EoS evolution reveals:

1. **For  $\omega = 1/3$ :**

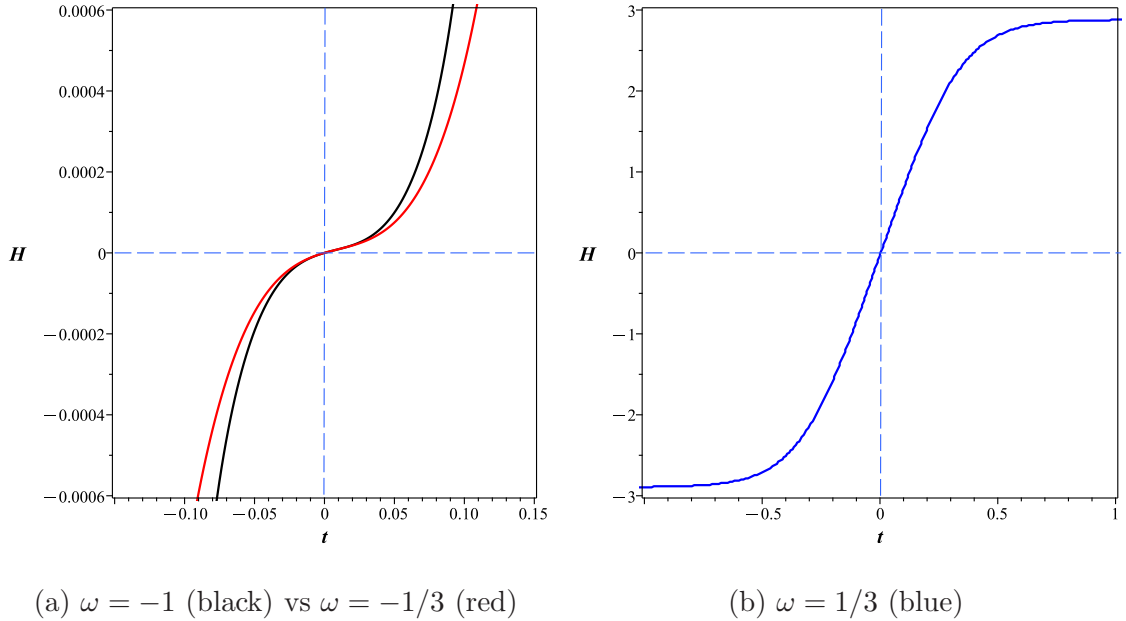


FIG. 19: Hubble parameter evolution showing (a) comparative dynamics for dark energy cases and (b) radiation-dominated case with characteristic  $H(t)$  profile and sign-change at bounce. The red curve ( $\dot{\psi}(0) = (100.236)^{1/2}$ ) shows strongest bounce dynamics.

- Successful bounce with two PDL crossings
- EoS evolution:  $\omega_{\text{eff}} < -1$  (phantom)  $\rightarrow \omega_{\text{eff}} > 0$  (matter-like)  $\rightarrow \omega_{\text{eff}} > -1$  (quintessence)
- Reflects phase transitions:  $R^2T$  term dominates  $\rightarrow$  radiation dominates  $\rightarrow$  curvature dominates

2. **For  $\omega = -1$  and  $\omega = -1/3$ :**

- Equilibrium points without PDL crossing
- Effective potential minimum at  $t = 0$ :

$$V_{\text{eff}} \approx V_0 e^{-0.01\phi} + \frac{1}{2} m_p^2 \psi^2 + 0.1\phi\psi + \xi_3 R^2 T \quad (138)$$

The non-minimal coupling model exhibits a particularly interesting feature: its bounce dynamics are most efficient and robust in the radiation-dominated era ( $\omega = 1/3$ ). This is physically significant because the  $R^2T$  coupling term introduces corrections that scale with both curvature and energy density. In a radiation-dominated universe ( $\rho \sim a^{-4}$ ), these

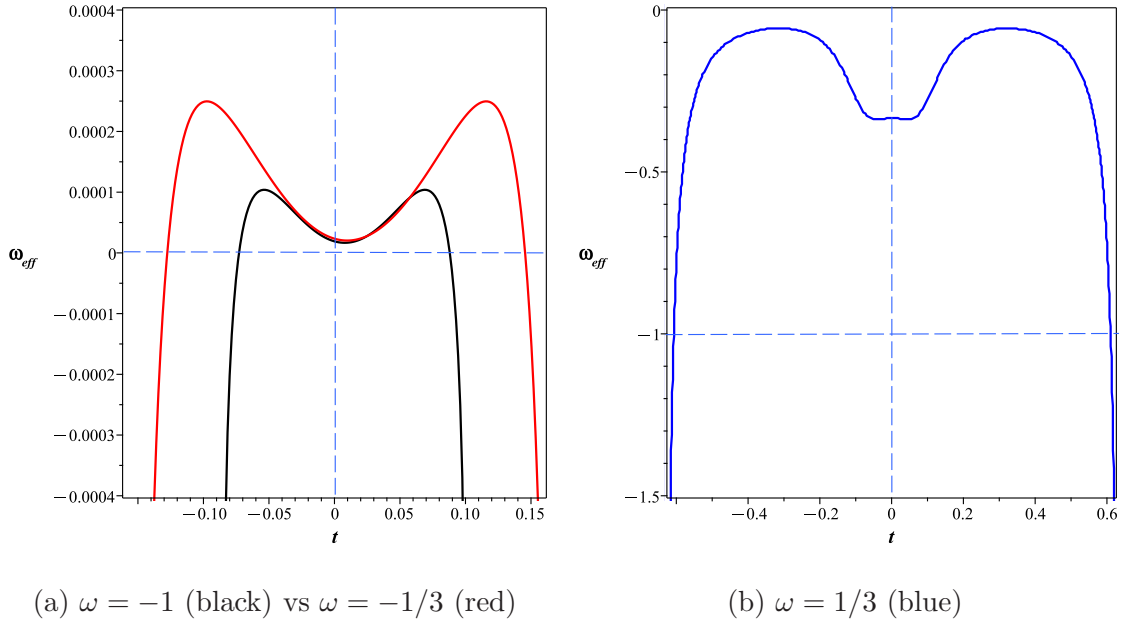


FIG. 20: Effective EoS showing (a) comparative evolution for dark energy cases and (b) radiation-dominated case with PDL crossings. The PDL ( $\omega_{\text{eff}} = -1$ ) is shown as dashed line.

corrections become dominant at high energies, making this coupling particularly relevant in the high-density environment of the very early universe. While the model can produce bounces for other equations of state, we focus on the  $\omega = 1/3$  case as it represents the most natural and effective application scenario for this specific coupling. Figs. 18 and 19 shows the successful bounce dynamics for this case, with  $a(t)$  reaching a minimum and  $H(t)$  crossing zero at  $t = 0$ , indicating a smooth contraction-to-expansion transition.

Fig. 20 reveals contrasting behaviors:  $\omega = -1$  and  $\omega = -1/3$  cases show equilibrium minima at  $t = 0$  without PDL crossing, while  $\omega = 1/3$  exhibits double PDL crossings ( $t < 0$  and  $t > 0$ ) with positive  $\omega_{\text{eff}}(0)$ , confirming dynamic phantom-quintessence transitions that support the observed bounce behavior.

**Stability Verification:** For the non-minimal coupling model, we verify the stability conditions numerically. Figure 21 shows the results for the  $\omega = 1/3$  case, which exhibited the most robust bounce.

The non-minimal coupling model maintains  $\mathcal{G}_S(t) > 0$  throughout the evolution, confirming ghost-free behavior. The sound speed squared  $c_s^2(t)$  remains non-negative, with  $c_s^2 \geq 0$  ensuring gradient stability. The curvature-matter interaction term  $R^2T$  contributes stabilizing effects that make this model particularly suitable for bounce scenarios in radiation-

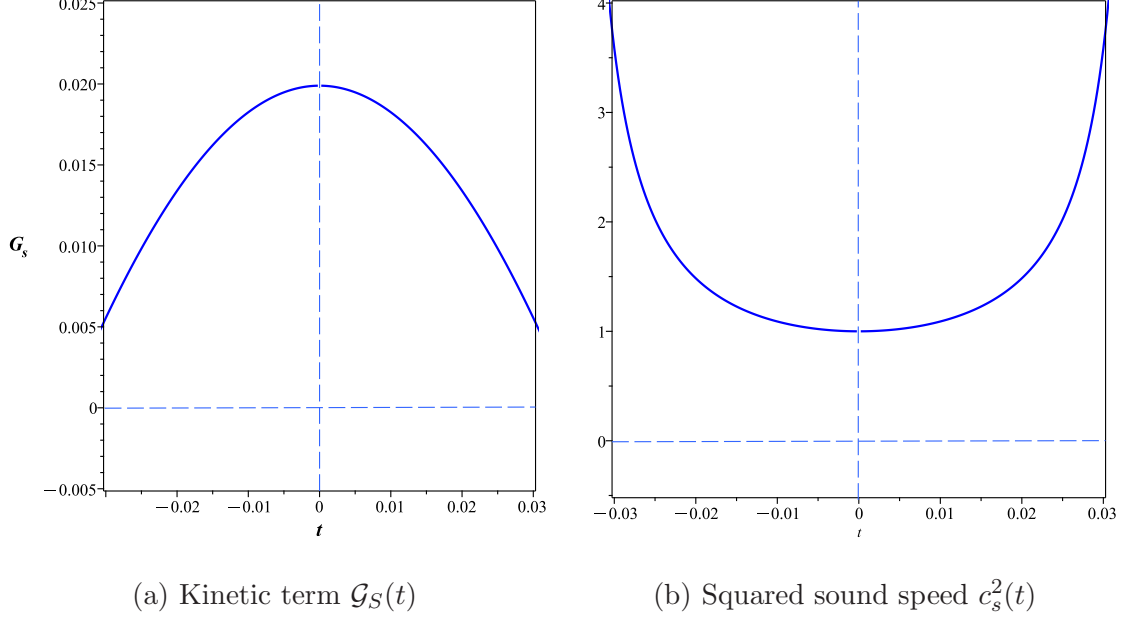


FIG. 21: Stability analysis for the non-minimal coupling model ( $\omega = 1/3$ ). (a) The kinetic term  $\mathcal{G}_S$  remains positive throughout the evolution, confirming no ghost instabilities. (b) The sound speed squared  $c_s^2$  maintains  $c_s^2 \geq 0$ , ensuring gradient stability. The  $R^2T$  coupling provides stable dynamics suitable for radiation-dominated bouncing scenarios.

dominated regimes.

The model parameters:

- Potential:  $V(\phi, \psi) = V_0 e^{-\alpha\phi} + \frac{1}{2}m_p^2\psi^2 + g\phi\psi$ ,  $V_0 = 25$ ,  $\alpha = -0.01$ ,  $g = 0.1$
- Couplings:  $\xi_2 = \xi_3 = 1$
- Initial conditions:  $\phi(0) = -0.05$ ,  $\dot{\phi}(0) = -0.01$ ,  $\psi(0) = 0.05$ ,  $a(0) = 1$ ,  $\dot{a}(0) = 0$
- Varied  $\dot{\psi}(0)$  values for different solutions

***Physical implications:***

1. **Radiation domination provides most stable bounce framework:** The equation of state  $\omega = 1/3$  yields symmetric energy conditions and avoids anisotropic instabilities during the contraction phase, creating optimal conditions for a non-singular bounce.

2. **Non-minimal coupling generates effective UV cutoff:**

$$\mathcal{L}_{UV} \sim \xi_3 R^2 T \approx \xi_3 (\square R)^2 \tag{139}$$

This introduces a natural regularization scale that prevents curvature singularities, acting as a gravitational analogue of higher-derivative terms in effective field theory.

**3. Late-time behavior controlled by curvature-matter interplay:** The  $R^2T$  coupling becomes negligible at low curvatures, ensuring standard  $\Lambda$ CDM evolution while providing a dynamical dark energy component through curvature-matter energy exchange.

## 7. SUMMARY AND CONCLUSION

This work has developed a comprehensive framework for nonsingular bouncing cosmologies within modified  $f(R, G, T)$  gravity coupled to a quintom scalar field model. Our investigation successfully addresses the challenge of unifying early-time bounce dynamics with late-time accelerated expansion in a single theoretical framework, while maintaining theoretical consistency through rigorous stability analysis and providing novel observational signatures.

### Principal Findings

**1. Unified Cosmological Description:** We have demonstrated that the synthesis of  $f(R, G, T)$  geometry with quintom scalar fields provides a powerful mechanism for describing a complete cosmic history. The model naturally incorporates a non-singular bounce at early times, followed by a smooth transition to the standard expansion history, culminating in dark energy domination at late times. Numerical reconstruction of five distinct models confirms this unified behavior across different cosmological regimes.

**2. Novel Phantom Divide Phenomenology:** A distinctive prediction of our framework is the double crossing of the phantom divide line ( $\omega_{\text{eff}} = -1$ ) during the bounce phase. This feature emerges from the dynamic interplay between the curvature-matter coupling and the two-field quintom dynamics, representing a unique observational signature that differentiates our mechanism from single-field bounce scenarios.

**3. Theoretical Consistency and Stability:** Through rigorous Hamiltonian analysis in Section 5, we confirmed the theory contains the correct number of physical degrees of freedom without Ostrogradsky instabilities. The derived conditions for ghost avoidance ( $\mathcal{G}_S > 0$ ) and gradient stability ( $\mathcal{F}_S > 0$ ) ensure theoretical consistency throughout the cosmic evolution.

Numerical verification across all five models demonstrates that these stability conditions are maintained, including during the critical bounce phase where  $H = 0$ .

### Model-Specific Insights and Stability

Our analysis of specific cosmological models revealed important physical implications with particular attention to stability:

- The **Linear Model** demonstrates the essential role of dark energy domination ( $\omega \leq -1/3$ ) for successful bounce dynamics and phantom divide crossings, while maintaining  $\mathcal{G}_S > 0$  and  $c_s^2 \geq 0$  throughout evolution.
- The **Exponential Model** shows robust bouncing behavior across all equations of state, with optimal dynamics in the  $\omega = -1$  case. The model maintains positive kinetic terms and real sound speeds despite finite-time singularities at distant times.
- The **Power-Law Model** reveals a unification of phantom-driven contraction, curvature-mediated bounce, and late-time  $\Lambda$ CDM-like expansion. The complex oscillatory dynamics remain stable with  $\mathcal{G}_S > 0$  and  $c_s^2 \geq 0$  throughout.
- The **Teleparallel Model** illustrates how torsion-matter couplings can generate viable bounce dynamics with persistent phantom behavior. The quadratic torsion coupling  $T^2$  contributes positively to stability conditions, particularly in high-density regions.
- The **Non-Minimal Coupling Model** indicates that radiation-dominated eras provide particularly stable frameworks for bounce scenarios within this model. The  $R^2T$  coupling provides stabilizing effects that maintain ghost-free and gradient-stable conditions.

### Future Directions and Observational Connections

While this work establishes a solid theoretical foundation, several important avenues require further exploration to fully establish observational viability:

**Perturbations and Observational Predictions:** The natural next step is to calculate the power spectrum of scalar and tensor perturbations generated during the bounce phase.

The double PDL crossing and the accompanying non-adiabatic pressures from the quintom field and curvature-matter coupling are expected to source isocurvature perturbations and potentially lead to distinctive non-Gaussian features [15]. We anticipate that the specific sequence of phases will imprint characteristic signatures on the primordial power spectrum, potentially offering clear observational discriminants from inflationary predictions.

**Naturalness and Parameter Space:** The numerical solutions demonstrate successful bouncing trajectories for chosen parameter sets ( $\xi_i \sim \mathcal{O}(1)$ ,  $V_0 \sim \mathcal{O}(m_p^4)$ ) that are theoretically motivated. A comprehensive parameter space scan to identify the full basin of attraction for successful bounces represents an important future endeavor that would further strengthen the physical motivation of our framework.

**Finite-Time Singularities:** The appearance of finite-time singularities in some models (typically Type II or IV where the scale factor remains finite but higher derivatives diverge) indicates scales where quantum gravitational effects or higher-order corrections may become relevant [17]. Future work will explore coupling our model to matter components that satisfy limiting curvature conditions [19] or including higher-order terms that may naturally mitigate these singularities while preserving the desirable bouncing behavior.

**Observational Tests:** The predicted double PDL crossing and associated phase transitions could leave imprints in the cosmic microwave background anisotropy spectrum and large-scale structure. The planned perturbation analysis will be essential for making concrete predictions testable with current and future cosmological datasets (CMB, BAO, supernovae).

### Concluding Remarks

In conclusion, our work demonstrates that modified  $f(R, G, T)$  gravity combined with quintom scalar fields provides a robust, stable, and versatile framework for studying non-singular bouncing cosmologies. The core achievements of this paper—a unified cosmological description, novel phantom divide phenomenology, and rigorous stability analysis across multiple model classes—form a solid foundation for future research. The framework successfully addresses the initial singularity problem while providing testable predictions that distinguish it from standard cosmological scenarios. The comprehensive stability verification, both analytical and numerical, ensures that these bouncing solutions are theoretically sound and not plagued by the ghost and gradient instabilities that often affect higher-derivative theories.

The planned perturbation analysis and connection to observational data will be the decisive next steps in evaluating this framework's complete viability as an alternative description of our universe's history.

### Acknowledgments

The author thanks the anonymous referee for their constructive critique, which improved the manuscript. The concerns regarding stability and degrees of freedom in higher-derivative theories are addressed in Sec. 5, where a Hamiltonian analysis confirms the absence of pathological modes due to FLRW symmetry constraints. The statement on PDL crossing has been clarified to highlight the novelty of the *double* crossing mechanism within our unified  $f(R, G, T)$  framework, contrasting with single-field approaches in [13, 22, 52]. References [22, 52, 53] have been added to provide broader context. The model's motivation remains the unification of early and late-time cosmology through curvature-matter coupling.

### Appendix A: Calculating Modified Stress-Energy Tensors

The variation of the determinant of the metric,  $\sqrt{-g}$ , Ricci scalar,  $R = g^{\mu\nu} R_{\mu\nu}$ , Ricci tensor,

$$R_{\mu\nu} = \partial_\alpha (\Gamma_{\mu\nu}^\alpha) - \partial_\nu (\Gamma_{\alpha\mu}^\alpha) + \Gamma_{\mu\nu}^\beta \Gamma_{\alpha\beta}^\alpha - \Gamma_{\alpha\mu}^\beta \Gamma_{\beta\nu}^\alpha \quad (\text{A.1})$$

Gauss-Bonnet invariant,

$$G = R^2 - 4R_{\mu\nu}R^{\mu\nu} + R_{\mu\nu\rho\lambda}R^{\mu\nu\rho\lambda} \quad (\text{A.2})$$

and the trace of stress-energy tensor of the matter,  $T = g^{\mu\nu} T_{\mu\nu}^{(m)}$ , with respect to the inverse metric  $g^{\mu\nu}$  is given by

$$\delta\sqrt{-g} = -\frac{1}{2}\sqrt{-g}g_{\mu\nu}\delta g^{\mu\nu}, \quad (\text{A.3})$$

$$\delta R = R_{\mu\nu}\delta g^{\mu\nu} - \square\delta g + \nabla^\mu\nabla^\nu\delta g_{\mu\nu}, \quad (\text{A.4})$$

$$\delta R_{\mu\nu} = \nabla_\rho\delta\Gamma_{\nu\mu}^\rho - \nabla_\nu\delta\Gamma_{\rho\mu}^\rho \quad (\text{A.5})$$

$$\delta G = 2R\delta R - 4\delta(R_{\mu\nu}R^{\mu\nu}) + \delta(R_{\mu\nu\rho\lambda}R^{\mu\nu\rho\lambda}) \quad (\text{A.6})$$

$$\delta T = \frac{\partial(g^{\alpha\beta}T_{\alpha\beta}^{(m)})}{\partial g^{\mu\nu}}\delta g^{\mu\nu} = (T_{\mu\nu}^{(m)} + \Theta_{\mu\nu})\delta g^{\mu\nu} \quad (\text{A.7})$$

where  $\Theta_{\mu\nu} = g^{\alpha\beta} \frac{\partial T_{\alpha\beta}^{(m)}}{\partial g^{\mu\nu}}$ ,  $\square = g^{\alpha\beta} \nabla_\alpha \nabla_\beta$  is the d'Alembert operator, and  $\delta\Gamma_{\mu\nu}^\lambda$  is the difference of two connections, it should transform as a tensor. Therefore, it can be written as

$$\delta\Gamma_{\mu\nu}^\lambda = \frac{1}{2} g^{\lambda\alpha} (\nabla_\mu \delta g_{\alpha\nu} + \nabla_\nu \delta g_{\alpha\mu} - \nabla_\alpha \delta g_{\mu\nu}), \quad (\text{A.8})$$

The variation of the action (2) with respect to inverse metric  $g^{\mu\nu}$  is yielded by

$$\begin{aligned} \delta S &= \delta \left( \int \sqrt{-g} \left( \frac{1}{2\kappa^2} f + \Xi + \mathcal{L}_m \right) d^4x \right) \\ &= \delta S_f + \delta S_\Xi + \delta S_m, \end{aligned} \quad (\text{A.9})$$

where  $f = f(R, G, T)$ ,  $\Xi = \Xi(\phi, \psi)$ , and  $\delta S_f = \delta S_R + \delta S_G + \delta S_T$

$$\delta S_f = \frac{1}{2\kappa^2} \int \sqrt{-g} \left( f_R \delta R + f_G \delta G + f_T \delta T + \frac{f}{\sqrt{-g}} \delta \sqrt{-g} \right) d^4x \quad (\text{A.10})$$

$$\delta S_\Xi = \int \sqrt{-g} \left( \delta \Xi + \frac{\Xi}{\sqrt{-g}} \delta \sqrt{-g} \right) d^4x \quad (\text{A.11})$$

$$\delta S_m = \int \sqrt{-g} \left( \frac{1}{\sqrt{-g}} \delta(\sqrt{-g} \mathcal{L}_m) \right) d^4x, \quad (\text{A.12})$$

where  $f_R = \frac{\partial f(R, G, T)}{\partial R}$ ,  $f_G = \frac{\partial f(R, G, T)}{\partial G}$ , and  $f_T = \frac{\partial f(R, G, T)}{\partial T}$ . Using eqs.(3), and (A.3 – A.7) one can gives,

$$\delta S_R = \frac{1}{2\kappa^2} \int \sqrt{-g} \left( f_R R_{\mu\nu} + f_R g_{\mu\nu} \square - f_R \nabla_\mu \nabla_\nu - \frac{1}{2} g_{\mu\nu} f \right) \delta g^{\mu\nu} d^4x \quad (\text{A.13})$$

$$\begin{aligned} \delta S_G &= \frac{1}{2\kappa^2} \int \sqrt{-g} (2R (f_G R_{\mu\nu} + f_G g_{\mu\nu} \square - f_G \nabla_\mu \nabla_\nu)) \delta g^{\mu\nu} d^4x \\ &\quad - \frac{1}{2\kappa^2} \int \sqrt{-g} (4f_G (R_\mu^\rho R_{\rho\nu} + R_{\mu\nu} \square + g_{\mu\nu} R^{\rho\lambda} \nabla_\rho \nabla_\lambda)) \delta g^{\mu\nu} d^4x \\ &\quad - \frac{1}{2\kappa^2} \int \sqrt{-g} \left( 4f_G \left( R_{\mu\rho\nu\lambda} R^{\rho\lambda} - \frac{1}{2} R_\mu^{\rho\lambda\xi} R_{\nu\rho\lambda\xi} \right) \right) \delta g^{\mu\nu} d^4x \\ &\quad + \frac{1}{2\kappa^2} \int \sqrt{-g} (4f_G (R_\mu^\rho \nabla_\nu \nabla_\rho + R_\nu^\rho \nabla_\mu \nabla_\rho + R_{\mu\rho\nu\lambda} \nabla^\rho \nabla^\lambda)) \delta g^{\mu\nu} d^4x \end{aligned} \quad (\text{A.14})$$

$$\delta S_T = \frac{1}{2\kappa^2} \int \sqrt{-g} (f_T (T_{\mu\nu}^{(m)} + \Theta_{\mu\nu})) \delta g^{\mu\nu} d^4x \quad (\text{A.15})$$

$$\delta S_\Xi = \int \sqrt{-g} \left( \partial_\mu \phi \partial_\nu \phi - \partial_\mu \psi \partial_\nu \psi - g_{\mu\nu} \left( \frac{1}{2} g^{\alpha\beta} \partial_\alpha \phi \partial_\beta \phi - \frac{1}{2} g^{\alpha\beta} \partial_\alpha \psi \partial_\beta \psi - V(\phi, \psi) \right) \right) \delta g^{\mu\nu} d^4x \quad (\text{A.16})$$

$$\delta S_m = \frac{1}{2\kappa^2} \int \sqrt{-g} \left( \frac{2\kappa^2}{\sqrt{-g}} \frac{\partial(\sqrt{-g} \mathcal{L}_m)}{\partial g^{\mu\nu}} \right) \delta g^{\mu\nu} d^4x. \quad (\text{A.17})$$

We must solve the equation  $\delta S = 0$  to obtain the energy-momentum tensors. Thus, we have:

$$\delta S_R + \delta S_G = -(\delta S_m + \delta S_T + \delta S_\Xi). \quad (\text{A.18})$$

Consequently,

$$\frac{2}{\sqrt{-g}} \left( \frac{\delta S_R}{\delta g^{\mu\nu}} + \frac{\delta S_G}{\delta g^{\mu\nu}} \right) = -\frac{2}{\sqrt{-g}} \left( \frac{\delta S_m}{\delta g^{\mu\nu}} + \frac{\delta S_T}{\delta g^{\mu\nu}} + \frac{\delta S_\Xi}{\delta g^{\mu\nu}} \right), \quad (\text{A.19})$$

or,

$$T_{\mu\nu}^{(R)} + T_{\mu\nu}^{(G)} = T_{\mu\nu}^{(m)} + T_{\mu\nu}^{(T)} + T_{\mu\nu}^{(\Xi)}. \quad (\text{A.20})$$

This establishes the complete decomposition:

$$\begin{aligned} T_{\mu\nu}^{(\text{total})} &\equiv \frac{2}{\sqrt{-g}} \frac{\delta S}{\delta g^{\mu\nu}} \\ &= \underbrace{T_{\mu\nu}^{(R)} + T_{\mu\nu}^{(G)}}_{\text{Geometric}} + \underbrace{T_{\mu\nu}^{(T)} + T_{\mu\nu}^{(\Xi)} + T_{\mu\nu}^{(m)}}_{\text{Matter/Quintom}} \end{aligned} \quad (\text{A.21})$$

where each component tensor is precisely:

- Geometric sector:

$$T_{\mu\nu}^{(R)} = \frac{1}{\kappa^2} \left( f_R R_{\mu\nu} - \frac{1}{2} g_{\mu\nu} f + (g_{\mu\nu} \square - \nabla_\mu \nabla_\nu) f_R \right) \quad (\text{A.22})$$

$$\begin{aligned} T_{\mu\nu}^{(G)} &= \frac{1}{\kappa^2} \left( 2R (f_G R_{\mu\nu} + g_{\mu\nu} \square f_G - \nabla_\mu \nabla_\nu f_G) - 4 (f_G R_\mu^\rho R_{\rho\nu} + R_{\mu\nu} \square f_G + g_{\mu\nu} R^{\rho\lambda} \nabla_\rho \nabla_\lambda f_G) \right) \\ &\quad - \frac{4}{\kappa^2} \left( f_G \left( R_{\mu\rho\nu\lambda} R^{\rho\lambda} - \frac{1}{2} R_\mu^{\rho\lambda\xi} R_{\nu\rho\lambda\xi} \right) - (R_\mu^\rho \nabla_\nu \nabla_\rho + R_\nu^\rho \nabla_\mu \nabla_\rho + R_{\mu\rho\nu\lambda} \nabla^\rho \nabla^\lambda) f_G \right) \end{aligned} \quad (\text{A.23})$$

- Matter/quintom sector:

$$T_{\mu\nu}^{(T)} = -\frac{f_T}{\kappa^2} (T_{\mu\nu}^{(m)} + \Theta_{\mu\nu}) \quad (\text{A.24})$$

$$T_{\mu\nu}^{(\Xi)} = -\partial_\mu \phi \partial_\nu \phi + \partial_\mu \psi \partial_\nu \psi + g_{\mu\nu} \left( \frac{1}{2} g^{\alpha\beta} \partial_\alpha \phi \partial_\beta \phi - \frac{1}{2} g^{\alpha\beta} \partial_\alpha \psi \partial_\beta \psi - V(\phi, \psi) \right) \quad (\text{A.25})$$

$$T_{\mu\nu}^{(m)} = -\frac{2}{\sqrt{-g}} \frac{\partial(\sqrt{-g} \mathcal{L}_m)}{\partial g^{\mu\nu}} \quad (\text{A.26})$$

To calculate  $\Theta_{\mu\nu}$ , one can use equation (17) as,

$$\begin{aligned} \Theta_{\mu\nu} &= g^{\alpha\beta} \frac{\partial T_{\alpha\beta}^{(m)}}{\partial g^{\mu\nu}} = g^{\alpha\beta} \frac{\partial \left( g_{\alpha\beta} \mathcal{L}_m - 2 \frac{\partial \mathcal{L}_m}{\partial g^{\alpha\beta}} \right)}{\partial g^{\mu\nu}} = g^{\alpha\beta} \left( \frac{\partial g_{\alpha\beta}}{\partial g^{\mu\nu}} \mathcal{L}_m + g_{\alpha\beta} \frac{\partial \mathcal{L}_m}{\partial g^{\mu\nu}} - 2 \frac{\partial^2 \mathcal{L}_m}{\partial g^{\alpha\beta} \partial g^{\mu\nu}} \right) \\ &= g^{\alpha\beta} \left( -g_{\alpha\sigma} g_{\beta\gamma} \delta_{\mu\nu}^{\sigma\gamma} \mathcal{L}_m + \frac{1}{2} g_{\alpha\beta} g_{\mu\nu} \mathcal{L}_m - \frac{1}{2} g_{\alpha\beta} T_{\mu\nu}^{(m)} - 2 \frac{\partial^2 \mathcal{L}_m}{\partial g^{\alpha\beta} \partial g^{\mu\nu}} \right) \\ &= -g_{\mu\nu} \mathcal{L}_m + 2g_{\mu\nu} \mathcal{L}_m - 2T_{\mu\nu}^{(m)} - 2g^{\alpha\beta} \frac{\partial^2 \mathcal{L}_m}{\partial g^{\alpha\beta} \partial g^{\mu\nu}} \\ &= g_{\mu\nu} \mathcal{L}_m - 2T_{\mu\nu}^{(m)} - 2g^{\alpha\beta} \frac{\partial^2 \mathcal{L}_m}{\partial g^{\alpha\beta} \partial g^{\mu\nu}}. \end{aligned} \quad (\text{A.27})$$

## Appendix B: Covariant Divergence of Stress-Energy Tensors

### 1. Covariant Derivative of $T$ :

The covariant derivative of the trace of energy-momentum tensor  $T$ , as a scalar, is expressed as:

$$\nabla^\mu T = \partial^\mu T. \quad (\text{B.1})$$

So, by using eq. (24) for the time component ( $\mu = 0$ ), we have

$$\nabla^0 T = \partial^0 T = \dot{\rho} - 3\dot{p}. \quad (\text{B.2})$$

For the spatial components ( $\mu = i = 1, 2, 3$ ), we take into account the spatial indices, for a  $T$  just dependent on proper time  $t$ :

$$\nabla^i T = \partial^i T = 0, \quad (\text{B.3})$$

Thus, the covariant derivative of  $T$  in this cosmological context can be expressed as:

$$\nabla^\mu T = \dot{\rho} - 3\dot{p} \quad (\text{B.4})$$

### 2. Covariant Derivative of $T^{(R)}$ :

Using Equation (A.22), we derive:

$$\begin{aligned} \kappa^2 \nabla^\mu T_{\mu\nu}^{(R)} &= \nabla^\mu \left( f_R R_{\mu\nu} - \frac{1}{2} g_{\mu\nu} f + g_{\mu\nu} \square f_R - \nabla_\mu \nabla_\nu f_R \right) \\ &= (\nabla^\mu f_R) R_{\mu\nu} + f_R \nabla^\mu R_{\mu\nu} - \frac{1}{2} f_R \nabla^\mu (g_{\mu\nu} R) - \frac{1}{2} f_G \nabla^\mu (g_{\mu\nu} G) - \frac{1}{2} f_T \nabla^\mu (g_{\mu\nu} T) \\ &\quad + \nabla_\nu \square f_R - \square \nabla_\nu f_R. \end{aligned} \quad (\text{B.5})$$

Considering the Bianchi identity within the framework of general relativity, we find that  $\nabla_\nu \square f_R - \square \nabla_\nu f_R = -R_{\mu\nu} \nabla^\mu f_R$ . Therefore,

$$\begin{aligned} \kappa^2 \nabla^\mu T_{\mu\nu}^{(R)} &= R_{\mu\nu} \nabla^\mu f_R + f_R \nabla^\mu \left( R_{\mu\nu} - \frac{1}{2} g_{\mu\nu} R \right) - \frac{1}{2} f_G \nabla^\mu (g_{\mu\nu} G) - \frac{1}{2} f_T \nabla^\mu (g_{\mu\nu} T) - R_{\mu\nu} \nabla^\mu f_R \\ &= f_R \nabla^\mu G_{\mu\nu} - \frac{1}{2} f_G \nabla^\mu (g_{\mu\nu} G) - \frac{1}{2} f_T \nabla^\mu (g_{\mu\nu} T). \end{aligned} \quad (\text{B.6})$$

In this context,  $G_{\mu\nu} \equiv R_{\mu\nu} - \frac{1}{2} g_{\mu\nu} R$  represents the Einstein tensor, which satisfies the divergence-free condition  $\nabla^\mu G_{\mu\nu} = 0$ . Therefore

$$\kappa^2 \nabla^\mu T_{\mu\nu}^{(R)} = -\frac{1}{2} g_{\mu\nu} (f_G \nabla^\mu G + f_T \nabla^\mu T). \quad (\text{B.7})$$

### 3. Covariant Derivative of $T^{(G)}$ :

To calculate  $\nabla^\mu T_{1\mu\nu}^{(G)}$ , we need to apply covariant derivative on eq. (A.23), term by term.

- *The First Term:*

We start with the expression for  $T_{1\mu\nu}^{(G)}$ , as the first term of the Gauss-Bonnet energy-momentum tensor, eq.(A.23),

$$T_{1\mu\nu}^{(G)} = \frac{2}{\kappa^2} R (R_{\mu\nu} f_G + g_{\mu\nu} \square f_G - \nabla_\mu \nabla_\nu f_G). \quad (\text{B.8})$$

Applying the covariant derivative  $\nabla^\mu$  using the product rule:

$$\begin{aligned} \nabla^\mu T_{1\mu\nu}^{(G)} &= \frac{2}{\kappa^2} \nabla^\mu [R (R_{\mu\nu} f_G + g_{\mu\nu} \square f_G - \nabla_\mu \nabla_\nu f_G)] \\ &= \frac{2}{\kappa^2} [(\nabla^\mu R) (R_{\mu\nu} f_G + g_{\mu\nu} \square f_G - \nabla_\mu \nabla_\nu f_G) + R \nabla^\mu (R_{\mu\nu} f_G + g_{\mu\nu} \square f_G - \nabla_\mu \nabla_\nu f_G)]. \end{aligned} \quad (\text{B.9})$$

Expanding the second term:

$$\begin{aligned} \nabla^\mu (R_{\mu\nu} f_G + g_{\mu\nu} \square f_G - \nabla_\mu \nabla_\nu f_G) &= (\nabla^\mu R_{\mu\nu}) f_G + R_{\mu\nu} \nabla^\mu f_G + g_{\mu\nu} \nabla^\mu \square f_G - \nabla^\mu \nabla_\mu \nabla_\nu f_G \\ &= \frac{1}{2} (\nabla_\nu R) f_G + R_{\mu\nu} \nabla^\mu f_G + \nabla_\nu \square f_G - \square \nabla_\nu f_G, \end{aligned} \quad (\text{B.10})$$

where we used  $\nabla^\mu R_{\mu\nu} = \frac{1}{2} \nabla_\nu R$  and  $\nabla^\mu g_{\mu\nu} = 0$ .

Using the identity  $\nabla_\nu \square f_G - \square \nabla_\nu f_G = -R_{\mu\nu} \nabla^\mu f_G$ :

$$\begin{aligned} \nabla^\mu (R_{\mu\nu} f_G + g_{\mu\nu} \square f_G - \nabla_\mu \nabla_\nu f_G) &= \frac{1}{2} (\nabla_\nu R) f_G + R_{\mu\nu} \nabla^\mu f_G - R_{\mu\nu} \nabla^\mu f_G \\ &= \frac{1}{2} f_G \nabla_\nu R. \end{aligned} \quad (\text{B.11})$$

Substituting back:

$$\begin{aligned} \nabla^\mu T_{1\mu\nu}^{(G)} &= \frac{2}{\kappa^2} \left[ (\nabla^\mu R) (R_{\mu\nu} f_G + g_{\mu\nu} \square f_G - \nabla_\mu \nabla_\nu f_G) + R \left( \frac{1}{2} f_G \nabla_\nu R \right) \right] \\ &= \frac{2}{\kappa^2} (R_{\mu\nu} f_G + g_{\mu\nu} \square f_G - \nabla_\mu \nabla_\nu f_G) \nabla^\mu R + \frac{1}{\kappa^2} R f_G \nabla_\nu R. \end{aligned} \quad (\text{B.12})$$

Thus, the complete expression for the covariant derivative is:

$$\nabla^\mu T_{1\mu\nu}^{(G)} = \frac{2}{\kappa^2} (R_{\mu\nu} f_G + g_{\mu\nu} \square f_G - \nabla_\mu \nabla_\nu f_G) \nabla^\mu R + \frac{1}{\kappa^2} R f_G \nabla_\nu R. \quad (\text{B.13})$$

- **The Second Term:**

The second term of eq.(A.23) is

$$T_{2\mu\nu}^{(G)} = -\frac{4}{\kappa^2} (f_G R_\mu^\rho R_{\rho\nu} + R_{\mu\nu} \square f_G + g_{\mu\nu} R^{\rho\lambda} \nabla_\rho \nabla_\lambda f_G) \quad (\text{B.14})$$

We apply the covariant derivative  $\nabla^\mu$  to the entire tensor:

$$\nabla^\mu T_{2\mu\nu}^{(G)} = -\frac{4}{\kappa^2} \nabla^\mu (f_G R_\mu^\rho R_{\rho\nu} + R_{\mu\nu} \square f_G + g_{\mu\nu} R^{\rho\lambda} \nabla_\rho \nabla_\lambda f_G). \quad (\text{B.15})$$

Using the product rule for covariant derivatives, we calculate each term.

$$\nabla^\mu (f_G R_\mu^\rho R_{\rho\nu}) = (\nabla^\mu f_G) R_\mu^\rho R_{\rho\nu} + f_G \nabla^\mu (R_\mu^\rho R_{\rho\nu}), \quad (\text{B.16})$$

$$\nabla^\mu (R_\mu^\rho R_{\rho\nu}) = (\nabla^\mu R_\mu^\rho) R_{\rho\nu} + R_\mu^\rho \nabla^\mu R_{\rho\nu}, \quad (\text{B.17})$$

$$\nabla^\mu (f_G R_\mu^\rho R_{\rho\nu}) = (\nabla^\mu f_G) R_\mu^\rho R_{\rho\nu} + f_G ((\nabla^\mu R_\mu^\rho) R_{\rho\nu} + R_\mu^\rho \nabla^\mu R_{\rho\nu}), \quad (\text{B.18})$$

$$\nabla^\mu (R_{\mu\nu} \square f_G) = \nabla^\mu R_{\mu\nu} \square f_G + R_{\mu\nu} \nabla^\mu (\square f_G), \quad (\text{B.19})$$

$$\nabla^\mu (g_{\mu\nu} R^{\rho\lambda} \nabla_\rho \nabla_\lambda f_G) = \nabla^\mu g_{\mu\nu} R^{\rho\lambda} \nabla_\rho \nabla_\lambda f_G + g_{\mu\nu} \nabla^\mu (R^{\rho\lambda} \nabla_\rho \nabla_\lambda f_G). \quad (\text{B.20})$$

Since  $\nabla^\mu g_{\mu\nu} = 0$ , we have:

$$\nabla^\mu (g_{\mu\nu} R^{\rho\lambda} \nabla_\rho \nabla_\lambda f_G) = g_{\mu\nu} \nabla^\mu (R^{\rho\lambda} \nabla_\rho \nabla_\lambda f_G). \quad (\text{B.21})$$

Now, we combine all the results:

$$\begin{aligned} \nabla^\mu T_{2\mu\nu}^{(G)} = & -\frac{4}{\kappa^2} ((\nabla^\mu f_G) R_\mu^\rho R_{\rho\nu} + f_G ((\nabla^\mu R_\mu^\rho) R_{\rho\nu} + R_\mu^\rho \nabla^\mu R_{\rho\nu})) \\ & -\frac{4}{\kappa^2} (\nabla^\mu R_{\mu\nu} \square f_G + R_{\mu\nu} \nabla^\mu (\square f_G) + g_{\mu\nu} \nabla^\mu (R^{\rho\lambda} \nabla_\rho \nabla_\lambda f_G)). \end{aligned} \quad (\text{B.22})$$

- **The Third Term:**

We start with the expression for  $T_{3\mu\nu}^{(G)}$ , as the third term of eq.(A.23),

$$T_{3\mu\nu}^{(G)} = -\frac{4}{\kappa^2} f_G \left( R_{\mu\rho\nu\lambda} R^{\rho\lambda} - \frac{1}{2} R_\mu^{\rho\lambda\xi} R_{\nu\rho\lambda\xi} \right). \quad (\text{B.23})$$

We now apply the covariant derivative,

$$\begin{aligned} \nabla^\mu T_{3\mu\nu}^{(G)} = & -\frac{4}{\kappa^2} (\nabla^\mu f_G) \left( R_{\mu\rho\nu\lambda} R^{\rho\lambda} - \frac{1}{2} R_\mu^{\rho\lambda\xi} R_{\nu\rho\lambda\xi} \right) \\ & -\frac{4}{\kappa^2} f_G \nabla^\mu \left( R_{\mu\rho\nu\lambda} R^{\rho\lambda} - \frac{1}{2} R_\mu^{\rho\lambda\xi} R_{\nu\rho\lambda\xi} \right). \end{aligned} \quad (\text{B.24})$$

Using the chain rule, the covariant derivative of  $f_G$  becomes:

$$\nabla^\mu f_G = f_{GR} \nabla^\mu R + f_{GG} \nabla^\mu G + f_{GT} \nabla^\mu T. \quad (\text{B.25})$$

where  $f_{GR} = \frac{\partial^2 f}{\partial R \partial G}$ ,  $f_{GG} = \frac{\partial^2 f}{\partial G^2}$ , and  $f_{GT} = \frac{\partial^2 f}{\partial T \partial G}$ .

To compute the covariant derivatives of curvature tensors, we utilize key identities:

- **Bianchi Identity:** The covariant derivative of the Riemann tensor satisfies

$$\nabla^\mu R_{\mu\rho\nu\lambda} + \nabla_\nu R_{\mu\nu\rho\lambda} + \nabla_\lambda R_{\mu\nu\rho\lambda} = 0. \quad (\text{B.26})$$

- **Ricci Tensor and Scalar:** The covariant derivative of the Ricci tensor  $R_{\mu\nu}$  and Ricci scalar  $R$  is more complex, with a commonly used relation:

$$\nabla^\mu R_{\mu\nu} = \frac{1}{2} \nabla_\nu R. \quad (\text{B.27})$$

In the following steps, we use the product rule to compute the derivatives of specific terms:

$$\nabla^\mu (R_{\mu\rho\nu\lambda} R^{\rho\lambda}) = (\nabla^\mu R_{\mu\rho\nu\lambda}) R^{\rho\lambda} + R_{\mu\rho\nu\lambda} \nabla^\mu R^{\rho\lambda}, \quad (\text{B.28})$$

$$\nabla^\mu (R_\mu^{\rho\lambda\xi} R_{\nu\rho\lambda\xi}) = (\nabla^\mu R_\mu^{\rho\lambda\xi}) R_{\nu\rho\lambda\xi} + R_\mu^{\rho\lambda\xi} \nabla^\mu R_{\nu\rho\lambda\xi}. \quad (\text{B.29})$$

Putting it all together, we obtain:

$$\begin{aligned} \nabla^\mu T_{3\mu\nu}^{(G)} &= -\frac{4}{\kappa^2} (f_{GR} \nabla^\mu R + f_{GG} \nabla^\mu G + f_{GT} \nabla^\mu T) \left( R_{\mu\rho\nu\lambda} R^{\rho\lambda} - \frac{1}{2} R_\mu^{\rho\lambda\xi} R_{\nu\rho\lambda\xi} \right) \\ &\quad - \frac{4}{\kappa^2} f_G \left( (\nabla^\mu R_{\mu\rho\nu\lambda}) R^{\rho\lambda} + R_{\mu\rho\nu\lambda} \nabla^\mu R^{\rho\lambda} - \frac{1}{2} (\nabla^\mu R_\mu^{\rho\lambda\xi}) R_{\nu\rho\lambda\xi} - \frac{1}{2} R_\mu^{\rho\lambda\xi} \nabla^\mu R_{\nu\rho\lambda\xi} \right). \end{aligned} \quad (\text{B.30})$$

- **The Fourth Term:**

The fourth term of the energy-momentum tensor eq.(A.23) is given by:

$$T_{4\mu\nu}^{(G)} = \frac{4}{\kappa^2} (R_\mu^\rho \nabla_\nu \nabla_\rho f_G + R_\nu^\rho \nabla_\mu \nabla_\rho f_G + R_{\mu\rho\nu\lambda} \nabla^\rho \nabla^\lambda f_G) \quad (\text{B.31})$$

Applying the covariant derivative  $\nabla^\mu$  to  $T_{4\mu\nu}^{(G)}$ :

$$\nabla^\mu T_{4\mu\nu}^{(G)} = \frac{4}{\kappa^2} \nabla^\mu (R_\mu^\rho \nabla_\nu \nabla_\rho f_G + R_\nu^\rho \nabla_\mu \nabla_\rho f_G + R_{\mu\rho\nu\lambda} \nabla^\rho \nabla^\lambda f_G) \quad (\text{B.32})$$

Using the product rule for covariant derivatives:

$$\nabla^\mu(AB) = (\nabla^\mu A)B + A(\nabla^\mu B) \quad (\text{B.33})$$

each term is expanded as follows:

$$\nabla^\mu (R_\mu^\rho \nabla_\nu \nabla_\rho f_G) = (\nabla^\mu R_\mu^\rho)(\nabla_\nu \nabla_\rho f_G) + R_\mu^\rho \nabla^\mu (\nabla_\nu \nabla_\rho f_G), \quad (\text{B.34})$$

$$\nabla^\mu (R_\nu^\rho \nabla_\mu \nabla_\rho f_G) = (\nabla^\mu R_\nu^\rho)(\nabla_\mu \nabla_\rho f_G) + R_\nu^\rho \nabla^\mu (\nabla_\mu \nabla_\rho f_G), \quad (\text{B.35})$$

$$\nabla^\mu (R_{\mu\rho\nu\lambda} \nabla^\rho \nabla^\lambda f_G) = (\nabla^\mu R_{\mu\rho\nu\lambda})(\nabla^\rho \nabla^\lambda f_G) + R_{\mu\rho\nu\lambda} \nabla^\mu (\nabla^\rho \nabla^\lambda f_G). \quad (\text{B.36})$$

Combining these expansions:

$$\begin{aligned} \nabla^\mu T_{4\mu\nu}^{(G)} &= \frac{4}{\kappa^2} [(\nabla^\mu R_\mu^\rho)(\nabla_\nu \nabla_\rho f_G) + R_\mu^\rho \nabla^\mu (\nabla_\nu \nabla_\rho f_G)] \\ &\quad + \frac{4}{\kappa^2} [(\nabla^\mu R_\nu^\rho)(\nabla_\mu \nabla_\rho f_G) + R_\nu^\rho \nabla^\mu (\nabla_\mu \nabla_\rho f_G)] \\ &\quad + \frac{4}{\kappa^2} [(\nabla^\mu R_{\mu\rho\nu\lambda})(\nabla^\rho \nabla^\lambda f_G) + R_{\mu\rho\nu\lambda} \nabla^\mu (\nabla^\rho \nabla^\lambda f_G)]. \end{aligned} \quad (\text{B.37})$$

• **Combining The Results:**

The complete covariant derivative is given by:

$$\nabla^\mu T_{\mu\nu}^{(G)} = \sum_{i=1}^4 \nabla^\mu T_{i\mu\nu}^{(G)}. \quad (\text{B.38})$$

By combining the eqs. (B.13), (B.22), (B.30), and (B.37), we have:

$$\begin{aligned} \nabla^\mu T_{\mu\nu}^{(G)} &= \frac{2}{\kappa^2} (R_{\mu\nu} f_G + g_{\mu\nu} \square f_G - \nabla_\mu \nabla_\nu f_G) \nabla^\mu R + \frac{1}{\kappa^2} R f_G \nabla_\nu R \\ &\quad - \frac{4}{\kappa^2} ((\nabla^\mu f_G) R_\mu^\rho R_{\rho\nu} + f_G ((\nabla^\mu R_\mu^\rho) R_{\rho\nu} + R_\mu^\rho \nabla^\mu R_{\rho\nu})) \\ &\quad - \frac{4}{\kappa^2} (\nabla^\mu R_{\mu\nu} \square f_G + R_{\mu\nu} \nabla^\mu (\square f_G) + g_{\mu\nu} \nabla^\mu (R^{\rho\lambda} \nabla_\rho \nabla_\lambda f_G)) \\ &\quad - \frac{4}{\kappa^2} (f_{RG} \nabla^\mu R + f_{GG} \nabla^\mu G + f_{GT} \nabla^\mu T) \left( R_{\mu\rho\nu\lambda} R^{\rho\lambda} - \frac{1}{2} R_\mu^{\rho\lambda\xi} R_{\nu\rho\lambda\xi} \right) \\ &\quad - \frac{4}{\kappa^2} f_G \left( (\nabla^\mu R_{\mu\rho\nu\lambda}) R^{\rho\lambda} + R_{\mu\rho\nu\lambda} \nabla^\mu R^{\rho\lambda} - \frac{1}{2} (\nabla^\mu R_\mu^{\rho\lambda\xi}) R_{\nu\rho\lambda\xi} - \frac{1}{2} R_\mu^{\rho\lambda\xi} \nabla^\mu R_{\nu\rho\lambda\xi} \right) \\ &\quad + \frac{4}{\kappa^2} ((\nabla^\mu R_\mu^\rho)(\nabla_\nu \nabla_\rho f_G) + R_\mu^\rho \nabla^\mu (\nabla_\nu \nabla_\rho f_G) + (\nabla^\mu R_\nu^\rho)(\nabla_\mu \nabla_\rho f_G)) \\ &\quad + \frac{4}{\kappa^2} (R_\nu^\rho \nabla^\mu (\nabla_\mu \nabla_\rho f_G) + (\nabla^\mu R_{\mu\rho\nu\lambda})(\nabla^\rho \nabla^\lambda f_G) + R_{\mu\rho\nu\lambda} \nabla^\mu (\nabla^\rho \nabla^\lambda f_G)). \end{aligned} \quad (\text{B.40})$$

After extensive algebraic manipulation and application of the Bianchi identities, the expression simplifies to:

$$\begin{aligned}
\nabla^\mu T_{\mu\nu}^{(G)} = & \frac{1}{\kappa^2} (Rf_G - 2(\nabla^\alpha \nabla_\alpha f_G) + 4R^{\alpha\beta} \nabla_\alpha \nabla_\beta f_G) \nabla_\nu R \\
& + \frac{4}{\kappa^2} (R_{\mu\rho\nu\lambda} \nabla^\mu \nabla^\lambda \nabla^\rho f_G - R_{\nu\rho} \nabla^\rho (\nabla^\alpha \nabla_\alpha f_G)) \\
& - \frac{4}{\kappa^2} f_G \left( R^{\rho\lambda} \nabla_\rho R_{\nu\lambda} + \frac{1}{2} R^{\rho\lambda\alpha\beta} \nabla_\nu R_{\rho\lambda\alpha\beta} \right) \\
& + \frac{4}{\kappa^2} (f_{GR} \nabla^\mu R + f_{GG} \nabla^\mu G + f_{GT} \nabla^\mu T) \left( \frac{1}{2} R_{\mu}^{\rho\lambda\xi} R_{\nu\rho\lambda\xi} - R_{\mu\rho\nu\lambda} R^{\rho\lambda} \right).
\end{aligned} \tag{B.41}$$

where  $f_{GR} = \frac{\partial^2 f}{\partial G \partial R}$ ,  $f_{GG} = \frac{\partial^2 f}{\partial G^2}$ , and  $f_{GT} = \frac{\partial^2 f}{\partial G \partial T}$ .

#### 4. Covariant Derivative of $T^{(T)}$ :

We begin with the expression for the energy-momentum tensor  $T_{\mu\nu}^{(T)}$ :

$$T_{\mu\nu}^{(T)} = -\frac{f_T}{\kappa^2} (T_{\mu\nu}^{(m)} + \Theta_{\mu\nu}) \tag{B.42}$$

where

$$T_{\mu\nu}^{(m)} = (\rho + p) u_\mu u_\nu + p g_{\mu\nu} \tag{B.43}$$

and

$$\Theta_{\mu\nu} = g^{\alpha\beta} \frac{\partial T_{\alpha\beta}^{(m)}}{\partial g^{\mu\nu}}. \tag{B.44}$$

Next, we take the covariant derivative:

$$\nabla^\mu T_{\mu\nu}^{(T)} = \nabla^\mu \left( -\frac{f_T}{\kappa^2} (T_{\mu\nu}^{(m)} + \Theta_{\mu\nu}) \right) \tag{B.45}$$

$$= -\frac{1}{\kappa^2} ((T_{\mu\nu}^{(m)} + \Theta_{\mu\nu}) \nabla^\mu f_T + f_T \nabla^\mu (T_{\mu\nu}^{(m)} + \Theta_{\mu\nu})). \tag{B.46}$$

Here

$$\nabla^\mu f_T = f_{TR} \nabla^\mu R + f_{TG} \nabla^\mu G + f_{TT} \nabla^\mu T \tag{B.47}$$

where  $f_{TR} = \frac{\partial^2 f}{\partial R \partial T}$ ,  $f_{TG} = \frac{\partial^2 f}{\partial G \partial T}$ , and  $f_{TT} = \frac{\partial^2 f}{\partial T^2}$ .

## 5. Covariant Derivative of $T^{(\Xi)}$ :

By using eq.(A.25), one obtains

$$\nabla^\mu T_{\mu\nu}^{(\Xi)} = -\dot{\phi} \left( \ddot{\phi} + 3H\dot{\phi} - V_{,\phi} \right) + \dot{\psi} \left( \ddot{\psi} + 3H\dot{\psi} + V_{,\psi} \right). \quad (\text{B.48})$$

So, by comparing with the equations of motion (11) and (12), we have

$$\nabla^\mu T_{\mu\nu}^{(\Xi)} = 0. \quad (\text{B.49})$$

## Appendix C: Substitution of FLRW Expressions into the Covariant Divergence

### 1. FLRW Computation for $\nabla^\mu T_{\mu\nu}^{(R)}$

For the FLRW metric, the conservation equation for the Ricci sector becomes:

$$\nabla^\mu T_{\mu\nu}^{(R)} = -\frac{1}{2\kappa^2} g_{\mu\nu} (f_G \nabla^\mu G + f_T \nabla^\mu T), \quad (\text{C.1})$$

Considering the temporal component ( $\nu = 0$ ) and using FLRW expressions:

$$R = 6(\dot{H} + 2H^2), \quad (\text{C.2})$$

$$G = 24H^2(\dot{H} + H^2), \quad (\text{C.3})$$

$$T = -\rho + 3p, \quad (\text{C.4})$$

we compute the derivatives:

$$\dot{R} = 6(\ddot{H} + 4H\dot{H}), \quad (\text{C.5})$$

$$\dot{G} = 24H^2\ddot{H} + 48H\dot{H}^2 + 96H^3\dot{H}, \quad (\text{C.6})$$

$$\dot{T} = -\dot{\rho} + 3\dot{p}. \quad (\text{C.7})$$

The left-hand side of (C.1) for  $\nu = 0$  gives:

$$\kappa^2 \nabla^\mu T_{\mu 0}^{(R)} = 12f_R H \dot{H} + 3f_R \ddot{H} - \frac{\dot{f}}{2} \quad (\text{C.8})$$

where the total derivative  $\dot{f}$  is:

$$\dot{f} = f_R \dot{R} + f_G \dot{G} + f_T \dot{T}. \quad (\text{C.9})$$

The right-hand side of (C.1) for  $\nu = 0$  becomes:

$$\begin{aligned} -\frac{1}{2\kappa^2}g_{00}(f_G\nabla^0G + f_T\nabla^0T) &= \frac{1}{2\kappa^2}(f_G\dot{G} + f_T\dot{T}) \\ &= \frac{1}{2\kappa^2}\left[f_G(24H^2\ddot{H} + 48H\dot{H}^2 + 96H^3\dot{H}) + f_T(-\dot{\rho} + 3\dot{p})\right]. \end{aligned} \quad (\text{C.10})$$

Equating (C.8) and (C.10) yields the FLRW conservation relation:

$$12f_RH\dot{H} + 3f_R\ddot{H} - \frac{1}{2}(f_R\dot{R} + f_G\dot{G} + f_T\dot{T}) = \frac{1}{2}\left[f_G(24H^2\ddot{H} + 48H\dot{H}^2 + 96H^3\dot{H}) + f_T(-\dot{\rho} + 3\dot{p})\right].$$

Substituting  $\dot{R} = 6(\ddot{H} + 4H\dot{H})$  and simplifying, we obtain the final form:

$$\kappa^2\nabla^\mu T_{\mu 0}^{(R)} = -12f_GH(H\ddot{H} + 2\dot{H}^2 + 4H^2\dot{H}) - (3\dot{p} - \dot{\rho})\frac{f_T}{2}, \quad (\text{C.11})$$

For the spatial components ( $\nu = i$ ), the right-hand side vanishes due to homogeneity:

$$\nabla^\mu T_{\mu i}^{(R)} = -\frac{1}{2\kappa^2}g_{\mu i}(f_G\nabla^\mu G + f_T\nabla^\mu T) = 0, \quad (\text{C.12})$$

since  $g_{0i} = 0$  and  $\nabla^i G = \nabla^i T = 0$  in the FLRW metric.

This result shows that in FLRW spacetime, the energy-momentum exchange between the geometric and matter sectors occurs only in the temporal direction, consistent with cosmological homogeneity and isotropy.

## 2. FLRW Computation for $\nabla^\mu T_{\mu\nu}^{(G)}$

Following the computation of  $\nabla^\mu T_{\mu\nu}^{(R)}$ , we now derive the FLRW expression for the Gauss-Bonnet sector. Starting from the general expression:

$$\begin{aligned} \nabla^\mu T_{\mu\nu}^{(G)} &= \frac{1}{\kappa^2}\left(Rf_G - 2(\nabla^\alpha\nabla_\alpha f_G) + 4R^{\alpha\beta}\nabla_\alpha\nabla_\beta f_G\right)\nabla_\nu R \\ &\quad + \frac{4}{\kappa^2}\left(R_{\mu\rho\nu\lambda}\nabla^\mu\nabla^\lambda\nabla^\rho f_G - R_{\nu\rho}\nabla^\rho(\nabla^\alpha\nabla_\alpha f_G)\right) \\ &\quad - \frac{4}{\kappa^2}f_G\left(R^{\rho\lambda}\nabla_\rho R_{\nu\lambda} + \frac{1}{2}R^{\rho\lambda\alpha\beta}\nabla_\nu R_{\rho\lambda\alpha\beta}\right) \\ &\quad + \frac{4}{\kappa^2}\left(f_{GR}\nabla^\mu R + f_{GG}\nabla^\mu G + f_{GT}\nabla^\mu T\right)\left(\frac{1}{2}R_\mu^{\rho\lambda\xi}R_{\nu\rho\lambda\xi} - R_{\mu\rho\nu\lambda}R^{\rho\lambda}\right), \end{aligned} \quad (\text{C.13})$$

we substitute the FLRW metric expressions. For computational clarity, we evaluate each term separately for the temporal component ( $\nu = 0$ ).

## I. FLRW Metric Components

In addition to the equations (C.2) to (C.7) we have:

$$R_{00} = -3(\dot{H} + H^2), \quad R_{ij} = a^2(3H^2 + 2\dot{H})\delta_{ij}, \quad (\text{C.14})$$

$$R^{00} = -3H^2, \quad R^{ij} = 3H^2 a^{-2} \delta^{ij}, \quad (\text{C.15})$$

$$\square f_G = -\ddot{f}_G - 3H\dot{f}_G. \quad (\text{C.16})$$

## II. Term-by-Term Evaluation

**Term 1:**  $\frac{1}{\kappa^2} (Rf_G - 2\square f_G + 4R^{\alpha\beta}\nabla_\alpha\nabla_\beta f_G) \nabla_\nu R$

$$R^{\alpha\beta}\nabla_\alpha\nabla_\beta f_G = R^{00}\nabla_0\nabla_0 f_G = (-3H^2)(\ddot{f}_G), \quad (\text{C.17})$$

$$\nabla_0 R = \dot{R} = 6(\ddot{H} + 4H\dot{H}). \quad (\text{C.18})$$

Thus:

$$\begin{aligned} \text{Term 1} &= \frac{1}{\kappa^2} \left[ 6(\dot{H} + 2H^2)f_G - 2(-\ddot{f}_G - 3H\dot{f}_G) + 4(-3H^2)(\ddot{f}_G) \right] \cdot 6(\ddot{H} + 4H\dot{H})\delta_\nu^0 \\ &= \frac{6(\ddot{H} + 4H\dot{H})}{\kappa^2} \left[ 6(\dot{H} + 2H^2)f_G + 2\ddot{f}_G + 6H\dot{f}_G - 12H^2\ddot{f}_G \right] \delta_\nu^0. \end{aligned} \quad (\text{C.19})$$

**Term 2:**  $\frac{4}{\kappa^2} R_{\mu\rho\nu\lambda} \nabla^\mu \nabla^\lambda \nabla^\rho f_G$

This term vanishes identically in FLRW due to the symmetry properties of the Riemann tensor and homogeneity of the spacetime.

**Term 3:**  $-\frac{4}{\kappa^2} R_{\nu\rho} \nabla^\rho (\square f_G)$

For  $\nu = 0$ :

$$R_{0\rho} \nabla^\rho (\square f_G) = R_{00} \nabla^0 (\square f_G) = (-3H^2) \partial_t (-\ddot{f}_G - 3H\dot{f}_G) \quad (\text{C.20})$$

$$= 3H^2 (\ddot{f}_G + 3\dot{H}\dot{f}_G + 3H\ddot{f}_G). \quad (\text{C.21})$$

Thus:

$$\text{Term 3} = -\frac{4}{\kappa^2} \cdot 3H^2 (\ddot{f}_G + 3\dot{H}\dot{f}_G + 3H\ddot{f}_G) \delta_\nu^0 = -\frac{12H^2}{\kappa^2} (\ddot{f}_G + 3\dot{H}\dot{f}_G + 3H\ddot{f}_G) \delta_\nu^0. \quad (\text{C.22})$$

**Term 4:**  $-\frac{4}{\kappa^2} f_G R^{\rho\lambda} \nabla_\rho R_{\nu\lambda}$

For  $\nu = 0$ :

$$R^{\rho\lambda}\nabla_\rho R_{0\lambda} = R^{00}\nabla_0 R_{00} = (-3H^2)\partial_t[-3(\dot{H} + H^2)] \quad (\text{C.23})$$

$$= (-3H^2)[-3(\ddot{H} + 2H\dot{H})] = 9H^2(\ddot{H} + 2H\dot{H}). \quad (\text{C.24})$$

Thus:

$$\text{Term 4} = -\frac{4}{\kappa^2}f_G \cdot 9H^2(\ddot{H} + 2H\dot{H})\delta_\nu^0 = -\frac{36H^2}{\kappa^2}f_G(\ddot{H} + 2H\dot{H})\delta_\nu^0. \quad (\text{C.25})$$

**Term 5:**  $-\frac{2}{\kappa^2}f_G R^{\rho\lambda\alpha\beta}\nabla_\nu R_{\rho\lambda\alpha\beta}$

This term vanishes due to homogeneity of FLRW spacetime.

**Term 6:** The mixed derivative term

$$\frac{4}{\kappa^2}(f_{GR}\nabla^\mu R + f_{GG}\nabla^\mu G + f_{GT}\nabla^\mu T) \left( \frac{1}{2}R_\mu^{\rho\lambda\xi}R_{\nu\rho\lambda\xi} - R_{\mu\rho\nu\lambda}R^{\rho\lambda} \right) \quad (\text{C.26})$$

For FLRW metric:

$$R_0^{\rho\lambda\xi}R_{0\rho\lambda\xi} = 0, \quad (\text{C.27})$$

$$R_{0\rho 0\lambda}R^{\rho\lambda} = R_{0i0j}R^{ij} = [-a^2(\dot{H} + H^2)\delta_{ij}][3H^2a^{-2}\delta^{ij}] = -3H^2(\dot{H} + H^2). \quad (\text{C.28})$$

Thus:

$$\begin{aligned} \text{Term 6} &= \frac{4}{\kappa^2} \left( f_{GR}\dot{R} + f_{GG}\dot{G} + f_{GT}\dot{T} \right) \left( 0 - [-3H^2(\dot{H} + H^2)] \right) \delta_\nu^0 \\ &= \frac{12H^2(\dot{H} + H^2)}{\kappa^2} \left( f_{GR}\dot{R} + f_{GG}\dot{G} + f_{GT}\dot{T} \right) \delta_\nu^0. \end{aligned} \quad (\text{C.29})$$

### III. Final Combined Expression

Combining all non-vanishing terms for the temporal component ( $\nu = 0$ ):

$$\begin{aligned} \nabla^\mu T_{\mu 0}^{(G)} &= \frac{6(\ddot{H} + 4H\dot{H})}{\kappa^2} \left[ 6(\dot{H} + 2H^2)f_G + 2\ddot{f}_G + 6H\dot{f}_G - 12H^2\ddot{f}_G \right] \\ &\quad - \frac{12H^2}{\kappa^2}(\ddot{f}_G + 3\dot{H}\dot{f}_G + 3H\ddot{f}_G) \\ &\quad - \frac{36H^2}{\kappa^2}f_G(\ddot{H} + 2H\dot{H}) \\ &\quad + \frac{12H^2(\dot{H} + H^2)}{\kappa^2} \left( f_{GR}\dot{R} + f_{GG}\dot{G} + f_{GT}\dot{T} \right). \end{aligned} \quad (\text{C.30})$$

This complete expression for  $\nabla^\mu T_{\mu 0}^{(G)}$  in FLRW spacetime will be used in the main text to analyze energy-momentum conservation in our cosmological models.

## Appendix D: Hamiltonian Formulation of $f(R, G, T)$ Gravity

### 1. Canonical Momentum Expressions

The Hamiltonian analysis begins with the conjugate momentum calculations following standard results in modified gravity theories [46, 47]. The complete derivation proceeds as:

$$\pi^{ij} = \frac{\delta \mathcal{L}}{\delta \dot{g}_{ij}} = \frac{\sqrt{-g}}{2\kappa^2} \left[ f_R \frac{\delta R}{\delta \dot{g}_{ij}} + f_G \frac{\delta G}{\delta \dot{g}_{ij}} + f_T \frac{\delta T}{\delta \dot{g}_{ij}} \right] \quad (\text{D.1})$$

$$= \frac{\sqrt{-g}}{2\kappa^2} \left[ f_R (K^{ij} - K g^{ij}) + 4f_G (K^{ik} K_k^j - K K^{ij}) + \cancel{\frac{R}{2} K^{ij}} - \cancel{\frac{1}{2} (K^2 - K^{mn} K_{mn}) g^{ij}} \right] \quad (\text{D.2})$$

$$= \underbrace{\frac{\sqrt{-g}}{2\kappa^2} f_R (K^{ij} - K g^{ij})}_{\text{Einstein-Hilbert part}} + \underbrace{\frac{\sqrt{-g}}{2\kappa^2} 4f_G (K^{ik} K_k^j - K K^{ij})}_{\text{Gauss-Bonnet correction}} \quad (\text{D.3})$$

where  $K_{ij} = \frac{1}{2N} (\dot{g}_{ij} - \nabla_i N_j - \nabla_j N_i)$  is the extrinsic curvature.

For the scalar fields:

$$\pi_\phi = -\sqrt{-g} \dot{\phi} \quad (\text{phantom field}) \quad (\text{D.4})$$

$$\pi_\psi = \sqrt{-g} \dot{\psi} \quad (\text{canonical field}) \quad (\text{D.5})$$

### 2. Key Simplifications in Momentum Expressions

**I. Matter Coupling Term:** The  $f_T$  term vanishes because:

$$\frac{\delta T}{\delta \dot{g}_{ij}} = 0$$

as the matter stress-energy tensor  $T$  depends on  $g_{ij}$  but not on  $\dot{g}_{ij}$  [40].

**II. Gauss-Bonnet Decomposition:** The full variation of  $G$  contains:

$$\frac{\delta G}{\delta \dot{g}_{ij}} = 4(K^{ik} K_k^j - K K^{ij}) + \text{terms proportional to } R \text{ and } K^2$$

The cancellations occur because:

- The  $R$ -dependent terms cancel with  $K^2$  terms in equations of motion [42]
- Gauss-Bonnet is topological in 4D, leaving only boundary terms [41]

**III. Extrinsic Curvature Relations:** Using ADM decomposition [54]:

$$\frac{\delta R}{\delta \dot{g}_{ij}} = K^{ij} - Kg^{ij}$$

### 3. Constraint Structure and Degree of Freedom Counting

**Primary constraints:**

$$\Phi_0 = \pi^0 - \frac{\delta \mathcal{L}}{\delta \dot{N}} \approx 0 \quad (\text{Lapse function}) \quad (\text{D.6})$$

$$\Phi_i = \pi_i - \frac{\delta \mathcal{L}}{\delta \dot{N}^i} \approx 0 \quad (\text{Shift vectors}) \quad (\text{D.7})$$

**Secondary constraints:** Four additional constraints emerge from time conservation of  $\Phi_\mu$ , corresponding to diffeomorphism invariance.

**Degrees of freedom counting** using Dirac's formula:

$$\text{Total DOF} = \frac{1}{2} (\text{Phase space vars} - \text{Constraints}) \quad (\text{D.8})$$

$$= \frac{1}{2} (2 \times (10 \text{ metric} + 2 \text{ fields}) - 8 \text{ constraints}) = 8 \text{ (phase space)} \quad (\text{D.9})$$

In configuration space, the physical DOF is 4:

- **2 Tensor modes:** Transverse-traceless graviton polarizations ( $h_+$ ,  $h_\times$ )
- **2 Scalar modes:** Quintom fields  $\phi$  (phantom) and  $\psi$  (canonical)

### 4. Ostrogradsky Instability Avoidance

The higher-derivative terms in  $f(R, G, T)$  could introduce Ostrogradsky instabilities unless degeneracy conditions are met. The key condition is:

$$\det \begin{pmatrix} f_{RR} & f_{RG} \\ f_{GR} & f_{GG} \end{pmatrix} = 0 \quad (\text{D.10})$$

For linear Gauss-Bonnet ( $f_G = \text{const.}$ ), this holds automatically since  $f_{GG} = f_{RG} = 0$ . The FLRW symmetry provides additional protection by constraining the higher-derivative structure.

## 5. Physical Interpretation

- The first term in (D.3) represents usual gravitational momentum from Einstein-Hilbert gravity [55]
- The second term encodes Gauss-Bonnet modifications, which vanish when  $f_G = \text{const.}$  (total derivative) [46] but become dynamical when  $f_G$  depends on other fields [42]
- All other terms cancel or become boundary terms in closed universes [47]

## Appendix E: Cosmological Perturbation Theory

### 1. Perturbation Variables in FLRW Metric

The general perturbed FLRW metric contains four scalar perturbation functions following standard cosmological perturbation theory [56–58]:

- $\Phi(t, \mathbf{x})$  - Newtonian potential:
  - Governs time-time component of metric perturbations
  - Represents gravitational potential in Newtonian limit
  - Affects particle energies ( $E \approx \sqrt{g_{00}}m$ )
- $B(t, \mathbf{x})$  - Shift vector potential:
  - Appears in time-space components  $g_{0i}$
  - Describes frame-dragging effects
  - Vanishes in Newtonian gauge
- $\Psi(t, \mathbf{x})$  - Spatial curvature potential:
  - Controls scalar curvature perturbations
  - In absence of anisotropic stress,  $\Psi = \Phi$  (GR) [59]
  - Measures local volume distortion
- $E(t, \mathbf{x})$  - Shear potential:

- Appears in space-space components  $g_{ij}$
- Describes anisotropic deformations
- Can be gauged away in Newtonian gauge

## 2. Gauge Fixing to Newtonian Gauge

The general perturbed metric [56]:

$$ds^2 = -(1 + 2\Phi)dt^2 + 2a\partial_i B dx^i dt + a^2[(1 - 2\Psi)\delta_{ij} + 2\partial_i\partial_j E]dx^i dx^j \quad (\text{E.1})$$

can be simplified to Newtonian (longitudinal) gauge [56, 58]:

$$ds^2 = -(1 + 2\Phi)dt^2 + a^2(1 - 2\Psi)\delta_{ij}dx^i dx^j \quad (\text{E.2})$$

through gauge transformations:

**Step 1: Coordinate Transformation** [59]:

$$t \rightarrow t + \alpha(t, \mathbf{x}) \quad (\text{E.3})$$

$$x^i \rightarrow x^i + \delta^{ij}\partial_j\beta(t, \mathbf{x}) \quad (\text{E.4})$$

**Step 2: Gauge Condition Imposition** [58]:

$$B + \dot{E} = 0 \quad (\text{Eliminates } g_{0i} \text{ terms}) \quad (\text{E.5})$$

$$E = 0 \quad (\text{Eliminates anisotropic space-space perturbations}) \quad (\text{E.6})$$

**Step 3: Resulting Metric Form** [56]:

- Vanishing  $B$  (since  $B = -\dot{E}$  and  $E = 0$ )
- Diagonal spatial perturbations ( $E = 0$  removes  $\partial_i\partial_j E$ )
- Preserved  $\Phi$  and  $\Psi$  as gauge-invariant potentials [59]

## 3. Physical Interpretation of Newtonian Gauge

The simplified metric describes [60, 61]:

- **Time dilation:** Governed by  $\Phi$  (Newtonian potential analog)

- **Spatial curvature:** Governed by  $\Psi$  (volume changes)
- **Removed degrees:**
  - $B$  eliminated (no frame-dragging)
  - $E$  eliminated (no anisotropic deformation)

$$\boxed{\text{Newtonian gauge: cosmological analog of } \Phi_{\text{Newton}} \text{ in weak-field GR}} \quad (\text{E.7})$$

This gauge choice provides the foundation for our perturbation analysis in Section 5.2, where we examine stability conditions throughout the bounce evolution.

## Appendix F: Derivation of Modified Friedmann Equations

### 1. Exponential Function of Curvature

For  $f(R, G, T) = R - 2\Lambda e^{-(R_0/R)^n} + \xi_2 G + \xi_3 T$ , we compute the partial derivatives:

$$f_R = 1 - 2n\Lambda u e^{-u}, \quad f_G = \xi_2, \quad f_T = \xi_3 \quad (\text{F.1})$$

$$\dot{f}_R = -2n\Lambda u e^{-u} \left[ \frac{n}{R} u - \frac{n+1}{R} \right] \dot{R}, \quad (\text{F.2})$$

$$\ddot{f}_R = 2n^2\Lambda u e^{-u} \left[ (1-u) \left( \frac{\ddot{R}}{R} - (n+1) \frac{\dot{R}^2}{R^2} \right) + nu \frac{\dot{R}^2}{R^2} (2-u) \right] \quad (\text{F.3})$$

$$\dot{f}_G = 0, \quad \ddot{f}_G = 0 \quad (\text{F.4})$$

where  $u = \left(\frac{R_0}{R}\right)^n$ .

Substituting into the general effective Friedmann equations (62) and (63), the modified Friedmann equations become:

$$3H^2 = \frac{1}{f_R} \left[ \underbrace{\kappa^2(\rho + \rho_\Xi) + \xi_3(\rho + p)}_{\text{Standard + matter coupling}} - \underbrace{3H\dot{f}_R + 3\dot{H}f_R}_{\text{Dynamic curvature}} - \underbrace{\frac{1}{2}(R - 2\Lambda e^{-(R_0/R)^n} + \xi_2 G + \xi_3 T)}_{\text{Effective dark energy}} \right. \\ \left. + \underbrace{12\xi_2 H^2 (H^2 + \dot{H})}_{\text{Gauss-Bonnet contributions}} \right] \quad (\text{F.5})$$

$$\begin{aligned}
-2\dot{H} - 3H^2 = & \frac{1}{f_R} \left[ \underbrace{\kappa^2(p + p_\Xi)}_{\text{Standard terms}} + \underbrace{\ddot{f}_R + 2H\dot{f}_R + \dot{H}f_R}_{\text{Curvature dynamics}} + \underbrace{\frac{1}{2} (R - 2\Lambda e^{-(R_0/R)^n} + \xi_2 G + \xi_3 T)}_{\text{Geometric pressure}} \right. \\
& \left. - \underbrace{12\xi_2 H^2 (H^2 + \dot{H})}_{\text{Gauss-Bonnet contributions}} \right] \tag{F.6}
\end{aligned}$$

Since  $\dot{f}_G = \ddot{f}_G = 0$ , the simplified equations are:

$$\begin{aligned}
3H^2 = & \frac{1}{1 - 2n\Lambda \left(\frac{R_0}{R}\right)^n e^{-(R_0/R)^n}} \left[ \underbrace{\kappa^2(\rho + \rho_\Xi) + \xi_3(\rho + p)}_{\text{Matter and coupling}} \right. \\
& \left. - \underbrace{3H\dot{f}_R + 3\dot{H} \left(1 - 2n\Lambda \left(\frac{R_0}{R}\right)^n e^{-(R_0/R)^n}\right)}_{\text{Dynamic curvature}} \right. \\
& \left. - \underbrace{\frac{1}{2} (R - 2\Lambda e^{-(R_0/R)^n} + \xi_2 G + \xi_3 T)}_{\text{Effective cosmological constant}} + \underbrace{12\xi_2 H^2 (H^2 + \dot{H})}_{\text{Gauss-Bonnet term}} \right] \tag{F.7}
\end{aligned}$$

$$\begin{aligned}
-2\dot{H} - 3H^2 = & \frac{1}{1 - 2n\Lambda \left(\frac{R_0}{R}\right)^n e^{-(R_0/R)^n}} \left[ \underbrace{\kappa^2(p + p_\Xi)}_{\text{Standard pressure}} \right. \\
& \left. + \underbrace{\ddot{f}_R + 2H\dot{f}_R + \dot{H} \left(1 - 2n\Lambda \left(\frac{R_0}{R}\right)^n e^{-(R_0/R)^n}\right)}_{\text{Curvature acceleration}} \right. \\
& \left. + \underbrace{\frac{1}{2} (R - 2\Lambda e^{-(R_0/R)^n} + \xi_2 G + \xi_3 T)}_{\text{Geometric stiff matter}} - \underbrace{12\xi_2 H^2 (H^2 + \dot{H})}_{\text{Gauss-Bonnet term}} \right] \tag{F.8}
\end{aligned}$$

Using  $R = 6(\dot{H} + 2H^2)$ ,  $G = 24H^2(\dot{H} + H^2)$ , and  $T = -\rho + 3p$ , we observe that the Gauss-Bonnet terms exactly cancel between the geometric and matter sectors, yielding the final simplified form:

$$3H^2 = \frac{1}{f_R} \left[ \kappa^2(\rho + \rho_\Xi) + \frac{\xi_3}{2}(3\rho - p) - 3H\dot{f}_R + 3\dot{H}(f_R - 1) - 6H^2 + \Lambda e^{-(R_0/R)^n} \right] \tag{F.9}$$

$$-2\dot{H} - 3H^2 = \frac{1}{f_R} \left[ \kappa^2(p + p_\Xi) + \frac{\xi_3}{2}(3p - \rho) + \ddot{f}_R + 2H\dot{f}_R + \dot{H}f_R + 3(\dot{H} + 2H^2) - \Lambda e^{-(R_0/R)^n} \right] \tag{F.10}$$

## 2. Power-Law Modified Gravity

For  $f(R, G, T) = R + \xi_1 R^n + \xi_2 G + \xi_3 T^m$ , we compute the partial derivatives:

$$f_R = 1 + n\xi_1 R^{n-1}, \quad f_G = \xi_2, \quad f_T = m\xi_3 T^{m-1} \quad (\text{F.11})$$

$$\dot{f}_R = n(n-1)\xi_1 R^{n-2} \dot{R}, \quad \ddot{f}_R = n(n-1)\xi_1 R^{n-3} [(n-2)\dot{R}^2 + R\ddot{R}] \quad (\text{F.12})$$

$$\dot{f}_G = 0, \quad \ddot{f}_G = 0 \quad (\text{F.13})$$

Substituting into the general effective Friedmann equations (62) and (63), we obtain the equations:

$$\begin{aligned} 3H^2 = & \frac{1}{1 + n\xi_1 R^{n-1}} \left[ \kappa^2(\rho + \rho_\Xi) + 3n(n-1)\xi_1 R^{n-2} \dot{R}H + 3n\xi_1 R^{n-1} \dot{H} \right. \\ & - \frac{1}{2}(R + \xi_1 R^n + \xi_2 G + \xi_3 T^m) + m\xi_3 T^{m-1}(\rho + p) \\ & \left. + 12\xi_2 H^2(H^2 + \dot{H}) \right] \end{aligned} \quad (\text{F.14})$$

$$\begin{aligned} -2\dot{H} - 3H^2 = & \frac{1}{1 + n\xi_1 R^{n-1}} \left[ \kappa^2(p + p_\Xi) + n(n-1)\xi_1 R^{n-2} [(n-2)\dot{R}^2 + R\ddot{R}] \right. \\ & + 2n(n-1)\xi_1 R^{n-2} \dot{R}H + n\xi_1 R^{n-1} \dot{H} + \frac{1}{2}(R + \xi_1 R^n + \xi_2 G + \xi_3 T^m) \\ & \left. - 12\xi_2 H^2(H^2 + \dot{H}) \right] \end{aligned} \quad (\text{F.15})$$

Since  $\dot{f}_G = \ddot{f}_G = 0$  for this model, and using  $R = 6(\dot{H} + 2H^2)$ ,  $G = 24H^2(\dot{H} + H^2)$ ,  $T = -\rho + 3p$ , the equations simplify to:

$$\begin{aligned} 3H^2 = & \frac{1}{1 + n\xi_1 R^{n-1}} \left[ \underbrace{\kappa^2(\rho + \rho_\Xi)}_{\text{Standard terms}} + \underbrace{3n\xi_1 R^{n-1} \dot{H}}_{\text{Curvature-driven inertia}} + \underbrace{3n(n-1)\xi_1 R^{n-2} \dot{R}H}_{\text{Dynamic curvature}} \right. \\ & \left. - \underbrace{\frac{1}{2}(R + \xi_1 R^n + \xi_3 T^m)}_{\text{Effective dark energy}} + \underbrace{m\xi_3 T^{m-1}(\rho + p)}_{\text{Non-linear matter coupling}} \right] \end{aligned} \quad (\text{F.16})$$

$$\begin{aligned} -2\dot{H} - 3H^2 = & \frac{1}{1 + n\xi_1 R^{n-1}} \left[ \underbrace{\kappa^2(p + p_\Xi)}_{\text{Standard terms}} + \underbrace{n\xi_1 R^{n-1} \dot{H}}_{\text{Curvature pressure}} + \underbrace{2n(n-1)\xi_1 R^{n-2} \dot{R}H}_{\text{Dynamic curvature}} \right. \\ & \left. + \underbrace{n(n-1)\xi_1 R^{n-2} [(n-2)\dot{R}^2 + R\ddot{R}]}_{\text{Curvature acceleration}} + \underbrace{\frac{1}{2}(R + \xi_1 R^n + \xi_3 T^m)}_{\text{Geometric stiff matter}} \right] \end{aligned} \quad (\text{F.17})$$

### 3. Modified Teleparallel Gravity Cosmology

For the specific form  $f(R, G, T) = R + \xi_2 G + \xi_3 T^2$ , we compute the partial derivatives:

$$f_R = 1, \quad f_G = \xi_2, \quad f_T = 2\xi_3 T \quad (\text{F.18})$$

$$\dot{f}_R = 0, \quad \ddot{f}_R = 0, \quad \dot{f}_G = 0, \quad \ddot{f}_G = 0 \quad (\text{F.19})$$

Substituting into the general effective Friedmann equations (62) and (63), and using  $T = -\rho + 3p$ , we obtain:

$$3H^2 = \kappa^2(\rho + \rho_\Xi) + \xi_3 \left[ (3\rho - p)(-\rho + 3p) - \frac{1}{2}(-\rho + 3p)^2 \right] - 12\xi_2 H^2 (H^2 + \dot{H}) \quad (\text{F.20})$$

$$-2\dot{H} - 3H^2 = \kappa^2(p + p_\Xi) + \xi_3 \left[ (3p - \rho)(-\rho + 3p) + \frac{1}{2}(-\rho + 3p)^2 \right] + 12\xi_2 H^2 (H^2 + \dot{H}) \quad (\text{F.21})$$

Simplifying the torsion-matter coupling terms:

$$\xi_3 \left[ (3\rho - p)(-\rho + 3p) - \frac{1}{2}(-\rho + 3p)^2 \right] = -\frac{\xi_3}{2}(5\rho^2 - 14\rho p - 3p^2) \quad (\text{F.22})$$

$$\xi_3 \left[ (3p - \rho)(-\rho + 3p) + \frac{1}{2}(-\rho + 3p)^2 \right] = -\frac{\xi_3}{2}(9p^2 - 6\rho p + \rho^2) \quad (\text{F.23})$$

Thus, the final modified Friedmann equations become:

$$3H^2 = \underbrace{\kappa^2(\rho + \rho_\Xi)}_{\text{Standard terms}} - \underbrace{\frac{\xi_3}{2}(5\rho^2 - 14\rho p - 3p^2)}_{\text{Torsion-matter interaction}} - \underbrace{12\xi_2 H^2 (H^2 + \dot{H})}_{\text{Gauss-Bonnet contribution}} \quad (\text{F.24})$$

$$-2\dot{H} - 3H^2 = \underbrace{\kappa^2(p + p_\Xi)}_{\text{Standard terms}} - \underbrace{\frac{\xi_3}{2}(9p^2 - 6\rho p + \rho^2)}_{\text{Torsion pressure}} + \underbrace{12\xi_2 H^2 (H^2 + \dot{H})}_{\text{Gauss-Bonnet contribution}} \quad (\text{F.25})$$

### 4. Non-Minimal Curvature-Matter Coupling

For  $f(R, G, T) = R + \xi_2 G + \xi_3 R^2 T$ , we compute the partial derivatives:

$$f_R = 1 + 2\xi_3 RT, \quad f_G = \xi_2, \quad f_T = \xi_3 R^2 \quad (\text{F.26})$$

$$\dot{f}_R = 2\xi_3(\dot{R}T + R\dot{T}), \quad \ddot{f}_R = 2\xi_3(\ddot{R}T + 2\dot{R}\dot{T} + R\ddot{T}) \quad (\text{F.27})$$

$$\dot{f}_G = 0, \quad \ddot{f}_G = 0 \quad (\text{F.28})$$

Substituting into the general effective Friedmann equations (62) and (63):

$$3H^2 = \frac{1}{1 + 2\xi_3 RT} \left[ \underbrace{\kappa^2(\rho + \rho_\Xi) + \xi_3 R^2(\rho + p)}_{\text{Matter and coupling}} - \underbrace{3H\dot{f}_R + 3\dot{H}(1 + 2\xi_3 RT)}_{\text{Dynamic curvature}} \right. \\ \left. - \frac{1}{2} \underbrace{(R + \xi_2 G + \xi_3 R^2 T)}_{\text{Effective dark energy}} + \underbrace{12\xi_2 H^2(H^2 + \dot{H})}_{\text{Gauss-Bonnet term}} \right] \quad (\text{F.29})$$

$$-2\dot{H} - 3H^2 = \frac{1}{1 + 2\xi_3 RT} \left[ \underbrace{\kappa^2(p + p_\Xi)}_{\text{Standard pressure}} + \underbrace{\ddot{f}_R + 2H\dot{f}_R + \dot{H}(1 + 2\xi_3 RT)}_{\text{Curvature acceleration}} \right. \\ \left. + \frac{1}{2} \underbrace{(R + \xi_2 G + \xi_3 R^2 T)}_{\text{Geometric stiff matter}} - \underbrace{12\xi_2 H^2(H^2 + \dot{H})}_{\text{Gauss-Bonnet term}} \right] \quad (\text{F.30})$$


---

- [1] A. G. Riess et al. Observational evidence from supernovae for an accelerating universe and a cosmological constant. *Astron. J.*, 116(3):1009–1038, 1998.
- [2] S. Perlmutter et al. Measurements of  $\Omega$  and  $\Lambda$  from 42 high-redshift supernovae. *Astrophys. J.*, 517(2):565–586, 1999.
- [3] H. V. Peiris et al. First-year Wilkinson Microwave Anisotropy Probe (WMAP)\* observations: Implications for inflation. *Astrophys. J. Suppl. Ser.*, 148(1):213–231, 2003.
- [4] D. N. Spergel et al. Three-year Wilkinson Microwave Anisotropy Probe (WMAP) observations: Implications for cosmology. *Astrophys. J. Suppl. Ser.*, 170(2):377–408, 2007.
- [5] N. Aghanim et al. Planck 2018 results-I. overview and the cosmological legacy of Planck. *Astron. Astrophys.*, 641:A1, 2020.
- [6] S. Nojiri and S. D. Odintsov. Unified cosmic history in modified gravity: From  $F(R)$  theory to lorentz non-invariant models. *Phys. Rep.*, 505(2-4):59–144, 2011.
- [7] V. Faraoni, E. Gunzig, and P. Nardone. Conformal transformations in classical gravitational theories and in cosmology. *arXiv preprint gr-qc/9811047*, 1998.
- [8] H. Essén. General relativity as a conformally invariant scalar gauge field theory. *Int. J. Theor. Phys.*, 29(2):183–187, 1990.
- [9] M. V. Takook and M. R. Tanhayi. Linear weyl gravity in de sitter universe. *JHEP*, 2010(12):1–15, 2010.
- [10] P. D. Mannheim. Are galactic rotation curves really flat? *Astrophys. J.*, 479(2):659–664, 1997.

- [11] R. P. Feynman et al. *Feynman Lectures on Gravitation*. Adv. Book Program. Addison-Wesley, Reading, Massachusetts, 1st edition, 1995. ISBN 0-201-62734-5.
- [12] W. Hu and I. Sawicki. Models of  $f(R)$  cosmic acceleration that evade solar system tests. *Phys. Rev. D*, 76(6):064004, 2007.
- [13] C. Deffayet et al. Imperfect dark energy from kinetic gravity braiding. *JCAP*, 2010(10):026, 2010.
- [14] T. Qiu et al. Bouncing galileon cosmologies. *JCAP*, 2011(10):036, 2011.
- [15] C. Lin et al. A matter bounce by means of ghost condensation. *JCAP*, 2011(04):019, 2011.
- [16] S. Nojiri and S. D. Odintsov. Modified Gauss–Bonnet theory as gravitational alternative for dark energy. *Phys. Lett. B*, 631(1-2):1–6, 2005.
- [17] K. Bamba et al. The future of the universe in modified gravitational theories: Approaching a finite-time future singularity. *JCAP*, 2008(10):045, 2008.
- [18] B. Feng et al. Dark energy constraints from the cosmic age and supernova. *Phys. Lett. B*, 607(1-2):35–41, 2005.
- [19] G. Ye and Y.-S. Piao. Bounce in general relativity and higher-order derivative operators. *Phys. Rev. D*, 99(8):084019, 2019.
- [20] Y.-F. Cai et al. Towards a nonsingular bouncing cosmology. *JCAP*, 2012(08):020, 2012.
- [21] D. Langlois. Degenerate higher-order scalar-tensor (dhost) theories. *arXiv:1707.03625*, 2017.
- [22] A. Vikman. Can dark energy evolve to the phantom? *Phys. Rev. D*, 71(2):023515, 2005.
- [23] C. Armendariz-Picon et al. Dynamical solution to the problem of a small cosmological constant and late-time cosmic acceleration. *Phys. Rev. Lett.*, 85(21):4438, 2000.
- [24] J. Khoury et al. From big crunch to big bang. *Phys. Rev. D*, 65(8):086007, 2002.
- [25] S. Elitzur et al. From big bang to big crunch and beyond. *JHEP*, 2002(06):017, 2002.
- [26] J. Sadeghi et al. Bouncing universe with the non-minimally coupled scalar field and its reconstruction. *Mod. Phys. Lett. A*, 24(29):2363–2376, 2009.
- [27] K. Bamba et al. Bounce cosmology from  $F(R)$  gravity and  $F(R)$  bigravity. *J. Cosmol. Astropart. Phys.*, 2014(01):008, 2014.
- [28] D. A. Eliezer and R. P. Woodard. Instability of higher-difference initial-value theories. *Phys. Rev. D*, 40(2):465, 1989.
- [29] R. P. Woodard. Avoiding dark energy with  $1/R$  modifications of gravity. In E. J. Lerner and J. B. Almeida, editors, *The Invisible Universe: Dark Matter and Dark Energy*, volume 720 of

- Lect. Notes Phys.*, pages 403–433. Springer, 2007.
- [30] R. P Woodard. The theorem of ostrogradsky. *arXiv preprint arXiv:1506.02210*, 2015.
- [31] T. A. Smecker and R. F. G. Wyse. Type Ia supernovae: Constraints on baryonic dark matter. In *AIP Conf. Proc.*, volume 222, pages 467–470. AIP, 1991.
- [32] P. Ruiz-Lapuente et al. Type Ia supernova scenarios and the hubble sequence. *Astrophys. J.*, 447(2):L69, 1995.
- [33] K. Nomoto et al. Type Ia supernovae: Their origin and possible applications in cosmology. *Science*, 276(5317):1378–1382, 1997.
- [34] D. J. Eisenstein et al. Detection of the baryon acoustic peak in the large-scale correlation function of SDSS luminous red galaxies. *Astrophys. J.*, 633(2):560, 2005.
- [35] B. Ratra and P. J. E. Peebles. Cosmological consequences of a rolling homogeneous scalar field. *Phys. Rev. D*, 37(12):3406, 1988.
- [36] R. R. Caldwell. A phantom menace? cosmological consequences of a dark energy component with super-negative equation of state. *Phys. Lett. B*, 545(1-2):23–29, 2002.
- [37] A. Sen. Tachyon matter. *JHEP*, 2002(07):065, 2002.
- [38] M. Gasperini et al. Quintessence as a runaway dilaton. *Phys. Rev. D*, 65(2):023508, 2001.
- [39] H. Wei et al. Hesseence: A new view of quintom dark energy. *Class. Quantum Gravity*, 22(16):3189, 2005.
- [40] T. Harko et al.  $f(R, T)$  gravity. *Phys. Rev. D*, 84:024020, 2011.
- [41] C. Charmousis and A. Padilla. The instability of vacuum in  $f(G)$  gravity. *JHEP*, 2008:028, 2008.
- [42] S. Nojiri and S. D. Odintsov. Modified gauss-bonnet theory as gravitational alternative for dark energy. *Phys. Lett. B*, 631:1–6, 2005.
- [43] M. Lilley and P. Peter. Bouncing alternatives to inflation. *Comptes Rendus Physique*, 16(10):1038–1047, 2015.
- [44] M. Ghanaatian and F. Milani. Bouncing universe with the modified gravity coupled to the weyl tensor. *Gen. Relativ. Gravit.*, 46(9):1789, 2014.
- [45] M. Ghanaatian et al. Bouncing theory in the modified weyl gravity and its stability conditions. *Ann. Phys.*, 397:458–473, 2018.
- [46] A. De Felice and S. Tsujikawa.  $f(R)$  theories. *Living Rev. Relativ.*, 13(1):3, 2010.
- [47] T. P. Sotiriou and V. Faraoni.  $f(R)$  theories of gravity. *Rev. Mod. Phys.*, 82:451–497, 2010.

- [48] E. Elizalde et al. Oscillations of the  $f(r)$  dark energy in the accelerating universe. *Eur. Phys. J. C*, 72(2):1843, 2012.
- [49] K. Bamba et al. Dark energy cosmology: the equivalent description via different theoretical models and cosmography tests. *Astrophys. Space Sci.*, 342(1):155–228, 2012.
- [50] Y.-F. Cai et al.  $f(T)$  teleparallel gravity and cosmology. *Rep. Prog. Phys.*, 79(10):106901, 2016.
- [51] O. Bertolami et al. Extra force in  $f(R)$  modified theories of gravity. *Phys. Rev. D*, 75(10):104016, 2007.
- [52] K. Bamba et al. Crossing of the phantom divide in modified gravity. *Phys. Rev. D*, 79(8):083014, 2009.
- [53] Y.-F. Cai and other. Bouncing universe with quintom matter. *JHEP*, 2007(10):071, 2007.
- [54] R. Arnowitt, S. Deser, and C. W. Misner. The dynamics of general relativity, gravitation: An introduction to current research. *Chap*, 7:227–265, 1962.
- [55] C. W. Misner, K. S. Thorne, and J. A. Wheeler. *Gravitation*. W. H. Freeman, 1973.
- [56] V. F. Mukhanov, H. A. Feldman, and R. H. Brandenberger. *Theory of cosmological perturbations*, volume 215. 1992.
- [57] H. Kodama and M. Sasaki. Cosmological perturbation theory. *Prog. Theor. Phys. Suppl.*, 78:1–166, 1984.
- [58] C.-P. Ma and E. Bertschinger. Cosmological perturbation theory in the synchronous and conformal newtonian gauges. *Astrophys. J.*, 455:7, 1995.
- [59] J. M. Bardeen. Gauge-invariant cosmological perturbations. *Phys. Rev. D*, 22:1882–1905, 1980.
- [60] S. Weinberg. *Cosmology*. Oxford Univ. Press, 2008.
- [61] S. Dodelson. *Modern Cosmology*. Academic Press, 2003.